

Response to Reviewers comments for
Photooxidants from Brown Carbon and Other Chromophores in Illuminated Particle Extracts

By Richie Kaur et. al.

Please note:

Reviewer comment is in black text.

Our response is in blue.

Please note that line numbers in the revised version are different due to changes in the manuscript.

Anonymous Referee #1

Received and published: 21 December 2018

This paper reports the results of a study that quantified $\cdot\text{OH}$, $^1\text{O}_2$ and triplet states in particulate matter aqueous extracts. As there are few or no studies on the subject, the topic is interesting and deserves publication. However, there are some clarity issues with the present version of the manuscript that should be solved. Moreover, it is not clear whether the procedure to determine the transient species was fully appropriate (in particular, the authors do not specify if and how they dealt with transient scavenging by the probe molecules, which is a confounding factor in this kind of measurements and could possibly explain the inconsistency between the $^1\text{O}_2$ and $^3\text{C}^*$ data). For these reasons, the manuscript should be revised following the recommendations reported below.

We thank this reviewer for their thorough review and the detailed, helpful comments. We have addressed each of them below.

Regarding probe molecules, while we tried to limit probe concentrations so that they were insignificant scavengers of the transient oxidants, we found that we had one condition (MBO used to measure $[\text{OH}^\cdot]$ in the dilution series of sample PME3D) where the probe was a significant sink. As described below (and in the revised manuscript), we corrected these $[\text{OH}^\cdot]$ values for the influence of MBO. For the other oxidant cases – $^1\text{O}_2^*$ and $^3\text{C}^*$, and $[\text{OH}^\cdot]$ measured in the other samples using benzene – our probe concentrations were low enough that they insignificantly perturbed oxidant kinetics. These determinations are also described below.

1. Page 5, bottom. Please specify the degree (approximate) by which the samples were diluted upon addition of H_2SO_4 . Moreover, measuring pH in a small sample might not be totally trivial: please provide details of the pH measurement device.

The dilution of the samples was always kept below 10%. For each sample, we acidified and measured the pH of a 1 mL aliquot using a pH microelectrode (MI-414 series, protected tip

needle, 16 gauge, 6 cm length; Microelectrodes, Inc.). We have added this information in Sect. 2.3 (Page 6, top).

2. Line 177. Is the pathlength measured in cm? Please specify.

Yes. Pathlength was measured in cm. We have clarified this (now Page 6, bottom).

3. Page 6, bottom. I suppose that the contributions of nitrate and nitrite to absorption were small. Anyway, that should be specified for completeness (approximately which percentage of absorbance would be accounted for by NO₂⁻/NO₃⁻ and which by DOM, of course it varies with wavelength but it is important to have an idea of that).

The contributions of NO₂⁻ / NO₃⁻ to light absorption were small and vary by wavelength. Integrated across the solar wavelengths, these species accounted for up to 7% of total absorption. We have added this information to Sect. 2.4 (top of page 7).

4. Line 190. Please spell out the “OM” and “OC” acronyms.

We apologize for the oversight. We have spelled out the acronyms OM (organic matter) and OC (organic carbon).

5. Section 2.5 and overall. Scavenging of the reactive species by probes can be a problem, because it decreases the transient steady-state concentration. Because of this, the steady-state concentration in the illuminated sample with the probe can be much different from the steady-state concentration in the sample without probe. If an issue like this occurred in the measurements of ¹O₂ and the triplet states, that could explain the inconsistency of the results (comparison between ¹O₂ and ³C* should be carried out in the samples without probes, by means of an extrapolation). Experiments with benzene were carried out at different initial concentrations, and by so doing there is a chance of correcting for probe scavenging (although it was not specified whether such a procedure was followed). In the case of FFA and the triplet probes the used concentration is not provided. This issue should be checked, corrected if necessary, and in any case discussed in the manuscript.

To minimize perturbations in the steady-state concentrations of the oxidants, we used low concentrations of probe compounds for ¹O₂* and ³C*. The concentrations of FFA and triplet probes (SYR and MeJA) were 10 μM each (Sections 2.5.2 and 2.5.3, respectively). The major sink for ¹O₂* in our samples is water, with a pseudo-first order rate constant of 2.2 × 10⁵ s⁻¹ (Bilski et al., 1997). In comparison, 10 μM of FFA (with a rate constant 1.2 × 10⁸ M⁻¹ s⁻¹; Wilkinson et al. (1995)) has a corresponding rate constant of 1.2 × 10³ s⁻¹, indicating that it reduces [¹O₂*] by less than 1 %.

For triplets, there are two major natural sinks: O₂, with a pseudo first-order rate constant, $k_{3C^*+O_2}[O_2]$, of 8.0 × 10⁵ s⁻¹ (see Eqn. 8) and dissolved organic compounds, which have an average pseudo-first-order rate constant with triplets of ~ (9 × 10⁷ L mol⁻¹C⁻¹)(3 × 10⁻³ mol L⁻¹) = 3 × 10⁴ s⁻¹ in the standard extracts. Together, these two sinks represent a total background rate

constant for triplet loss of approximately $8.3 \times 10^5 \text{ s}^{-1}$. In contrast, 10 μM of SYR (our most reactive triplet probe) has a pseudo-first-order rate constant of $k_{3\text{C}^*+\text{SYR}}[\text{SYR}] \approx (4 \times 10^9 \text{ M}^{-1} \text{ s}^{-1})(1 \times 10^{-5} \text{ M}) = 4 \times 10^4 \text{ s}^{-1}$. Thus the addition of SYR causes, on average, a decrease in the triplet concentration of only $\sim 5\%$.

The competition kinetics technique, which was used for most measurements of $\cdot\text{OH}$, uses a range of probe (benzene) concentrations so that the parameters P_{OH} , k'_{OH} and $[\cdot\text{OH}]$ can be determined under extrapolated conditions of zero added probe. For these cases the probe influence is accounted for in the method.

However, for our final case we found that the probe concentration was indeed too high. This is the dilution series of sample PME3D, where we used 75 μM methylbutenol (MBO) (Section S1). We had to use a high concentration because of analytical limitations: the high background absorbance in the standard extract made it difficult to detect MBO in our samples. However, in hindsight we should have adjusted the MBO concentration so that it was lower in the more dilute PM extracts. MBO has a rate constant with $\cdot\text{OH}$ of $7.4 \times 10^9 \text{ M}^{-1} \text{ s}^{-1}$ (Section S1), thus 75 μM corresponds to a pseudo-first-order rate constant for $\cdot\text{OH}$ loss of $5.6 \times 10^5 \text{ s}^{-1}$. With this relatively high value MBO is a significant, and in one case dominant, sink for $\cdot\text{OH}$ in the dilution series of PME3D. MBO is significantly suppressing $[\cdot\text{OH}]$ in the more dilute extracts, but not as much in the more concentrated extracts: our originally reported $[\cdot\text{OH}]$ values are too low by factors of 3.3, 1.4, 1.3, 1.2, and 1.1 for samples PME3D10, D2.5, D1.3, D1, and D0.5, respectively. We have added a description of this problem to the manuscript and corrected the $[\text{OH}]$ values in the PME3D dilution series. Because we correct our SYR probe results for the contribution of $\cdot\text{OH}$, we have also corrected the corresponding $^3\text{C}^*$ concentrations for the PME3D dilution samples, as well as our associated Figures and the extrapolations to aerosol liquid water conditions. Because $\cdot\text{OH}$ was a minor contributor to SYR loss, the corrections for $^3\text{C}^*$ are relatively small. We have indicated the problem with MBO determination of $\cdot\text{OH}$, and our correction, in the main text and supplemental material.

6. Lines 199-204. The procedure used here was different from the description of the irradiation experiments provided in section 2.3. Also the irradiated volume is different (5 mL vs. 1 mL), although the same HPLC was used in both cases which required the withdrawal of 100 μL aliquots. The reason for this difference should be provided for clarity.

We thank the reviewer for their attention to detail. At the beginning of Sect. 2.3, we mention that the procedure of using a 1 mL sample volume applies to all measurements except “ P_{OH} measurements” when it should have said “ $\cdot\text{OH}$ measurements using benzene” – this was an error that we have corrected. For all $\cdot\text{OH}$ measurements where benzene is used as a probe, we used a larger sample volume (5 mL instead of 1 mL) while withdrawing the same small aliquot for HPLC analysis (100 μL) in order to minimize the headspace in the reaction container. Since benzene is highly volatile, reducing headspace prevents loss of benzene due to volatilization. Since the other probes are less volatile, we were able to use a small volume (1 mL) for those experiments because the additional headspace in the container after a few aliquot withdrawals does not pose a complication, unlike in case of benzene. We have added this clarification in Sect. 2.5.1.

7. Line 201. “illuminated” should read “illumination”.

Thank you, we have corrected this.

8. Equation (4). Which is the rationale behind this equation? Is it assumed that light screening in ambient particles can be neglected? If so, why (there is a small pathlength there, but concentrations can be very high and compensate)? Please explain for clarity.

Yes, because of the very small pathlength in ambient particles the screening is negligible for our filtered samples. (Insoluble black carbon might cause screening in airborne particles, but our samples were filtered.) Although the particles are much more concentrated than our solutions (by approximately a factor of 10^3), the pathlength in the particles ($\sim 1 \mu\text{m}$) is smaller than in our solutions by a larger amount (approximately a factor of 10^4).

9. Page 8, top. To enable comparison between the two methods, please report reaction yields for benzene \Rightarrow phenol and for MBO.

The two techniques are not directly comparable. In the benzene technique, we measured the product of the reaction between benzene and $\cdot\text{OH}$, i.e., phenol. The yield for phenol from the benzene + $\cdot\text{OH}$ reaction is 73%; we have added this information to Sect. 2.5.1. On the other hand, when MBO was the probe, we measured the loss of MBO in solution, similar to FFA, SYR and MeJA. Because MBO can also react with $^1\text{O}_2^*$ and $^3\text{C}^*$, we corrected the MBO decay to account for these contributions and then calculated $[\cdot\text{OH}]$ from the fraction of MBO lost due to $\cdot\text{OH}$ alone (see Section S1.1 in the SI). On average, $55 (\pm 15) \%$ of MBO was lost by reaction with $\cdot\text{OH}$ in the PME3D dilution samples where MBO was used.

10. Section 2.5.2. Please specify the FFA concentration and the way $^1\text{O}_2$ scavenging by added Ffa was accounted for.

The concentration of FFA ($10 \mu\text{M}$) is specified near the beginning of Sect. 2.5.2. As we describe in our response to comment #5 above, this FFA concentration is low enough that it does not significantly affect the singlet oxygen concentration.

11. Line 232. Is it “faster” or slower? Please check.

Faster (as we had in the text) is correct. Since $^1\text{O}_2^*$ reacts more slowly with D_2O than H_2O , $[^1\text{O}_2^*]$ is higher in the D_2O solutions and thus FFA loss is faster.

12. Section 2.5.3. Also in this case, the probe concentration should be specified and its role as $^3\text{C}^*$ scavenger (or the way scavenging was corrected for) should be discussed, because the presence of the probe alters $[^3\text{C}^*]$.

The probe concentration of $10 \mu\text{M}$ is specified near the beginning of Sect. 2.5.3. As we discussed in our response to comment #5 above, our calculations indicate that the addition of SYR (or MeJA) does not significantly affect the triplet concentration. We have added a mention of this to the text.

13. Lines 269-272 and 279. the overall explanation here is not very clear. I imagine that a couple of matching triplets were used and the mole fractions were calculated so that it was possible to exactly match the experimental rate constant ratios. However, this should be explained better because it is definitely not straightforward to derive it from the text.

The reviewer is correct about how our technique works. We have added some text at the top of page 10 to try to clarify our description.

14. Lines 288-289. Canonica estimated $5 \times 10^5 \text{ s}^{-1}$ as the triplet deactivation rate constant. The data provided here suggest a higher value for the estimated rate constant. Which is the reason? Was a different $[\text{O}_2]$ assumed here in comparison with surface waters? Please explain better.

The triplet deactivation constant (units: s^{-1}) is the product of the second-order rate constant of triplet quenching by O_2 ($k_{3\text{C}+\text{O}_2}$; units: $\text{M}^{-1} \text{ s}^{-1}$) and the molar concentration of O_2 . We used Canonica's estimates for $k_{3\text{C}+\text{O}_2}$ (Canonica et al., 2000) for 3 model triplets, and to mimic natural triplets, we averaged them to get a value of $2.8 \times 10^9 \text{ M}^{-1} \text{ s}^{-1}$ (shown in Table S11). We used USGS estimates for dissolved oxygen concentration of $284 \mu\text{M}$ at our experimental temperature of $20 \text{ }^\circ\text{C}$ (USGS, 2018), which yields a triplet deactivation constant of $8 \times 10^5 \text{ s}^{-1}$. It is possible that some of the surface water studies were done at a different temperatures or used $k_{3\text{C}+\text{O}_2}$ for a single model triplet rather than the average value we used – either or both of those factors could be responsible for that difference. All of these details are given after Equation 8 in the main text.

15. Equation (9) and related discussion. I imagine that also R_{abs} was normalised to the winter solstice, otherwise there is no consistency. However, I do not understand the reason for using a double normalization. The quantum yield should be independent from the irradiation conditions, thus it should be the same (and better, to my opinion) to use the raw experimental data. If there are additional reasons for using normalized data, that should be explained.

We normalize measured rates of oxidant formation to winter solstice sunlight to correct for daily variations in the output of our lamp; this allows rates in different samples to be directly compared (and averaged). To be consistent, R_{abs} , the rate of light absorption in a sample, is calculated using the winter solstice actinic flux (Equation 2): while we could calculate the rate of light absorption for each experiment, values for different samples couldn't be properly compared because of variations in light output. So, while we are essentially double normalizing, it allows us to put all values on the same photon flux basis.

16. Line 345. How were the Absorption Angstrom Exponents calculated? Please specify (better by using a formula).

The AAE formula and calculation are described in the footnotes of Table S1 of the SI. In the interest of keeping our main text from getting any larger, we have not added the equation to the main text.

17. Line 362. Do you mean here that absorption declined faster with increasing wavelength? This may have implications for the molecular weight of DOM (higher molecular weight compounds experience a slower decrease of absorption with wavelength).

This is an interesting point. Yes, as shown in Fig. S5 of the SI, the particle extracts had a higher absorbance and mass absorption coefficient at shorter wavelengths. Consequently, the decline of absorbance with wavelength in the extracts was faster than in fog. However, a caveat to this data is that the figure compares the ratios of two specific samples (e.g., median absorbing PM extract with median absorbing fog), so it is unclear how representative each sample is. To better make this comparison we also calculated AAE values for the fog drops: the fog values are generally lower than the PM extract values (consistent with the Fig. S5 result), but the difference is small ($p = 0.56$; Table S1).

18. Lines 378,379. This statement means that PME are not more concentrated than for with respect to NO₃⁻ and NO₂⁻. Is there any idea as to the reason for this?

The reviewer is correct, but it's difficult to interpret this result since the gas-particle partitioning of HNO₃ under non-fog conditions is highly dependent upon the availability of ammonia.

19. Line 387. DOC concentration. It would be very useful for the readers to have a range of measured DOC values here.

We have added the range of measured DOC values.

20. Page 14, bottom. It may be interesting to recall that the IO₂ formation QY determined here is also not very distant from typical values found in surface waters.

This is a good point. We have added this comparison to the manuscript (on Page 15).

21. Page 15, bottom. Comparing steady-state concentrations in different studies is not very significant because they strongly depend on the irradiation conditions. It would be much better to compare the formation quantum yields.

The reviewer makes a good point. We have added a quantum yield comparison at the end of this section (on Page 16). The concentration comparison we had in the original manuscript (and which we've kept) is for the same winter-solstice sunlight conditions.

22. Page 16, top and middle (end of section 3.5). if it is not a consequence of unwanted transient scavenging by probes, this puzzling result might mean that the complicated approach followed here to measure 3C* was not very appropriate. In the context of surface waters, the use of 2,4,6-trimethylphenol as probe usually gives consistent results

between the $3C^*$ and $1O_2$ formation quantum yields. That could be discussed to place the used results and methodology into a clearer and more complete framework.

As we described earlier, our calculations indicate that our $^1O_2^*$ and $^3C^*$ probes did not significantly perturb the concentrations of these oxidants, so we do not think there is a problem with our method. It is possible that our PM results for $\Phi_{3C^*}/\Phi_{1O_2^*}$ are lower than the surface water results described by the reviewer because of differences in OM chemistry between the two types of samples; our result suggests that f_{Δ} is lower in atmospheric waters. But we also note that a recent study by Zhou et al. (2019) shows that the ratio $\Phi_{3C^*}/\Phi_{1O_2^*}$ for terrestrial NOM is approximately 0.5, similar to our result. The quantum yield for oxidizing triplets probably also depends on the probe used.

23. Lines 489,490. How is particle moisture estimated? Please specify.

Liquid water content for particles in California's Central Valley during winter were calculated based on particle composition and the component thermodynamics by Parworth et al. (2017). We used their values as an estimate for our samples, as described in Table S14 of the SI.

24. Line 524. In the case of $1O_2$ production, it is strange that saturation of absorbance was not observed even in the most concentrated samples. In the presence of a very high DOM amount, all or almost all incident radiation should be absorbed and a plateau [$1O_2$] trend should be observed as a consequence. Which was the absorbance in the most concentrated samples that were subject to irradiation?

Our highest absorbing samples had absorption coefficients of less than 0.6 cm^{-1} at 300 nm (e.g., Fig. 1) but we had a short pathlength (4 mm), so there was no significant screening of light in our experiments. Light screening factors (where a value of 1 indicates no screening) ranged from 0.84 to 0.99 (Table S1) and were accounted for in our calculations.

25. Page 18, 1st half. In the case of surface waters, you need $\text{DOC} \gg 20 \text{ mgC L}^{-1}$ to have significant scavenging of $3C^*$ by DOM. What is the situation here? Which were the DOC values of the most concentrated PME samples? It is important to discuss them for comparison.

The DOC values in $\mu\text{M-C}$ for all PME samples are given in Table S2 of the SI. Converted to mg-C L^{-1} , the values for the PME3D samples range from 4.3 to 86 mg-C L^{-1} . Thus, as the concentration. We have added a statement in the main text to indicate this.

26. Line 529. "(Wenk et al., 2011;2013) have shown" should read "Wenk et al. (2011; 2013) have shown".

Thank you, we have corrected this partially but somehow, we are unable to fix the formatting completely. It now reads "Wenk et al. (2011); (2013)". We are hoping this can be fixed during typesetting.

27. Lines 577 and 597-599. Role of $1O_2$ vs. $3C^*$ in PM water. There is a potential

inconsistency here, because $3C^*$ seem to play a minor role with the chosen model compounds but then one has to admit an important $3C^*$ scavenging by DOM. This seems to suggest that the choice of the five model compounds was not fully representative (they might tend to highlight $1O_2$ reactions). This issue should be discussed better.

This is an interesting point. We don't think that the duality of our results is because we picked compounds that are not representative, but rather that there are so many compounds (in number and/or quantity) that are reacting with triplets that its steady-state concentration is significantly suppressed in the PM condition (but its formation rate is unaffected). The result is that triplets do not appear to be very significant sinks for individual compounds, but they are significant in aggregate, i.e., when considered over all of the species that react with triplets. We have modified the text to describe this.

28. Line 615. "approximately" should read "approximate".

Thank you, we have corrected this sentence.

29. Line 622. 600 vs. 3000. According to Fig. 5 one has quite parallel increases of both $[1O_2]$ and $[3C^*]$ (the latter under the hypothesis of no plateau), while $3000/600 = 5$ which is quite a lot as difference. Are these numbers compatible with Figure 5 data? Please add a comment.

This is a good observation from the reviewer: while Fig. 5 considered only an extrapolation of the measured aqueous processes, in the text we also considered gas-phase mass transport and the expected organic sinks for oxidants in highly concentrated particles. To eliminate this confusion, we have modified Fig. 5 to show the expected oxidant concentrations in drops and particles considering both our aqueous measurements and the calculated impacts of organic sinks and mass transport from the gas phase. Under these conditions, the concentration of $^1O_2^*$ increases by a factor of 2400 from dilute drops to concentrated particles, while the concentration of oxidizing triplets increases by a factor of 30 (best fit) to 2000 (high estimate).

Anonymous Referee #2

Received and published: 2 January 2019

General comments This manuscript presents results of measurements of traditional and novel oxidants in PM extracts of ambient samples and importantly illustrates the potential for brown carbon to increase oxidant concentrations through the formation of triplet states. While many uncertainties exist, this study lays the groundwork for future studies into the role of brown carbon in generating photooxidants. The study presents a novel technique for measuring oxidants that appears to hold even under diluted conditions of aerosol extracts, and the results and conclusions drawn are supported by the available data. The abstract is concise enough, though it may benefit from further shortening and the title reflects the work as presented. The large volume of supplementary information will allow future work to build on this publication.

This work may help address the measurement/model discrepancies between the O/C ratio of ambient SOA and that predicted by chemical models. The manuscript is well presented with clear writing and legible figures. The work is also highly timely, and represents a step forward in our ability to understand the competing reactions taking place in aerosol and aerosol water (oxidant generation and loss). I have only two minor comments to improve the paper and one technical correction.

We thank this reviewer for their thoughtful review, encouraging comments, and specific suggestions for improvement of the manuscript. We had addressed each of the comments below.

Specific comments:

The abstract was a bit hard to get through, and could benefit from further shortening if the authors feel this is possible. For example, lines 34-38 may be omitted without loss of meaning.

We appreciate the reviewer's comment about the length of the abstract. To make it more concise, we have deleted lines 34-35. We left lines 36-38 as it is to provide an appropriate segue from discussing oxidant concentration measurements in dilute extracts to estimating them in ambient particles.

Lines 448-451: It was difficult to follow the relationship between $k'_{\text{SYR},3\text{C}^*}$ / $k'_{\text{MeJA},3\text{C}^*}$, and $k'_{\text{Probe},3\text{C}^*}$ ratio. Are these the same thing, but the latter is a general term? Please clarify.

Yes, the reviewer is correct – these refer to the same thing. The latter ($k'_{\text{Probe},3\text{C}^*}$ ratio) is a general term whereas $k'_{\text{SYR},3\text{C}^*}/k'_{\text{MeJA},3\text{C}^*}$ specifically mentions the probes. We have clarified this.

Technical corrections

Line 545: missing “is” between “it also”

We thank the reviewer for their attention to detail. We have made this correction.

Anonymous Referee #3

Received and published: 8 January 2019

This work mainly measured the concentrations of three important photooxidants formed from photoexcitation of brown carbon by collecting ambient particles during heavy residential wood-burning period in winter, extracting them in water, and illuminating the acidified aqueous extracts. The results in aqueous extracts were extrapolated to ambient particle water conditions and compared to the corresponding photooxidants in fog. The main conclusion of this work is that hydroxyl radical in particles had similar levels with fog and cloud drops while singlet oxygen and oxidizing triplet excited sites of organic matters are enhanced in particles. Their results indicate that singlet oxygen

and oxidizing triplet excited sites of organic matters formed from the photoexcitation of brown carbon can be important sinks for organic compounds in atmospheric particles. Although there are large uncertainties in the extrapolation to ambient particle water conditions, especially for oxidizing triplet excited sites of organic matters, this work provides the first measurement of singlet oxygen and oxidizing triplet excited sites of organic matters, which affect the lifetime of organic compounds in particle liquid water. The results are very helpful for the science community to improve our understanding of photooxidants and inspire more works for different seasons and locations, and implementing in current atmospheric models. I think this is an interesting and important work, and recommend for acceptance after comments below are addressed:

We thank this reviewer for their thoughtful review, encouraging comments, and specific suggestions for improvement of the manuscript. We had addressed each of the comments below.

1. Line 154, please explain “air-saturated”.

The term “air-saturated” refers to the fact that the particle extracts are saturated with O₂ by exposure to air. This is important because O₂ is a sink for triplets, and the lack of oxygen in solutions can artificially enhance the triplet steady-state concentration. During the course of the experiments, we stirred the solutions continuously and exposed the surface of the solution to air each time an aliquot was taken for HPLC analysis.

2. Line 379, the authors mentioned additional source can be photo-Fenton processes, I am wondering if Fe has been/can be measured in the samples. It would be interesting to compare to Fe data.

Unfortunately, we were not able to measure Fe in the solutions due to a lack of sample volumes. However, this is a very valid question that should be addressed in future studies of a similar nature.

3. Line 389-394, suggest adding some literature reviews on the destruction/sinks of OH in this section or in the introduction section.

We have added the references.

4. The authors made a couple comparisons between “standard” and “dilute” extracts throughout the manuscript. From the manuscript, the “standard” extraction was based on extracting particles into 1 mL water and the “dilute” was extracting in 2.5 mL water. It is an effect of dilution. It is not clear to me what is the purpose of comparing “standard” and “dilution” conditions. The authors have already studied extensively the effect of dilution using sample 3 in later experiments, so I don’t understand why repetitive comparison were made here or are there additional purposes of comparing “standard” and “dilute” extracts but were not well presented in the manuscript? The authors need to make it clearer.

We appreciate the reviewer’s comments on this. The comparisons between standard and dilute extracts arise mainly because we started out measuring the oxidant concentrations in the

dilute extracts. After a few samples, we realized that the “dilute” extracts closely resembled fog samples in terms of oxidant concentrations. We then switched to a higher concentration, i.e., extracting the particles in 1 mL water instead of 2.5 mL and we established this as the “standard” condition. The benefits of showing both results in the paper are to illuminate how even this small concentration factor changes oxidant concentrations and how dilute particle extracts essentially mimic fog droplet photochemistry.

5. Method section: sample extracts were mixed with photooxidant probes and then illuminated in light. The authors will need to address whether illumination will affect the probes or the products formed from probes and targeted photooxidants. For example, benzene traps OH radicals and form phenol. How does illumination experiments affect the product phenol. Do the authors concern about the photodegradation or photoenhancement of phenol, therefore, resulting in underestimation or overestimation of the OH concentration? Same concerns will also be needed to address for singlet oxygen and triplets cases.

This is a good question. Briefly, for measuring $\cdot\text{OH}$, we only illuminated solutions spiked with benzene for time periods where linear increase in phenol concentration was observed (Fig. S1 in the SI). Had there been any secondary chemistry, the concentration of phenol would no longer increase linearly. This is evidence that measuring $\cdot\text{OH}$ from phenol formation within our experimental time frame was not confounded by secondary reactions. Similarly, for $^1\text{O}_2^*$ and $^3\text{C}^*$, the loss of the probes follow first order kinetics (Figs. S2 and S8 in the SI).

6. Line 339, following the last comment, another concern is the effect of illumination on the light absorbance of brown carbon. For example, a recent study by Wong et al. 2017 EST (Changes in Light Absorptivity of Molecular Weight Separated Brown Carbon Due to Photolytic Aging) showed that light Absorptivity of brown carbon changes due to photolytic aging. Please discuss how change of absorptivity affects the conclusions in this work.

This is an interesting question. Part of the photolytic aging of brown carbon are likely the reactions of the dissolved organics with transient oxidants such as $\cdot\text{OH}$, $^1\text{O}_2^*$ and $^3\text{C}^*$. With respect to photolytic aging affecting the experimental outcomes, since we are measuring photooxidant formation in approximately the same time frame as the Wong et. al. study cited by the reviewer (i.e. about 2 hours), it is possible that some transformation of organics does occur. However, since the loss of probe compounds followed first-order kinetics in all cases and our probes do not undergo direct photolysis, we don't suspect the aging process to have affected photooxidant formation.

References:

- Bilski, P., Holt, R. N., and Chignell, C. F.: Properties of singlet molecular oxygen O₂ (1Δ_g) in binary solvent mixtures of different polarity and proticity, *Journal of Photochemistry and Photobiology A: Chemistry*, 109, 243-249, 1997.
- Canonica, S., Hellrung, B., and Wirz, J.: Oxidation of phenols by triplet aromatic ketones in aqueous solution, *J. Phys. Chem. A*, 104, 1226-1232, 2000.
- Parworth, C. L., Young, D. E., Kim, H., Zhang, X., Cappa, C. D., Collier, S., and Zhang, Q.: Wintertime water-soluble aerosol composition and particle water content in Fresno, California, *J. Geophys. Res. Atmos.*, 122, 3155-3170, 2017.
- USGS: U.S. Geological Survey. Water Properties - Dissolved Oxygen. Available at <https://water.usgs.gov/edu/dissolvedoxygen.html> [last accessed: January 23, 2018], 2018.
- Wilkinson, F., Helman, W. P., and Ross, A. B.: Rate constants for the decay and reactions of the lowest electronically excited singlet state of molecular oxygen in solution. An expanded and revised compilation, *J. Phys. Chem. Ref. Data*, 24, 663-677, 1995.
- Zhou, H., Yan, S., Lian, L., and Song, W.: Triplet-state Photochemistry of Dissolved Organic Matter: Triplet-state Energy Distribution and Surface Electric Charge Conditions, *Environ. Sci. Technol.*, 53, 2482–2490, 2019.

Photooxidants from Brown Carbon and Other Chromophores in Illuminated Particle Extracts

Richie Kaur¹, Jacqueline R. Labins¹, Scarlett S. Helbock¹, Wenqing Jiang², Keith J. Bein³, Qi Zhang², Cort Anastasio^{1,*}

¹Department of Land, Air and Water Resources, University of California-Davis, One Shields Avenue, Davis, CA 95616-8627, USA

²Department of Environmental Toxicology, University of California-Davis, One Shields Avenue, Davis, CA 95616-8627, USA

³Center for Health and the Environment, University of California-Davis, One Shields Avenue, Davis, CA 95616-8627, USA

Correspondence to: C. Anastasio (canastasio@ucdavis.edu)

Abstract

While photooxidants are important in atmospheric condensed phases, there are very few measurements in particulate matter (PM). Here we measure light absorption and the concentrations of three photooxidants – hydroxyl radical ($\cdot\text{OH}$), singlet molecular oxygen ($^1\text{O}_2^*$) and oxidizing triplet excited states of organic matter ($^3\text{C}^*$) – in illuminated aqueous extracts of wintertime particles from Davis, California. $^1\text{O}_2^*$ and $^3\text{C}^*$, which are formed from photoexcitation of brown carbon (BrC), have not been previously measured in PM. In the extracts, mass absorption coefficients for dissolved organic compounds (MAC_{DOC}) at 300 nm range between 13,000–30,000 $\text{cm}^2 \text{g}^{-1}$ and are approximately twice as high as previous values in Davis fogs. The average ($\pm 1\sigma$) $\cdot\text{OH}$ steady-state concentration in particle extracts is $4.4 (\pm 2.3) \times 10^{-16} \text{M}$, which is very similar to previous values in fog, cloud and rain: although our particle extracts are more concentrated, the resulting enhancement in the rate of $\cdot\text{OH}$ photoproduction is essentially cancelled out by a corresponding enhancement in concentrations of natural sinks for $\cdot\text{OH}$. In contrast, concentrations of the two oxidants formed primarily from brown carbon (i.e., $^1\text{O}_2^*$ and $^3\text{C}^*$) are both enhanced in the particle extracts compared to Davis fogs, a result of higher concentrations of dissolved organic carbon and faster rates of light absorption in the extracts. The average $^1\text{O}_2^*$ concentration in the PM extracts is $1.6 (\pm 0.5) \times 10^{-12} \text{M}$, seven times higher than past fog measurements, while the average concentration of oxidizing triplets is $1.0 (\pm 0.4) \times 10^{-13} \text{M}$, nearly double the average Davis fog value.

32 Additionally, the rates of $^1\text{O}_2^*$ and $^3\text{C}^*$ photoproduction are both well correlated with the rate of
33 sunlight absorption.

34 ~~While concentrations of $^1\text{O}_2^*$ and $^3\text{C}^*$ are higher in our PM extracts compared to fog, the~~
35 ~~extracts are approximately 1000 times more dilute than water containing ambient PM. Since we~~
36 cannot experimentally measure photooxidants under ambient [particle water](#) conditions, we
37 measured the effect of PM dilution on oxidant concentrations and then extrapolated to ambient
38 particle conditions. As the particle mass concentration in the extracts increases, measured
39 concentrations of $\cdot\text{OH}$ remain relatively unchanged, $^1\text{O}_2^*$ increases linearly, and $^3\text{C}^*$
40 concentrations increase less than linearly, likely due to quenching by dissolved organics. Based
41 on our measurements, and accounting for additional sources and sinks that should be important
42 under PM conditions, we estimate that [$\cdot\text{OH}$] in particles is [somewhat lower than in dilute](#)
43 [cloud/fog drops, while](#) [$^3\text{C}^*$] is [30 to 2000 times](#) higher in PM [than in drops](#), and [$^1\text{O}_2^*$] is
44 enhanced by a factor of roughly [2400 in PM compared to drops](#). Because of these enhancements
45 in $^1\text{O}_2^*$ and $^3\text{C}^*$ concentrations, the lifetimes of some highly soluble organics appear to be much
46 shorter in particle liquid water than under foggy/cloudy conditions. Based on extrapolating [our](#)
47 [measured](#) rates of formation [in PM extracts](#), BrC-derived singlet molecular oxygen and triplet
48 excited states are [overall](#) the dominant sinks for organic compounds in particle liquid water, with
49 an aggregate rate of reaction for each oxidant that is approximately 200 – 300 times higher than
50 the aggregate rate of reactions for organics with $\cdot\text{OH}$. For individual, highly soluble reactive
51 organic compounds it appears that $^1\text{O}_2^*$ is [often](#) the major sink in particle water, [which is a new](#)
52 [finding](#). Triplet excited states are likely also important in the fate of individual particulate
53 organics, but assessing this requires additional measurements of triplet interactions with
54 dissolved organic carbon in natural samples.

55

56 **1 Introduction**

57 Photochemically generated oxidants largely drive atmospheric chemistry, both in the gas
58 phase (Thompson, 1992; Finlayson-Pitts and Pitts Jr, 1999; Seinfeld and Pandis, 2012) and in
59 aqueous drops, where they largely govern the reactions and lifetimes of organic compounds (Lim
60 et al., 2005; Lim et al., 2010; Ervens et al., 2011; He et al., 2013; Herrmann et al., 2015; Blando
61 and Turpin, 2000). Similarly, photooxidants can be important for transformations in water-
62 containing particulate matter (PM): they make new PM mass by functionalizing gaseous volatile
63 organics to oxygenated lower-volatility products, and decrease PM mass by fragmenting large

64 organics into smaller, more volatile species (Jimenez et al., 2009). Oxidants in condensed phases
65 can come from the gas phase (e.g., the mass transport of hydroxyl radical, $\cdot\text{OH}$) or can be formed
66 photochemically within the particle or drop (Herrmann et al., 2010b). Our focus in this paper is
67 on the latter pathway.

68 Of the photooxidants formed in airborne particles, hydroxyl radical ($\cdot\text{OH}$) is the most
69 widely studied. While its concentrations have been measured in cloud/fog drops, rain and dew
70 (Arakaki and Faust, 1998; Arakaki et al., 1999; Anastasio and McGregor, 2001; Kaur and
71 Anastasio, 2017), there are only four known measurements of $\cdot\text{OH}$ photoproduction rates,
72 lifetimes, and steady-state concentrations in ambient particles, all from coastal or marine
73 locations (Anastasio and Jordan, 2004; Arakaki et al., 2006; Anastasio and Newberg, 2007;
74 Arakaki et al., 2013). Based on these and other measurements (e.g., Tong et al. (2017)) and
75 complementary modeling work (Herrmann et al., 2010b; Herrmann et al., 2015), the major
76 sources of $\cdot\text{OH}$ include photolysis of nitrate, nitrite, and hydrogen peroxide (HOOH) as well as
77 reactions of Fe(II) with HOOH or organic peroxides. The major sinks of $\cdot\text{OH}$ are organic
78 molecules since these reactions typically have nearly diffusion-controlled rate constants (Arakaki
79 et al., 2013; Herrmann et al., 2010a; Herrmann et al., 2015).

80 Photoexcitation of organic chromophores, i.e., light-absorbing brown carbon (BrC), can
81 also form oxidants in particles and drops. For example, sunlight absorption by organic
82 chromophores can promote the molecules from their ground states to reactive triplet excited
83 states (McNeill and Canonica, 2016; Kaur and Anastasio, 2018b). Triplets can both directly
84 oxidize organics via electron transfer reactions and form other photooxidants, including singlet
85 molecular oxygen ($^1\text{O}_2^*$) (Zepp et al., 1985) and hydrogen peroxide (Anastasio et al., 1997). In
86 this work we examine oxidizing triplets, which we refer to as $^3\text{C}^*$ or simply “triplets” for
87 simplicity. Such species are important in surface waters, where they rapidly oxidize several
88 classes of compounds including phenols, anilines, phenylurea herbicides, and sulfonamide
89 antibiotics (Cannonica et al., 1995; Cannonica and Hoigné, 1995; Boreen et al., 2005; Cannonica et
90 al., 2006; Bahnmüller et al., 2014).

91 There has been growing interest in the role and reactivity of triplets formed from
92 particulate brown carbon, especially their role in forming aqueous secondary organic aerosol
93 (SOA(aq)) (Smith et al., 2014; 2015; Yu et al., 2014; Yu et al., 2016; Laskin et al., 2015). There
94 is evidence that triplet-forming, light-absorbing species, e.g., imidazoles and pyrazines, are
95 formed in drops and particles (De Haan et al., 2009; 2010; Hawkins et al., 2018) and a few
96 laboratory studies have examined how illuminated imidazole particles can oxidize isoprene or

97 other alkenes to increase PM mass (Aregahegn et al., 2013; Rossignol et al., 2014). But the
98 formation of SOA(aq) from such reactions appears not to be significant under environmentally
99 relevant conditions where concentrations of triplet precursors are much lower (Tsui et al., 2017).
100 While we recently made the first measurements of triplet concentrations in fog waters (Kaur and
101 Anastasio, 2018b), there are no measurements of $^3\text{C}^*$ in particles, making it difficult to assess
102 their significance. This is doubly difficult because triplets are not a single oxidant, but rather a
103 suite of species with a wide range of reactivities (McNeill and Canonica, 2016).

104 Another important photooxidant in atmospheric and surface waters is singlet molecular
105 oxygen ($^1\text{O}_2^*$), which is formed by energy transfer from a triplet excited state to dissolved
106 oxygen, and lost via deactivation by water (Zepp et al., 1977; Haag and Hoigné, 1986; Haag and
107 Gassman, 1984; Faust and Allen, 1992). Similar to triplets, singlet oxygen has been studied
108 widely in surface waters (Zepp et al., 1977; Haag and Gassman, 1984; Haag and Hoigné, 1986;
109 Tratnyek and Hoigné, 1994) and reacts rapidly with electron-rich organics such as phenols,
110 polycyclic aromatic hydrocarbons, amino acids, and reduced sulfur species (Wilkinson et al.,
111 1995). However, there are only four measurements of $^1\text{O}_2^*$ concentrations in atmospheric waters
112 (Anastasio and McGregor, 2001; Kaur and Anastasio, 2017; Albinet et al., 2010; Faust and
113 Allen, 1992) and none in aqueous particles.

114 To address this gap, we measured $\cdot\text{OH}$, $^1\text{O}_2^*$, and $^3\text{C}^*$ in illuminated aqueous extracts of
115 fine particles collected from the Central Valley of California during winter, a period of heavy
116 residential wood burning. The goals of this study are to: 1) quantify $\cdot\text{OH}$, $^1\text{O}_2^*$, and $^3\text{C}^*$ kinetics
117 and concentrations in particle extracts, 2) compare light absorption and photooxidant kinetics
118 with previous measurements made in fog, 3) measure the dependence of oxidant concentrations
119 on particle dilution to predict photooxidant concentrations in ambient particle liquid water, and
120 4) assess the importance of particle photooxidants in processing organic compounds in the
121 atmosphere.

122 **2 Experimental**

123 **2.1 Chemicals**

124 All chemicals were used as received. Furfuryl alcohol (98%), syringol (99%), methyl
125 jasmonate (95%), benzene ($\geq 99.9\%$), 2-methyl-3-buten-2-ol (98%), deuterium oxide (99.9%
126 atom D), and 2-nitrobenzaldehyde (98%) were from Sigma-Aldrich and sulfuric acid (trace metal
127 grade) was from Fisher. All chemical solutions and particulate matter extracts were prepared

128 using purified water (Milli-Q water) from a Milli-Q Advantage A10 system (Millipore; ≥ 18.2
129 $M\Omega\text{ cm}$) with an upstream Barnstead activated carbon cartridge; total organic carbon
130 concentrations were below 10 ppb C.

131 **2.2 Particle collection and extraction**

132 Wintertime particles were collected in a residential neighborhood in Davis, California,
133 (38.5539° N , 121.7381° W , 16 m above sea level) during December 2015 and January 2016, a
134 period with significant wood burning. $PM_{2.5}$ was collected on 8×10 inch Teflon-coated quartz
135 filters (Pall Corporation, EmFabTM filters, type TX40HI20-WW) using a high-volume sampler
136 with a PM_{10} inlet (Graseby Anderson) followed by two offset, slotted impactor plates (Tisch
137 Environmental, Inc., 230 series) to remove particles greater than $2.5\ \mu\text{m}$. Due to technical
138 difficulties, the air flow rate was variable and typically ranged between 1130 and $1560\ \text{L min}^{-1}$,
139 corresponding to particle cut points of 2.5 to $1.6\ \mu\text{m}$. Particles were generally collected over two
140 to three consecutive nights between 5:30 pm and 7:30 am, but one sample (#3) was collected
141 continuously (day and night) for 72 hours (Table S1).

142 Immediately upon collection, samples were wrapped in aluminum foil (previously baked at
143 500°C for 8 h), sealed in ZiplockTM bags and stored at -20°C . On the day of extraction, several
144 $2\ \text{cm} \times 2\ \text{cm}$ pieces were cut (using stainless-steel tools) from the same filter, each was put into a
145 separate pre-cleaned 10 mL amber glass vial, Milli-Q water was added (see below), and the vial
146 was sealed and shaken for 3 hours in the dark. The extracts were filtered ($0.22\ \mu\text{m}$ PTFE ; Pall),
147 combined, and labeled as Particulate Matter Extract (PME). The standard condition was to use
148 1.0 mL of Milli-Q to extract each filter square, but in our initial work we used 2.5 mL of Milli-Q
149 per filter square; these latter “dilute extracts” are indicated by an asterisk and footnotes in the
150 figures and tables. We switched from dilute to standard conditions after PME1-3, but we include
151 both results in this work to compare the two types of extracts.

152 In addition, to study the effect of PM mass concentration, separate portions of filter #3
153 were extracted using five different extraction volumes between 0.5 and 10 mL (discussed later).
154 Those extracts are labeled as PME3Dx, where “x” is the extraction volume (e.g., PME3D1.3 for
155 filter squares extracted in 1.3 mL of Milli-Q). Upon extraction, each PME was stored in the
156 refrigerator (5°C) until the day of the illumination experiments. All illumination experiments and
157 analyses on a PME sample were completed within a week of its extraction.

158 2.3 Sample illumination and chemical analysis

159 For all illumination experiments except [•]OH measurements using benzene (discussed in
160 Sect. 2.5.1), on the day of the experiment a 1.0 mL aliquot of an air-saturated particle extract was
161 first acidified to pH 4.2 ± 0.2 using 10 mM sulfuric acid (with sample dilution $\leq 10\%$) to mimic
162 the particle water acidity in wintertime PM in California's Central Valley (Parworth et al., 2017).
163 The pH of the sample was measured using a pH microelectrode (MI-414 series, protected tip, 16
164 gauge needle, 6 cm length; Microelectrodes, Inc.). The acidified extract was then spiked with a
165 single photooxidant probe and put into a silicone-plugged, fully-filled GE021 quartz tube (4 mm
166 inner diameter, 6 cm length, 1.0 mL volume) and illuminated with a 1000 W xenon arc lamp
167 filtered with a water filter (to reduce sample heating), an AM 1.0 air mass filter (AM1D-3L,
168 Sciencetech) and 295 nm long-pass filter (20CGA-295, Thorlabs) to mimic tropospheric solar
169 light (Kaur and Anastasio, 2017). Because of the small tube size, samples were not stirred, but
170 the entire sample was illuminated in a chamber held at 20 °C. 100 μ L aliquots of illuminated
171 (and parallel dark) samples were periodically removed and analyzed for the concentration of
172 photooxidant probe (see below) using HPLC (Shimadzu LC-10AT pump, ThermoScientific
173 BetaBasic-18 C₁₈ column (250 \times 33 mm, 5 μ M bead), and Shimadzu-10AT UV-Vis detector).
174 The photon flux in the sample was measured on each experiment day using a 10 μ M solution of
175 2-nitrobenzaldehyde (2NB) in the same type of quartz tube as the sample (Galbavy et al., 2010).

176 Major anions and cations in the extracts (Table S2) were quantified using two Metrohm
177 ion chromatographs (881 Compact IC Pro) equipped with conductivity detectors (Ge et al., 2014;
178 Kaur and Anastasio, 2017). Dissolved organic carbon (DOC) in the filtered extracts was
179 measured using a Shimadzu TOC-VCPH analyzer (Yu et al., 2014).

180 2.4 Light Absorbance

181 Light absorbance was measured immediately after extraction using a Shimadzu UV-
182 2501PC spectrophotometer with 1-cm quartz cuvettes and a baseline of Milli-Q water.
183 Absorbance (A_λ) was converted to light absorption coefficients using

$$184 \quad \alpha_\lambda = \frac{A_\lambda}{l} \quad (1)$$

185 where l is the pathlength in cm. The rate of sunlight absorption (R_{abs} , mol-photons $\text{L}^{-1} \text{s}^{-1}$) in
186 each extract was calculated as:

$$187 \quad R_{\text{abs}} = 2.303 \times \frac{10^3}{N_A} \times \sum_{300\text{nm}}^{450\text{nm}} (\alpha_\lambda \times I_\lambda \times \Delta\lambda) \quad (2)$$

188 where 2.303 is for base conversion, 10^3 is for units conversion ($\text{cm}^3 \text{L}^{-1}$), N_A is Avogadro's
189 number, I_λ is the Davis winter-solstice actinic flux ($\text{photons cm}^{-2} \text{s}^{-1} \text{nm}^{-1}$) from the
190 Tropospheric Ultraviolet and Visible (TUV) Radiation Model version 4.1 (Madronich et al.,
191 2002), and $\Delta\lambda$ is the interval between adjacent wavelengths in the TUV output (nm).

192 Wavelength-dependent mass absorption coefficients for DOC (MAC_{DOC} ; $\text{cm}^2 \text{g}^{-1}$)
193 were estimated by subtracting the contributions of nitrite and nitrate from the measured
194 absorbance at each wavelength (which were small, $\leq 7\%$ of the total absorbance) and then
195 dividing the remainder by the DOC concentration:

$$196 \quad \text{MAC}_{\text{DOC},\lambda} = \frac{\alpha_{\text{DOC},\lambda} \times \ln(10) \times 10^3 \times 10^3}{[\text{DOC}]} \quad (3)$$

197 where $\alpha_{\text{DOC},\lambda}$ (cm^{-1}) is the sample absorbance coefficient at wavelength λ due to DOC (Kaur and
198 Anastasio (2017)); $\ln(10)$ is a base conversion factor; the two 10^3 factors are for unit conversion
199 ($\text{cm}^3 \text{L}^{-1}$ and mg g^{-1}), and the DOC concentration is in mg-C L^{-1} . Since the average organic
200 matter-to-organic carbon (OM/OC) ratio in California Central Valley particles is approximately
201 1.7 (Young et al., 2016), the absorption coefficients normalized by OM mass will be
202 approximately 60% of the MAC_{DOC} values.

203 **2.5 Measurement of photooxidants**

204 **2.5.1 Hydroxyl radical ($\cdot\text{OH}$)**

205 We quantified $\cdot\text{OH}$ kinetics using a benzene probe (Zhou and Mopper, 1990; Anastasio
206 and McGregor, 2001; Kaur and Anastasio, 2017). Briefly, four aliquots of each extract were
207 spiked with varying concentrations of benzene to trap $\cdot\text{OH}$ and form phenol (yield: 73%), which
208 is quantified (Fig. S1). Each benzene stock was made a day before the illumination experiment.
209 Similar to the other photooxidant experiments, all aliquots were air-saturated, acidified to an
210 initial pH of 4.2 (± 0.2), capped, and then constantly stirred during illumination in airtight 5.0
211 mL, 1-cm pathlength, rectangular quartz cuvettes with no initial headspace. For all $\cdot\text{OH}$
212 measurements where benzene is used as a probe, we used this larger sample volume (5 mL
213 instead of 1 mL) to minimize the headspace in the cuvette and prevent benzene loss due to
214 volatilization. Throughout the illumination period, 100 μL aliquots were collected through the
215 cap septum and analyzed for phenol using HPLC-UV (eluent of 30% acetonitrile: 70% Milli-Q,
216 flow rate of 0.6 mL/min, detection wavelength of 210 nm and column temperature of 35°C). As
217 described in Kaur and Anastasio (2017), we use these results to determine three experimental

218 quantities for $\cdot\text{OH}$: the rate of photoproduction ($P_{\text{OH,EXP}}$), the rate constant for $\cdot\text{OH}$ loss due to
219 natural sinks (k'_{OH}), and the steady-state concentration ($[\cdot\text{OH}]_{\text{EXP}}$). Measured rates of $\cdot\text{OH}$
220 formation and steady-state concentrations were normalized to values expected under midday,
221 Davis winter-solstice sunlight and were corrected for the small amount of internal light screening
222 due to light absorption by DOM:

$$[\cdot\text{OH}] = \left(\frac{[\cdot\text{OH}]_{\text{EXP}}}{S_{\lambda} \times j_{2\text{NB,EXP}}} \right) \times j_{2\text{NB,WIN}} \quad (4)$$

223 In this equation, S_{λ} is the internal light screening factor (Table S1), $j_{2\text{NB,WIN}}$ is the rate constant
224 for loss of 2-nitrobenzaldehyde at midday near the winter solstice in Davis (solar zenith angle =
225 62° , $j_{2\text{NB,WIN}} = 0.0070 \text{ s}^{-1}$; Anastasio and McGregor, (2001)), and $j_{2\text{NB,EXP}}$ is the measured rate
226 constant for loss of 2NB on the day of the experiment. [OH results are in Tables S3–S6.](#)

227 We also measured $\cdot\text{OH}$ steady-state concentrations in squares of particle filter #3 using
228 five different dilutions with water (discussed later). Because these sample volumes were too
229 small to use the benzene technique, we [determined](#) the steady-state concentration of $\cdot\text{OH}$ [by](#)
230 [measuring the loss of 2-methyl-3-buten-2-ol \(MBO\)](#) (Sect. S1). We then measured P_{OH} in a [1 cm](#)
231 [cuvette](#) using a high benzene concentration (1.5 mM) and determined the rate constant for $\cdot\text{OH}$
232 loss due to natural sinks by dividing the rate of photoproduction by the steady-state
233 concentration, $k'_{\text{OH}} = P_{\text{OH}} / [\cdot\text{OH}]$ (Sect. S1.3). ~~[OH results are in Tables S3–S6.](#)~~ [In contrast to the](#)
234 [benzene technique, there was some quenching of \$\cdot\text{OH}\$ by the probe MBO in our PME3 samples;](#)
235 [this quenching was most significant in the most dilute extract, PME3D10. We corrected](#)
236 [measured \$\cdot\text{OH}\$ concentrations for quenching by MBO in the PME3 samples \(Sect. S1\) and the](#)
237 [final, corrected values are given in the Tables mentioned above.](#)

238 **2.5.2 Singlet molecular oxygen ($^1\text{O}_2^*$)**

239 Singlet oxygen was quantified by measuring the loss of a furfuryl alcohol (FFA) probe
240 and using heavy water (D_2O) as a diagnostic tool (Kaur and Anastasio, 2017; Anastasio and
241 McGregor, 2001). Briefly, each extract was divided into two aliquots, acidified to pH 4.2 (± 0.2),
242 and diluted 50:50 using H_2O or D_2O . Both aliquots were spiked to $10 \mu\text{M}$ FFA and illuminated
243 in 1 mL quartz tubes. [\(At this concentration, FFA should decrease the steady-state concentration](#)
244 [of \$^1\text{O}_2^*\$ in air-saturated solutions by less than 1%.\)](#) FFA loss was detected using HPLC-UV
245 (eluent of 10% acetonitrile: 90% Milli-Q water, flow rate of 0.6 mL/min, detection wavelength
246 of 210 nm and column temperature of 35°C). The loss of FFA followed pseudo-first-order
247 kinetics and the slope of the plot of $\ln([\text{FFA}]_t / [\text{FFA}]_0)$ versus time is the negative of the pseudo-

248 first-order rate constant for loss of FFA (illustrated in Fig. S2). Loss of FFA in the D₂O-diluted
 249 aliquot is faster than in H₂O because H₂O is the dominant sink for ¹O₂*, which reacts less
 250 quickly with D₂O (Bilski et al., 1997). The differences in the pseudo-first-order rate constants for
 251 loss of FFA between the two aliquots of sample were used to calculate the steady-state
 252 concentration of ¹O₂* and the rate of singlet oxygen photoproduction (Anastasio and McGregor,
 253 2001). These were normalized to values expected in Davis winter-solstice sunlight (i.e., [¹O₂*]
 254 and P_{1O2*}) and corrected for internal light screening using an equation analogous to Eq. (4). ¹O₂*
 255 measurements are in Table S7.
 256

257 **2.5.3 Oxidizing triplet excited states of organic matter (³C*)**

258 Triplets were measured using the dual-probe technique we developed recently for fog
 259 waters (Kaur and Anastasio, 2018b): two 1.0 mL, pH 4.2 aliquots of each extract were spiked to
 260 10 μM of either syringol (SYR) or methyl jasmonate (MeJA) and the loss of each probe was
 261 measured during illumination in plugged quartz tubes (Sect. 2.3). The measured pseudo-first-
 262 order rate constant for probe loss (*k*'_{Probe,EXP}) was determined as the negative of the slope of the
 263 plot of ln([Probe]/[Probe]₀) versus illumination time. Values of *k*'_{Probe,EXP} were normalized to
 264 Davis winter-solstice sunlight and corrected for internal light screening using an analog of Eq.
 265 (4); the resulting rate constants are termed *k*'_{Probe} (s⁻¹) (Tables S8, S9 of the SI). This pseudo-
 266 first-order rate constant for loss of probe represents the sum of all loss pathways:
 267

$$268 \quad k'_{\text{Probe}} = k_{\text{Probe+OH}} [\cdot\text{OH}] + k_{\text{Probe+1O2*}} [^1\text{O}_2^*] + \Sigma(k_{\text{Probe+3C}_i^*}) [^3\text{C}_i^*] + j_{\text{Probe}} + \Sigma(k_{\text{Probe+Other}} [\text{Other}]) \quad (5)$$

269 where the first two terms are the contributions of [•]OH and ¹O₂* to probe loss; Σ(*k*_{Probe+3C*}[³C*])
 270 represents the sum of all triplet contributions to probe loss; *j*_{Probe} is the first-order rate constant
 271 for direct photodegradation of the probe, which is negligible for our illumination times (< 4.3 ×
 272 10⁻⁶ s⁻¹ and 4.8 × 10⁻⁷ s⁻¹ for SYR and MeJA, respectively, under Davis winter conditions); and
 273 Σ(*k*_{Probe+Other}[Other]) is the sum of contributions from all other oxidants. As described in Sect.
 274 S3, we estimate that these other oxidants (hydroperoxyl radical / superoxide radical anion, ozone,
 275 carbonate radical, hydrogen ion / aquated electron) contribute 12 % or less of the average
 276 measured syringol loss (Sect. S3) and so are ignored. We can then simplify and rearrange Eq. (5)
 277 to determine the triplet contribution to probe loss:
 278

$$279 \quad k'_{\text{Probe,3C*}} = \Sigma(k_{\text{Probe+3C}_i^*}) [^3\text{C}_i^*] = k'_{\text{Probe}} - (k_{\text{Probe+OH}} [\cdot\text{OH}] + k_{\text{Probe+1O2*}} [^1\text{O}_2^*]) \quad (6)$$

280 [In other probe techniques, the equivalent of Eq. 6 is rearranged so that \$\sum\[{}^3C_i^*\]\$ can be](#)
 281 [determined based on the measured value of \$k'_{\text{Probe},3C^*}\$ and the literature value of the second-order](#)
 282 [rate constant \$k_{\text{Probe}+3C_i}\$. However, because triplets represent a suite of unidentified compounds,](#)
 283 [there is no one value of \$k_{\text{Probe}+3C_i}\$. To estimate this second-order rate constant in each sample, we](#)
 284 [used a combination of rate constants from](#) four model triplets – 2-acetonaphthone (${}^3\text{2AN}^*$), 3'-
 285 methoxyacetophenone (${}^3\text{3MAP}^*$), 3,4-dimethoxybenzaldehyde (${}^3\text{DMB}^*$), and benzophenone
 286 (${}^3\text{BP}^*$) – that roughly span the range of triplet reactivities in natural samples. [We first identified](#)
 287 the “best match triplets”, i.e., the one or two model triplets that [match the](#) average oxidizing
 288 triplet reactivity in a given extract. To do this, we determined the model triplets [whose mole-](#)
 289 [fraction-weighted ratio of second-order rate constants \(i.e., \$k_{\text{SYR}+3C^*} / k_{\text{MeJA}+3C^*}\$ \) matches](#) the ratio
 290 of [the](#) measured [first-order](#) probe loss rate constants due to triplets ($k'_{\text{SYR},3C^*} / k'_{\text{MeJA},3C^*}$) in each
 291 extract [\(for more details, see Kaur and Anastasio \(2018b\)\)](#). [Ratios of the](#) second-order rate
 292 constants ($k_{\text{SYR}+3C^*} / k_{\text{MeJA}+3C^*}$) of the model triplets range from 1.7 for the most reactive species
 293 (${}^3\text{BP}^*$) to 100 for the least reactive, ${}^3\text{2AN}^*$ (Table S10). For each extract, we calculated two
 294 mole-fraction-weighted second-order rate constants for triplets [\(one for each probe\)](#) and used
 295 them to estimate the triplet steady-state concentration:

$$296 \quad \Sigma[{}^3C_i^*]_{\text{Probe}} = \frac{k'_{\text{Probe},3C^*}}{\chi_{3C1^*} \times k_{\text{Probe}+3C1^*} + \chi_{3C2^*} \times k_{\text{Probe}+3C2^*}} \quad (7)$$

297
 298 where χ_{3C1^*} and χ_{3C2^*} are the mole fractions of the two best match triplets (${}^3C_1^*$ and ${}^3C_2^*$), and
 299 $k_{\text{Probe}+3C1^*}$ and $k_{\text{Probe}+3C2^*}$ are the second-order reaction rate constants of the best model triplet
 300 matches. Eq. (7) gives us two estimates of the triplet steady-state concentration, one from each
 301 probe, i.e., $\Sigma[{}^3C_i^*]_{\text{SYR}}$ and $\Sigma[{}^3C_i^*]_{\text{MeJA}}$. We averaged the two to obtain the best value for the
 302 triplet steady-state concentration in each extract, $\Sigma[{}^3C_i^*]$.

303
 304 We next estimated the rate of triplet photoformation (P_{3C^*}):

$$305 \quad P_{3C^*} = \Sigma[{}^3C_i^*] \times (k_{3C^*+O_2}[O_2] + (k_{\text{rxn}} + k_Q)[\text{DOC}]) \quad (8)$$

306 where $k_{3C^*+O_2}$ is the average bimolecular rate constant for quenching of the model triplets by O_2
 307 ($= 2.8 \times 10^9 \text{ M}^{-1} \text{ s}^{-1}$; Table S11 and Canonica et al. (2000)), $[O_2]$ is the dissolved oxygen
 308 concentration of 284 μM at 20 °C (USGS, 2018), $k_{\text{rxn}} + k_Q$ is the overall reaction and quenching
 309 rate constant for triplets by DOC ($9.3 \times 10^7 \text{ L mol}^{-1} \text{ C}^{-1} \text{ s}^{-1}$; see below) and $[\text{DOC}]$ values are in
 310 Table S2. [At the concentrations we used \(10 \$\mu\text{M}\$ \), SYR and MeJA are negligible sinks for](#)
 311 [triplets](#). Measurements for triplets are in Tables S12 and S13.

312

313 For all three photooxidants, the quantum yield of formation was calculated as

$$314 \quad \Phi_{\text{Ox}} = \frac{P_{\text{Ox}}}{R_{\text{abs}}} \quad (9)$$

315 where P_{Ox} is the Davis winter-solstice-normalized rate of oxidant photoproduction and R_{abs} is the
316 rate of sunlight absorption by the extract.

317 | **2.5.4 PM mass concentration factor (CF)**

318 Due to the volume required for our probe techniques, we extract particles into Milli-Q
319 water, resulting in extracts that are approximately 1000 times more dilute than ambient particles.
320 To examine the impact of dilution on photooxidant concentrations, we extracted sample #3 in
321 five different volumes of Milli-Q water (0.5 to 10 mL) and measured $\cdot\text{OH}$, $^1\text{O}_2^*$ and $^3\text{C}^*$ steady-
322 state concentrations in the five extracts. We define the PM mass concentration factor (CF) as the
323 ratio of (PM mass) / (water mass) in a given extract relative to the most concentrated extract that
324 we can make:

$$325 \quad \text{CF} = \frac{V_{\text{MIN}}}{V_{\text{EXT}} + V_{\text{P}}} \quad (10)$$

326

327 where V_{MIN} is the minimum experimentally feasible volume of Milli-Q needed for extraction of
328 one filter square (0.5 mL), V_{EXT} is the volume of Milli-Q used to extract a given filter square (0.5
329 to 10 mL), and V_{P} is the volume of probe stock solution added (typically 20 μL). Values of CF
330 for the PME3D extracts ranged from 0.05 (least concentrated) to 0.96 (most concentrated) and
331 are listed in Table S14.

332

333 **2.5.5 Uncertainties**

334 In figures, error bars represent ± 1 standard error (SE) calculated by propagating the
335 uncertainties in each term used to calculate the plotted value.

336 **3 Results and discussion**

337 **3.1 General extract characteristics**

338 Similar to Davis fogs collected in 1997-98 (Anastasio and McGregor, 2001) and 2011
339 (Kaur and Anastasio, 2017), the most abundant ions in the particle extracts are ammonium
340 (NH_4^+ , 280–2600 μM) and nitrate (NO_3^- , 380–3300 μM) (Table S2). This is expected since

341 ammonium nitrate is the most significant inorganic component of wintertime particles in the
342 Central Valley (Herner et al., 2006; Heald et al., 2012; Young et al., 2016). The average values
343 of NO_3^- and NH_4^+ are not statistically different ($p > 0.5$) between the current particle extracts
344 (PME) and previous fogs, although the ranges are much wider in the particle extracts (Table S2).
345 Similar to nitrate, nitrite is another important source of hydroxyl radical in the aqueous phase
346 (Anastasio and McGregor, 2001), with an average concentration of $6.9 (\pm 2.9) \mu\text{M}$ in the particle
347 extracts, again statistically similar to the 2011 fog average. On the other hand, the average
348 concentration of potassium – commonly used as a tracer for biomass-burning (Silva et al., 1999;
349 Parworth et al., 2017) – is nearly 40 times higher in the particles than in the 2011 Davis fog
350 samples ($p = 0.019$), suggesting PME enrichment by residential wintertime wood-burning. This
351 is reflected in the dilute PM extracts as well: even though most characteristics in the dilute
352 extracts are similar to fog, the average K^+ ($38 \pm 7 \mu\text{M}$) in the dilute PMEs is 10 times higher than
353 the fog value. Dissolved organic carbon (DOC) in the standard extracts (mean: $3400 (\pm 760) \mu\text{M}$ -
354 C) is, on average, three times higher than both the dilute extracts and fog.

355 We employed two field blanks in this study, one each for dilute and standard extraction
356 conditions. Ions and DOC in both field blanks are lower than 10% of the corresponding PME
357 sample averages, with a few exceptions (Table S2).

358 **3.2 Light absorption in particle extracts**

359 As shown in Fig. 1a and Table S1, the pathlength-normalized absorbance (α , cm^{-1})
360 declines exponentially with wavelength, with values at 300 nm (α_{300}) between 0.27 and 0.58 cm^{-1}
361 ¹ for the standard extracts PME3–6. The average α_{300} value is nearly five times higher in standard
362 extracts than values in Davis fog samples (Table S1, Fig. S3, data available in Kaur and
363 Anastasio (2018a)), while the “dilute extracts” (PME1*, PME2*, and PME3D2.5*) have
364 | absorbances very similar to fog samples. [Values of the Absorption Angstrom Exponent \(AAE\)](#)
365 | for all PM extracts range between 6.2 and 7.9 (Table S1), similar to those reported previously for
366 water soluble particulate BrC from biomass burning (Hecobian et al., 2010; Kirchstetter and
367 Thatcher, 2012). For both the fog and PM extracts the calculated rate of sunlight absorption
368 between 300 and 450 nm (R_{abs}) is well-correlated with dissolved organic carbon (DOC) ($R^2 =$
369 | [0.89 and 0.67, respectively](#); Fig. S4), suggesting that BrC is mainly responsible for light
370 absorption. The R_{abs} values for the standard extracts are high, with an average value of $9.1 (\pm 4.1)$
371 $\times 10^{-6} \text{ mol-photon L}^{-1} \text{ s}^{-1}$, five times higher than the dilute extracts and past Davis fogs (Table
372 S1). Similar to fog (Kaur and Anastasio, 2018b), the average rate of sunlight absorbance in the

373 standard particle extracts is 17 times higher than the total formation rates of the three
374 photooxidants (discussed later), indicating that most of the (photo) energy absorbed is either
375 dissipated via non-reactive pathways or leads to formation of other products.

376 We next calculated mass absorption coefficients for the organics (MAC_{DOC}) by
377 subtracting the absorbance contributions by nitrite and nitrate from α and dividing by the DOC
378 concentration (Eq. (3)). Across both standard and dilute extracts, the average ($\pm \sigma$) MAC_{DOC}
379 value at 300 nm is $2.2 (\pm 0.7) \times 10^4 \text{ cm}^2 \text{ g-C}^{-1}$, 1.7 times higher than the fog sample average
380 (Figs. 1b and S3; data available at Kaur and Anastasio (2018a)). Both α and MAC_{DOC} in the
381 PME are generally higher than in fog, especially at shorter sunlight wavelengths (Fig. S5),
382 [although AAE values are similar in the extracts and fog \(Table S1\)](#). Since MAC_{DOC} accounts for
383 dilution (Eq. (3)), the higher values in PM extracts indicates that water-soluble organics in
384 particles are either more strongly light-absorbing (on a per-carbon basis), and/or less diluted with
385 non-absorbing DOC, compared to those in fog. Our PME mass-absorption coefficients at 300 nm
386 are very similar to values reported for the humic-like fraction of biomass-burning aerosols in the
387 Amazon basin (Hoffer et al., 2006) and for the water-soluble organic fractions of rural aerosols
388 (Varga et al., 2001; Sun et al., 2007) .

389 Compared to the samples, light absorption in the field blanks is negligible, representing
390 0.7% and 3% of the average α_{300} in the standard and dilute extracts, respectively (Table S1).

391 **3.3 Hydroxyl radical**

392 The average Davis winter-solstice-normalized rate of $\cdot\text{OH}$ photoproduction (P_{OH}) in the
393 standard extracts is $1.2 (\pm 0.5) \times 10^{-9} \text{ M s}^{-1}$ (i.e., $4.2 \pm 1.7 \mu\text{M h}^{-1}$), 3.3 times faster than the
394 average of previous Davis fogs (Table S3). In Davis fog, the main sources of $\cdot\text{OH}$ were nitrite
395 and nitrate photolysis, accounting for 70 – 90 % of measured P_{OH} (Anastasio and McGregor,
396 2001; Kaur and Anastasio, 2017). However, in the standard PM extracts, nitrite and nitrate
397 together account for an average of only $(34 \pm 14) \%$ of P_{OH} (Table S4), while other, unidentified
398 species account for the remaining $(66 \pm 14) \%$. While NO_2^- and NO_3^- concentrations in PME and
399 fog are similar, measured $\cdot\text{OH}$ photoproduction rates are much higher in the particle extracts. The
400 additional sources of $\cdot\text{OH}$ likely include photo-Fenton processes (Arakaki and Faust, 1998) and
401 organic peroxides (Tong et al., 2016; Tong et al., 2017; Lim and Turpin, 2015), although there is
402 only a modest correlation between DOC and P_{OH} due to unidentified sources (Fig. S6).

403 While organic compounds are potentially important sources of $\cdot\text{OH}$ in the particle
404 extracts, they are almost certainly the main $\cdot\text{OH}$ sink, as found previously for atmospheric and
405 surface waters (Brezonik and Fulkerson-Brekken, 1998; Dong et al., 2010; Arakaki et al., 2013).
406 The average ($\pm 1\sigma$) rate constant for $\cdot\text{OH}$ destruction, k'_{OH} , in the standard extracts is $2.5 (\pm 1.1)$
407 $\times 10^6 \text{ s}^{-1}$, three times higher than in dilute extracts and fog (Table S3); DOC concentrations in
408 the standard PM extracts are similarly enhanced, ranging between 2350 and 4090 $\mu\text{M-C}$ (Table
409 S2). Based on our calculations, inorganic species together account for no more than 10 % of k'_{OH}
410 in the PM extracts except for PME3D10 which is the most dilute sample and has the largest
411 uncertainty (Tables S5, S6). The rate constant for $\cdot\text{OH}$ destruction due to organics, i.e., $k'_{\text{OH,org}}$,
412 obtained by subtracting contributions of the inorganic sinks from k'_{OH} , is well correlated with
413 DOC concentrations ($R^2 = 0.73$) (Fig. S6). Arakaki et al. (2013) showed that the ratio $k'_{\text{OH,org}} /$
414 $[\text{DOC}]$ is relatively constant in atmospheric waters, with an average ($\pm 1\sigma$) value of $3.8 (\pm 1.9) \times$
415 $10^8 \text{ L (mol-C)}^{-1} \text{ s}^{-1}$. Our average ($\pm 1\sigma$) measured ratio in all particle extracts is nearly twice as
416 high, $7.1 (\pm 2.7) \times 10^8 \text{ L (mol-C)}^{-1} \text{ s}^{-1}$, but not statistically different (Table S3).

417 Davis winter-solstice-normalized $\cdot\text{OH}$ steady-state concentrations in all extracts are in the
418 range of $(1.7\text{--}7.9) \times 10^{-16} \text{ M}$, with an average ($\pm 1\sigma$) value of $5.1 (\pm 2.4) \times 10^{-16} \text{ M}$ in the
419 standard extracts (Fig. 2a, Table S3). While both the $\cdot\text{OH}$ photoproduction rate and rate constant
420 for $\cdot\text{OH}$ loss are approximately three times higher in the standard PM extracts compared to the
421 dilute extracts and fog, the two enhancements cancel out to give $\cdot\text{OH}$ steady-state concentrations
422 that are similar across all three sample types. This relative consistency of $\cdot\text{OH}$ concentrations has
423 been reported for a wide variety of atmospheric waters (Arakaki et al., 2013); our average
424 concentration is similar to most of these past results (Fig. S7). As we discuss in Sect. 3.6,
425 transport of $\cdot\text{OH}$ from the gas-phase is also an important source to drops and particles, but its
426 importance decreases with decreasing particle size.

427 We also calculated the quantum yield of hydroxyl radical formation, i.e., the fraction of
428 absorbed photons that result in $\cdot\text{OH}$ formation (Eq. (9)). The average ($\pm 1\sigma$) value of Φ_{OH} in all
429 particle extracts is $(0.014 \pm 0.010) \%$, which is statistically similar to the average fog result
430 (Table S3): while photoformation rates of $\cdot\text{OH}$ increase from fog to standard particle extracts
431 (Table S3), light absorption shows a similar trend (Table S1).

432 The rate of $\cdot\text{OH}$ photoproduction in the field blanks is negligible, representing 1 % and 6
433 % of the average rate in standard and dilute extracts, respectively. The rate constants for $\cdot\text{OH}$
434 destruction (k'_{OH}) in the standard (FB2) and dilute (FB1) field blanks represent 10 % and 43 %
435 of the corresponding PME averages. The latter result is puzzling, since the concentrations of $\cdot\text{OH}$

436 sinks measured in FB1 (i.e., DOC and NO_2^- ; Table S2) are much lower relative to the extract.
437 We discuss measurements of k'_{OH} in the blanks in more detail in Sect. S2. We do not subtract the
438 field blank results for k'_{OH} from the corresponding PM extract values and thus our sample results
439 are upper bounds.

440 3.4 Singlet molecular oxygen

441 The average ($\pm 1\sigma$) Davis winter solstice-normalized $^1\text{O}_2^*$ concentration in the dilute
442 extracts ($2.4 (\pm 0.7) \times 10^{-13}$ M) is very similar to the previous fog average (Fig. 2b). This is likely
443 because brown carbon is the source of $^1\text{O}_2^*$ (Faust and Allen, 1992; Zepp et al., 1977) and the
444 DOC concentrations in the fog and dilute extracts are very similar (Table S2). On the other hand,
445 the average [$^1\text{O}_2^*$] in the more concentrated, standard PM extracts (PME3–6), is $1.6 (\pm 0.5) \times 10^{-12}$
446 M, nearly seven times higher than the averages in Davis fog and dilute extracts (Fig. 2b, Table
447 S7). This is because the standard extracts have higher DOC concentrations but the same major
448 $^1\text{O}_2^*$ sink, i.e., water. Across all fog and particle extracts, the rate of singlet oxygen formation
449 ($P_{1\text{O}_2^*}$) is strongly correlated with the rate of sunlight absorption (R_{abs}) ($R^2 = 0.94$; Fig. 3a),
450 although this correlation is not evident in only the fog samples (Kaur and Anastasio, 2017).

451 | [As seen for \$\cdot\text{OH}\$](#) , quantum yields of $^1\text{O}_2^*$ are similar in the extracts (standard and dilute)
452 | and fog (Table S7); the slope of the $P_{1\text{O}_2^*}$ versus R_{abs} correlation line (Fig. 3a) gives an overall
453 | quantum yield of $^1\text{O}_2^*$ of $(3.8 \pm 0.2) \%$, i.e., across all samples roughly 4% of the photons
454 | absorbed lead to the formation of singlet oxygen. This is nearly 260 times higher than the
455 | average quantum yield of $\cdot\text{OH}$. [Our quantum yields for singlet oxygen formation in PM extracts](#)
456 | [are similar to values previously reported for surface water organics \(e.g., 2 – 5% in Zhou et al.](#)
457 | [\(2019\).](#)

458 3.5 Triplet excited states of organic matter ($^3\text{C}^*$)

459 We also determined the kinetics and concentrations of oxidizing “triplets”, by measuring
460 the loss of two probes, syringol (SYR) and methyl jasmonate (MeJA) (Fig. S8). In the standard
461 extracts, the average ($\pm \sigma$) Davis winter-normalized rate constants for loss of SYR and MeJA
462 (k'_{Probe}) are $(4.3 \pm 1.7) \times 10^{-4} \text{ s}^{-1}$ and $(2.6 \pm 0.7) \times 10^{-5} \text{ s}^{-1}$, which are equivalent to average
463 lifetimes of 0.70 (± 0.20) and 11 (± 3) h, respectively (Tables S8 and S9). Triplet probe lifetimes
464 in the dilute extracts are approximately three times longer and are very similar to fog values,
465 indicating that the main source of triplet precursors to fog drops is the BrC present in the fog
466 condensation nuclei rather than mass transport from the gas phase.

467 We correct the loss of triplet probes for oxidation by hydroxyl radical and singlet
468 molecular oxygen (Eq. (6)). In the standard extracts, $^1\text{O}_2^*$ and $\cdot\text{OH}$ account for an average of 13
469 % and 3 % of SYR loss, respectively (Table S8, Fig. S9); for methyl jasmonate, the
470 corresponding contributions are 37 % and 13 %.

471 Next we use the ratio of the pseudo-first-order rate constants for probe losses by triplets,
472 i.e., $k'_{\text{SYR},3\text{C}^*} / k'_{\text{MeJA},3\text{C}^*}$, to characterize the average reactivity of the triplet species in each
473 sample: a ratio close to 1 indicates higher reactivity, while a higher ratio indicates lower
474 reactivity. The $k'_{\text{Probe},3\text{C}^*}$ ratio (i.e., $k'_{\text{SYR},3\text{C}^*} / k'_{\text{MeJA},3\text{C}^*}$) in all extracts ranges between 7.9 and
475 37 (Table S12), which is a narrower range than in Davis fog samples (7.5 to 110) (Kaur and
476 Anastasio, 2018b). Based on the $k'_{\text{Probe},3\text{C}^*}$ ratios, triplets in the PM extracts generally have an
477 average reactivity similar to model aromatic triplets 3'-methoxyacetophenone ($^3\text{3MAP}^*$) and
478 3,4-dimethoxybenzaldehyde ($^3\text{DMB}^*$) (Fig. 2c, Table S12). The average ($\pm \sigma$) triplet steady-state
479 concentration in the standard extracts is $1.0 (\pm 0.4) \times 10^{-13}$ M (Fig. 2c, Table S13), which is
480 nearly twice the fog average, but not statistically significantly different. If we consider only the
481 PM and fog samples that have triplet reactivities similar to $^3\text{3MAP}^*$ and $^3\text{DMB}^*$ (i.e., the green
482 average lines in Fig. 2c), the average triplet concentration in the standard PM extracts is nearly
483 four times greater than in fog (Table S2), similar to the ratio of DOC concentrations.

484 In the standard extracts the average concentration of oxidizing triplets is 16 times lower
485 than [$^1\text{O}_2^*$] but nearly 200 times higher than [$\cdot\text{OH}$] from *in situ* sources. Our measurements of
486 oxidizing triplet concentrations lie at the higher end of measured and estimated concentrations of
487 total (i.e., oxidizing and energy transfer) triplets in surface waters, 10^{-15} – 10^{-13} M (Zepp et al.,
488 1985; Grebel et al., 2011). The average ($\pm 1 \sigma$) rate of triplet photoformation, $P_{3\text{C}^*}$, is $2.0 (\pm 1.0)$
489 $\times 10^{-7}$ M s $^{-1}$ (i.e., $720 (\pm 360)$ $\mu\text{M h}^{-1}$) in the standard extracts (Table S13). Thus the ratios of the
490 average production rates for $^1\text{O}_2^*$, $^3\text{C}^*$, and $\cdot\text{OH}$ are 290 : 170 : 1. There is a fair correlation
491 between $P_{3\text{C}^*}$ and R_{abs} (Fig. 3b), similar to the case for $P_{1\text{O}_2^*}$ (Fig. 3a), consistent with BrC as the
492 source of triplets. Sample-to-sample variability in the fraction of the total triplet pool that can
493 oxidize organics likely causes the $P_{3\text{C}^*}$ correlation ($R^2 = 0.81$) to be weaker than that of $P_{1\text{O}_2^*}$ (R^2
494 $= 0.94$). The average ($\pm 1 \sigma$) oxidizing triplet quantum yield in standard extracts is (2.4 ± 1.0) %
495 (Table S13), approximately two times lower than the value for $^1\text{O}_2^*$ (Table S7) but 150 times
496 higher than for $\cdot\text{OH}$ (Table S3). [Our triplet quantum yields are within the wide range of values](#)
497 [that has been reported for surface waters, approximately 0.4 – 7%](#) (Zepp et al., 1985; Grebel et
498 al., 2011; Zhou et al., 2019).

499 Triplet excited states have two main reaction pathways: energy transfer (e.g., to make
500 $^1\text{O}_2^*$) and electron transfer (e.g., to oxidize a phenol) (Zepp et al., 1985; McNeill and Canonica,
501 2016; Kaur and Anastasio, 2018b). Essentially all triplets possess enough energy to form $^1\text{O}_2^*$
502 (McNeill and Canonica, 2016), but only a subset of the triplet pool can oxidize organics via
503 electron transfer. Thus the quantum yield of $^1\text{O}_2^*$ can be used to estimate the total triplet
504 quantum yield, while our measurements of $\Phi_{3\text{C}^*}$ constrain the smaller subset of oxidizing triplets
505 (assuming energy transfer from triplets is the only source of $^1\text{O}_2^*$). The quantum yield for all
506 triplets can be estimated as $\Phi_{1\text{O}_2^*}/f_\Delta$, where f_Δ , the fraction of $^3\text{C}^*$ interactions with dissolved O_2
507 that yield $^1\text{O}_2^*$, is approximately 0.5 (McNeill and Canonica, 2016; Kaur and Anastasio, 2018b).
508 For our standard extracts, the average value of $\Phi_{1\text{O}_2^*}/f_\Delta$ is 0.078 ± 0.019 , i.e., approximately 8 %
509 of the photons absorbed by brown carbon chromophores make a triplet excited state. Next we use
510 the ratio $\Phi_{3\text{C}^*}/(\Phi_{1\text{O}_2^*}/f_\Delta)$ to estimate the fraction of all triplets that can participate in electron-
511 transfer (oxidation) reactions. The average value of this fraction is 0.35 ± 0.12 for all the PM
512 extracts, i.e., on average, [approximately a third](#) of all triplets are oxidizing (range = 18–50 %;
513 Table S13).

514 3.6 Predicting photooxidant concentrations in ambient particle water

515 Since our particle extracts are approximately 1000 times more dilute than ambient Davis
516 particles during winter, we want to be able to estimate oxidant concentrations under ambient
517 conditions. To do this we first measured photooxidant concentrations as a function of dilution for
518 the same sample and then extrapolated our results to ambient particle conditions. For the first
519 step, we extracted squares of filter #3 using five different volumes of Milli-Q water, from 10 to
520 0.50 mL (Sect. 2.5.4), corresponding to aqueous PM mass concentration factors (CF) of 0.05
521 (most dilute) to 0.96 (most concentrated) (Eq. (10)). For this sample, these are equivalent to PM
522 [solute](#) mass / water mass ratios typical for dilute to very concentrated cloud or fog drops, i.e.,
523 $(0.35 - 8.4) \times 10^{-4} \mu\text{g-PM} / \mu\text{g-H}_2\text{O}$; [in comparison, ambient particles have ratios of](#)
524 [approximately 1 \$\mu\text{g-PM} / \mu\text{g-H}_2\text{O}\$ and higher](#) (Table S14). The rate of light absorption increases
525 linearly with CF (Fig. 4a), indicating that BrC and other chromophores are efficiently extracted
526 for all Milli-Q volumes employed.

527 The change in photooxidant concentration with CF depends on how the ratio of sources
528 and sinks varies with dilution. In the case of hydroxyl radical, P_{OH} and k'_{OH} both increase as
529 extracts get more concentrated (i.e., as CF increases), resulting in an $\cdot\text{OH}$ concentration that [is](#)
530 [noisy but essentially unchanged over the](#) 20-fold increase in concentration factor ([Fig. 4b](#)). This

531 [result](#) is consistent with the relatively constant [$\cdot\text{OH}$] in our particle extracts relative to fog (Fig.
532 3a, black dashed lines) and with prior results showing very similar concentrations for rain, cloud,
533 fog, and marine PM extracts (Fig. S7 and Arakaki et al., 2013).

534 To estimate [$\cdot\text{OH}$] in particle liquid water, we use the measured linear dependences of the
535 rate of $\cdot\text{OH}$ photoproduction (P_{OH}) and loss rate constant (k'_{OH}) on concentration factor, which
536 corresponds to a measured PM mass / water mass ratio (Fig. S10). Under a typical wintertime,
537 Central Valley ambient particle water condition (1 $\mu\text{g-PM} / \mu\text{g-H}_2\text{O}$), the *in situ* P_{OH} and k'_{OH} are
538 estimated to be $4.2 \times 10^{-6} \text{ M s}^{-1}$ and $5.5 \times 10^9 \text{ s}^{-1}$, respectively (Fig. S10). This extrapolation of
539 only aqueous processes gives an $\cdot\text{OH}$ concentration in particle water of $7.6 \times 10^{-16} \text{ M}$, which is
540 similar to the average of the measurements in Fig. 4b. However, this estimate does not include
541 the contribution of mass transport of gas-phase $\cdot\text{OH}$ to the particles. As detailed in Sect. S4, we
542 estimate that the rate of $\cdot\text{OH}$ gas-to-particle transport [under particle conditions](#) is $4.2 \times 10^{-7} \text{ M s}^{-1}$,
543 [which is](#) approximately 10 % of the $\cdot\text{OH}$ photoformation rate from aqueous sources. [Figure 5](#)
544 [shows estimated \$\cdot\text{OH}\$ steady-state concentrations considering both aqueous reactions and gas-](#)
545 [phase mass transport across a wide range of drop to particle conditions: \[\$\cdot\text{OH}\$ \] decreases from \$5.4\$](#)
546 [\$\times 10^{-15} \text{ M}\$ under dilute drop conditions \(\$3 \times 10^{-5} \mu\text{g-PM}/\mu\text{g-H}_2\text{O}\$ \) to \$8.4 \times 10^{-16} \text{ M}\$ under the](#)
547 [much more concentrated particle conditions \(\$1 \mu\text{g-PM}/\mu\text{g-H}_2\text{O}\$ \). The calculated \[\$\cdot\text{OH}\$ \] values](#)
548 [\(orange line in Figure 5\) are higher than our measured values \(orange points in Figure 5\) because](#)
549 [of the gas-phase mass transport source. Changes in this source are also responsible for the slow](#)
550 [decrease in calculated \[\$\cdot\text{OH}\$ \] as conditions become more concentrated \(i.e., as \$\mu\text{g-PM}/\mu\text{g-H}_2\text{O}\$](#)
551 [increases\).](#) In the case of singlet oxygen, steady-state concentrations increase proportionally with
552 PM mass concentration factor (Fig. 4c). Our interpretation of this result is that the concentrations
553 of $^1\text{O}_2^*$ sources (i.e., BrC) increase proportionally with concentration factor, while the
554 concentration of the main sink for $^1\text{O}_2^*$ (i.e., water) is essentially unchanged. [At higher PM](#)
555 [mass/water mass ratios, we calculate that organic compounds become a significant sink for](#)
556 [singlet oxygen \(Sect. S4\), leading to a plateau in \[\$^1\text{O}_2^*\$ \] under the more concentrated conditions](#)
557 [of particles \(Fig. 5\). This extrapolation for ambient PM conditions \(\$1 \mu\text{g-PM} / \mu\text{g-H}_2\text{O}\$ \) predicts](#)
558 [an \$^1\text{O}_2^*\$ concentration in particle water of \$1.6 \times 10^{-10} \text{ M}\$ \(Table S15, Fig. 5\), which is 2400 times](#)
559 [higher than our prediction for dilute fog/cloud drops.](#) While there are no other measurements of
560 $^1\text{O}_2^*$ in particles, similar enhancements in $^1\text{O}_2^*$ concentrations (up to a factor of [roughly \$10^4\$](#))
561 have been found in cases where $^1\text{O}_2^*$ precursors become highly concentrated, e.g., in liquid-like
562 regions of ice (Bower and Anastasio, 2013) and in regions of hydrophobic CDOM in solution
563 (Latch and McNeill, 2006).

564 An increase in [extract concentration \(i.e., CF\)](#) also increases the triplet steady-state
565 concentration (Fig. 4d), but there is greater uncertainty in this trend, in part because there is more
566 uncertainty in measurements of $\Sigma[{}^3\text{C}_i^*]$. [As described in Sect. S4, we fit the data in Fig. 4d with](#)
567 [a hyperbolic regression under two cases: \(1\) a best fit, where parameters were adjusted to](#)
568 [minimize the regression error, and \(2\) a high estimate fit, where parameters were adjusted so that](#)
569 [the regression line passed near the upper portion of the error bar for the CF 0.96 data point.](#)
570 [These are the dashed and dotted lines in Fig. 4d, respectively.](#) In both cases the triplet
571 concentration initially rises more quickly with CF but then approaches a plateau at higher CF
572 values. Our interpretation of this behavior is that as CF increases, [DOM] and $P_{3\text{C}^*}$ increase
573 linearly but the dominant triplet sink switches from dissolved O_2 at low CF to DOM at high CF.
574 Wenk et al. (2011); (2013) have shown that surface water DOM can quench triplets [when DOM](#)
575 [concentrations are greater than \$20 \text{ mg-C L}^{-1}\$; in the PME3D extracts of Fig. 4, DOM ranges from](#)
576 [4.3 to \$86 \text{ mg-C L}^{-1}\$ \(Table S2\).](#) Based on our previous work, we believe that phenols from wood
577 combustion [are reacting with \(and physically quenching\) triplets](#) in our PM extracts (Smith et al.,
578 2014; 2015). As described in Sect. S5, by fitting a kinetic model to our triplet dilution data we
579 estimate that the total (reaction and quenching) rate constant for triplets with DOC in the PME3
580 extracts is $9.3 (\pm 1.3) \times 10^7 \text{ L mol-C}^{-1} \text{ s}^{-1}$.

581 These two extrapolations result in oxidizing triplet concentrations under PM conditions (1
582 $\mu\text{g-PM} / \mu\text{g-H}_2\text{O}$) of $2.3 \times 10^{-13} \text{ M}$ ([best fit](#)) and $1.3 \times 10^{-11} \text{ M}$ ([high estimate](#)). Taken together
583 with the other oxidant measurements, we estimate [that the](#) ratio of ${}^1\text{O}_2^* : {}^3\text{C}^* : \cdot\text{OH}$ concentrations
584 in ambient particle water [is](#) approximately $10^5 : 10^4 - 10^2 : 1$.

585

586 4 Implications

587 Our dilution experiments suggest that $\cdot\text{OH}$, ${}^1\text{O}_2^*$, and ${}^3\text{C}^*$ behave very differently as the
588 PM/water ratio increases from cloud and fog drop conditions to water-containing particles (Fig.
589 5). To understand what this implies for the fate of organic compounds, we estimated the gas-
590 aqueous partitioning and lifetimes of five model organic compounds for both fog and aqueous
591 aerosol (Fig. 6). We consider reactions with two gas-phase oxidants ($\cdot\text{OH}$, O_3) and four aqueous-
592 phase oxidants ($\cdot\text{OH}$, O_3 , ${}^1\text{O}_2^*$, ${}^3\text{C}^*$) (Table S16). Our model organics represent two groups in
593 terms of gas-aqueous partitioning: one group with modest Henry's law constants ($K_{\text{H}} \sim 10^4 \text{ M}$
594 atm^{-1}) and one with much higher values ($K_{\text{H}} = 10^9 - 10^{11} \text{ M atm}^{-1}$) (Fig. 6 and Table S17).

595 Fig. 6a shows the overall lifetimes of the five model organics and the fraction of each
596 present in fog and PM. For the organics with the lowest K_H values, approximately 10–20 % is
597 present in the aqueous-phase under fog conditions, but almost none is present in the particle
598 liquid water. Consequently, gas-phase reactions dominate their overall lifetimes, which are
599 approximately 2 to 3 hours for both fog and PM conditions. In contrast, the compounds with high
600 K_H values are partitioned strongly to the aqueous phase for both the fog and PM scenarios (Fig.
601 6a). But due to the overall higher oxidant concentrations in PM, the lifetimes of these organics
602 are predicted to be shorter – sometimes by large factors – in PM than in fog (Fig. 6a, Table S17).
603 Additionally, their main sinks change from fog to PM, shifting from aqueous $\cdot\text{OH}$, O_3 , and $^1\text{O}_2^*$
604 in fog to being generally dominated by $^1\text{O}_2^*$ in PM water (Fig. 6b). For example, for tyrosine
605 (compound 3), the predominant sink changes from aqueous O_3 in fog to $^1\text{O}_2^*$ in water-containing
606 particles, while its lifetime decreases from 1.6 h to 0.04 h (Fig. 6b and Table S17).

607 While triplets are negligible oxidants for individual organics in particles under the
608 conditions of Fig. 6, the picture changes if we move from the Fig. 6 triplet concentration of $2.3 \times$
609 10^{-13} M to the [high estimate](#) concentration (1.3×10^{-11} M; Fig. 5). Under this condition aqueous
610 oxidation still dominates the loss of the high- K_H compounds, but $^3\text{C}^*$ [becomes a much more](#)
611 [important](#) oxidant in PM and organic lifetimes get shorter by factors of [3](#) to [180](#) compared to fog
612 (Fig. S11). While there is large uncertainty in the triplet concentrations in PM, Figs. 6 and S11
613 both indicate that aqueous oxidants can control the fate of highly soluble species in aerosols and
614 that organic lifetimes can be shorter in PM because of an enhancement in oxidant concentrations.

615 Finally, [despite the uncertainty in triplet concentration under particle conditions](#), the
616 formation rate of $^3\text{C}^*$ is fast enough – and the fraction of triplets lost via reaction with organics is
617 high enough – that triplets represent, in aggregate, a significant sink for organic compounds in
618 particles. [While these two ideas might seem contradictory, we propose that the suite of reactive](#)
619 [organic compounds is suppressing the triplet concentrations enough that \$^3\text{C}^*\$ are small sinks for](#)
620 [individual organic compounds, but are significant sinks when integrated over all of the reactive](#)
621 [organics](#). As described in Sect. 3.5, the formation rates for $^1\text{O}_2^*$, $^3\text{C}^*$, and $\cdot\text{OH}$ have a ratio of
622 290 : 170 : 1, respectively, in the PM extracts; based on our dilution experiments (Fig. 4), we
623 expect similar ratios in ambient particle liquid water. Since organic compounds appear to be the
624 major sinks for all three oxidants under ambient particle conditions, and since each oxidant is at
625 steady-state, the ratio of formation rates is approximately the same as the ratio of total rates of
626 organic compound oxidation by each oxidant. Thus, while the steady-state concentration of $^3\text{C}^*$
627 might be significantly lower than that of $^1\text{O}_2^*$ in particle water, both oxidants appear to be

628 similarly important in the overall processing of particulate organics. In contrast, the total rate of
629 oxidation of organics by $\cdot\text{OH}$ appears to be 200–300 times slower, although $\cdot\text{OH}$ will be
630 relatively more important for less reactive organics. This comparison suggests that both singlet
631 molecular oxygen and triplet excited states [are important for the processing of organic](#)
632 [compounds in particle liquid water](#).

633

634 **5 Conclusions and Uncertainties**

635 We have made the first measurements of singlet molecular oxygen and oxidizing triplet
636 states in aqueous extracts of particles, in addition to measuring hydroxyl radical. Under our
637 standard condition, the particle extracts are approximately three times more concentrated than
638 wintertime Davis fog waters. The extracts contain significant amounts of brown carbon, with
639 DOC-normalized mass absorption coefficients between roughly 15,000 and 30,000 $\text{cm}^2 \text{g-C}^{-1}$
640 and Absorption Angstrom Exponents of 6.2 to 7.9. Upon absorbing light, BrC and other
641 chromophores in the samples form significant amounts of $\cdot\text{OH}$, $^1\text{O}_2^*$, and $^3\text{C}^*$. While
642 concentrations of $\cdot\text{OH}$ in the PM extracts are in the same range as found in fog waters,
643 concentrations of the oxidants derived primarily from BrC – i.e., $^1\text{O}_2^*$ and $^3\text{C}^*$ – are higher in the
644 extracts compared to in fog by factors of [approximately](#) seven and [two](#), respectively.

645 Dilution experiments indicate that the $\cdot\text{OH}$ concentration is essentially independent of the
646 PM mass concentration in solution, consistent with previous results, while $^1\text{O}_2^*$ and $^3\text{C}^*$ increase
647 with increasing aqueous PM concentration. Extrapolating our findings to the [much](#) more
648 concentrated conditions expected in ambient particle water suggests that hydroxyl radical
649 concentrations in particles will be [somewhat lower than](#) values in fog and cloud drops, [a result of](#)
650 [size-dependent changes in mass transport from the gas phase. In contrast](#), oxidants formed from
651 illumination of brown carbon will be enhanced in particles: [moving from very dilute drops \(\$3 \times\$](#)
652 [\$10^{-5}\$ \$\mu\text{g-PM}/\mu\text{g-H}_2\text{O}\$ \) to concentrated particles \(\$1 \mu\text{g-PM}/\mu\text{g-H}_2\text{O}\$ \) we predict that the](#)
653 [concentration of \$^1\text{O}_2^*\$ will increase](#) by approximately a factor of [2400](#), [while concentrations of](#)
654 [oxidizing triplets will increase](#) between a factor of [30](#) and [2000](#). The higher $^1\text{O}_2^*$ concentrations
655 predicted in particles lead to a large decrease in the lifetimes of highly water-soluble organic
656 compounds compared to foggy conditions, even though the liquid water content of the particles
657 is roughly 10^4 times lower than the fog. It [appears](#) that triplets are also more significant oxidants
658 [for individual organic compounds](#) in PM than in fog, but there is too much uncertainty in our
659 data to properly assess [this increase](#). In contrast, $\cdot\text{OH}$ is important for the oxidation of organics

660 that react only slowly with $^1\text{O}_2^*$ and $^3\text{C}^*$, but is otherwise a minor oxidant for the organics we
661 considered since the particulate $\cdot\text{OH}$ concentration is quite low.

662 While our results suggest that oxidants derived from brown carbon are very significant in
663 water-containing particles, there are several large uncertainties. Most significantly, because of
664 experimental limitations on the maximum PM concentration in our extracts, we need to
665 extrapolate oxidant measurements over a very large range (approximately a factor of 1000) to
666 predict oxidant levels in ambient water-containing particles. This results in very large
667 uncertainties. As part of this uncertainty, it is difficult to assess how reactions in the particles
668 might suppress concentrations of $^1\text{O}_2^*$ and $^3\text{C}^*$. Secondly, while calculations suggest that
669 unaccounted oxidants are minor sinks for our triplet probes, if these species are important our
670 triplet concentrations would be biased high. Finally, it is unclear how widely our results, which
671 are for one season and one location, can be applied to other particles containing brown carbon.
672 However, [PME3](#), our one sample collected during both daytime (with little biomass burning) and
673 night (with significant biomass burning) had similar reactivity to [the other](#) samples, [which were](#)
674 collected only at night. Regardless, since these are the first measurements of $^1\text{O}_2^*$ and $^3\text{C}^*$ in
675 particles, strengthening and improving our findings requires more measurements, especially for
676 other seasons and locations. Measurements under much higher [particle mass/water mass ratios](#),
677 ideally under ambient conditions, are also needed.

678 Despite the uncertainties, our results indicate that BrC-derived photooxidants such as
679 singlet molecular oxygen and organic triplet excited states can be important [oxidants](#) in
680 atmospheric particles. Currently these oxidants are not included in atmospheric models, although
681 our calculations suggest that $^1\text{O}_2^*$ and $^3\text{C}^*$ [can dominate](#) the processing of highly soluble organic
682 molecules in aerosol [particles](#).

683 **Competing Interests**

684 The authors declare that they have no conflict of interest.

685 **Author Contribution**

686 CA and RK developed the research goals and designed the experiments. KB lent and set up the
687 sampler, while RK, CA, and WJ collected samples. RK, JL, and SH performed the
688 photochemistry experiments while WJ analyzed ions and OC. RK analyzed the data and prepared
689 the manuscript with contributions from all co-authors. CA reviewed, wrote portions of, and

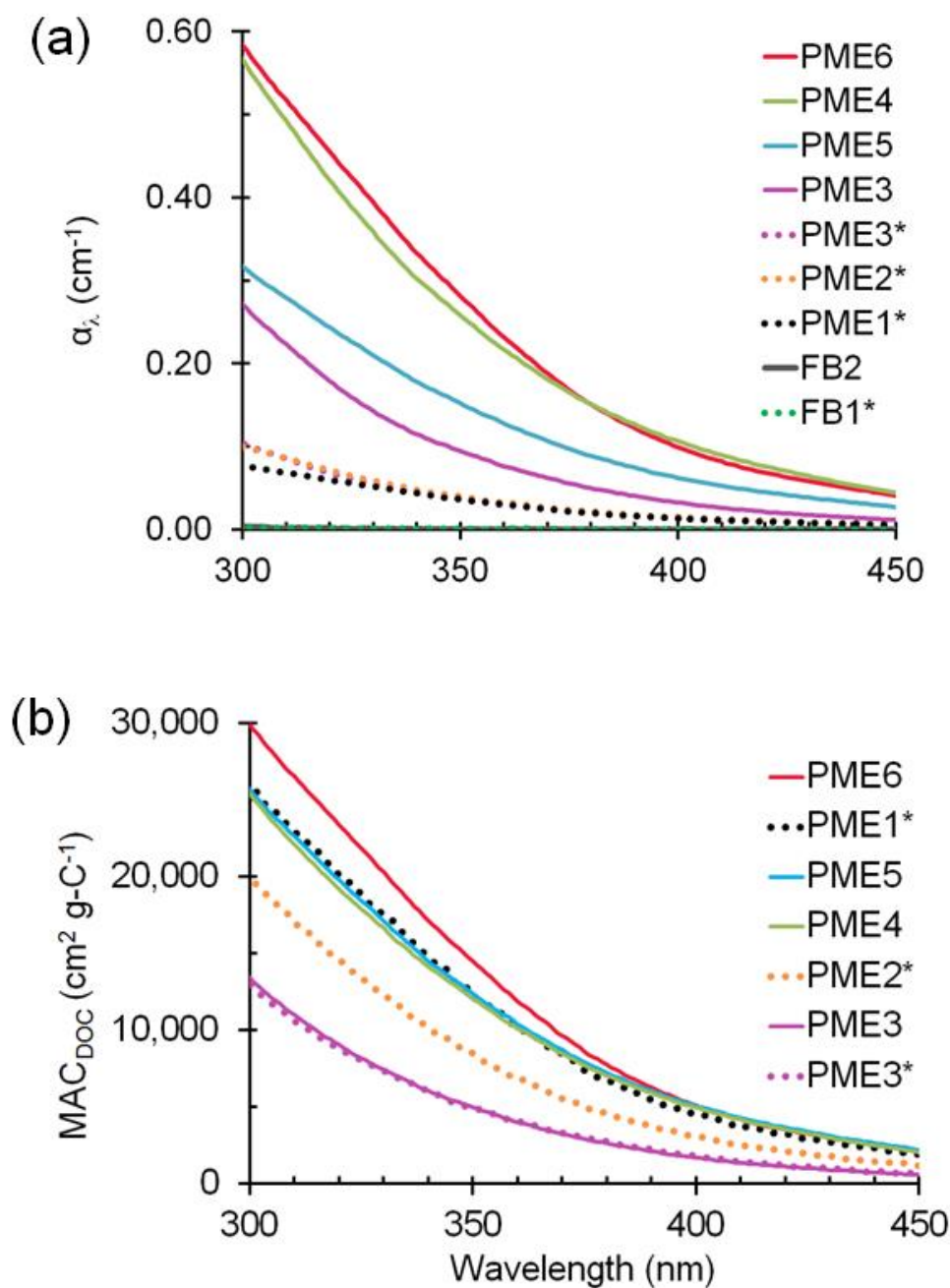
690 edited the manuscript. CA and QZ provided supervision and oversight during the experiments
691 and writing.

692 **Data Availability**

693 Light absorption data have been submitted to the data repository Pangaea, cited in the text and
694 are available at <https://doi.pangaea.de/10.1594/PANGAEA.896418>. Other data are available
695 upon request.

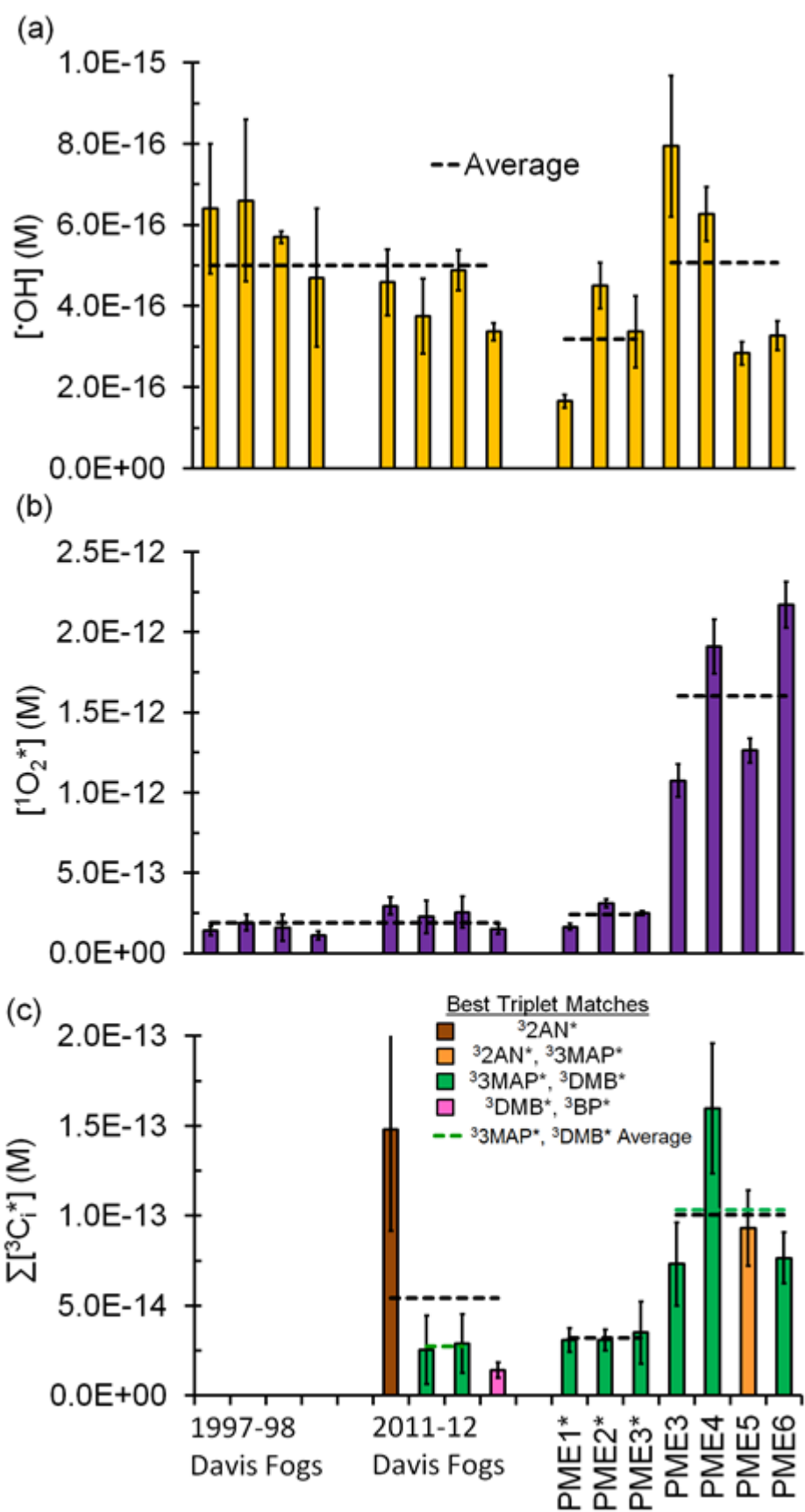
696 **Acknowledgments**

697 We thank Ann Dillner, Alexandra Boris, and April Chaney (UC Davis, Air Quality Research
698 Center) for use of a microbalance [and an anonymous reviewer for extensive and helpful](#)
699 [comments. Funding was provided by](#) the National Science Foundation (AGS-1649212),
700 [California Agricultural Experiment Station \(Project CA-D-LAW-6403-RR\)](#), a UC Guru Gobind
701 Singh Fellowship, a Donald G. Crosby Graduate Fellowship, and a James and Rita Seiber
702 International Student Support Award.



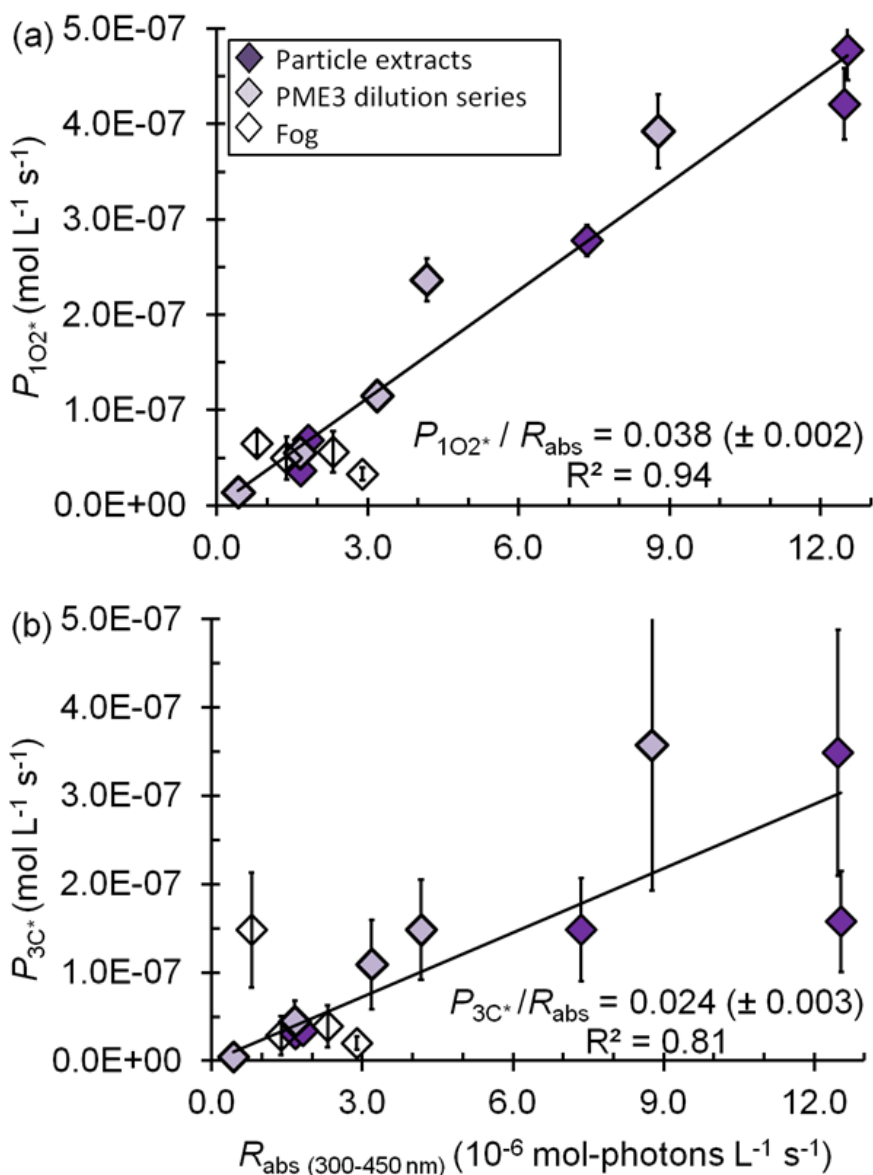
704

705 Figure 1. (a) Light absorption coefficients, α_λ , in particulate matter extracts (PME) (Eq. (1)) and
 706 field blanks (FB). The legend shows the sample identities, arranged from the highest absorbing
 707 (top) to lowest absorbing (bottom) at 300 nm. Solid and dotted lines represent standard and dilute
 708 extracts, respectively (with the latter indicated with an asterisk; Sect. 2.2). (b) Mass absorption
 709 coefficients of DOC in the particle extracts (Eq. (3)).



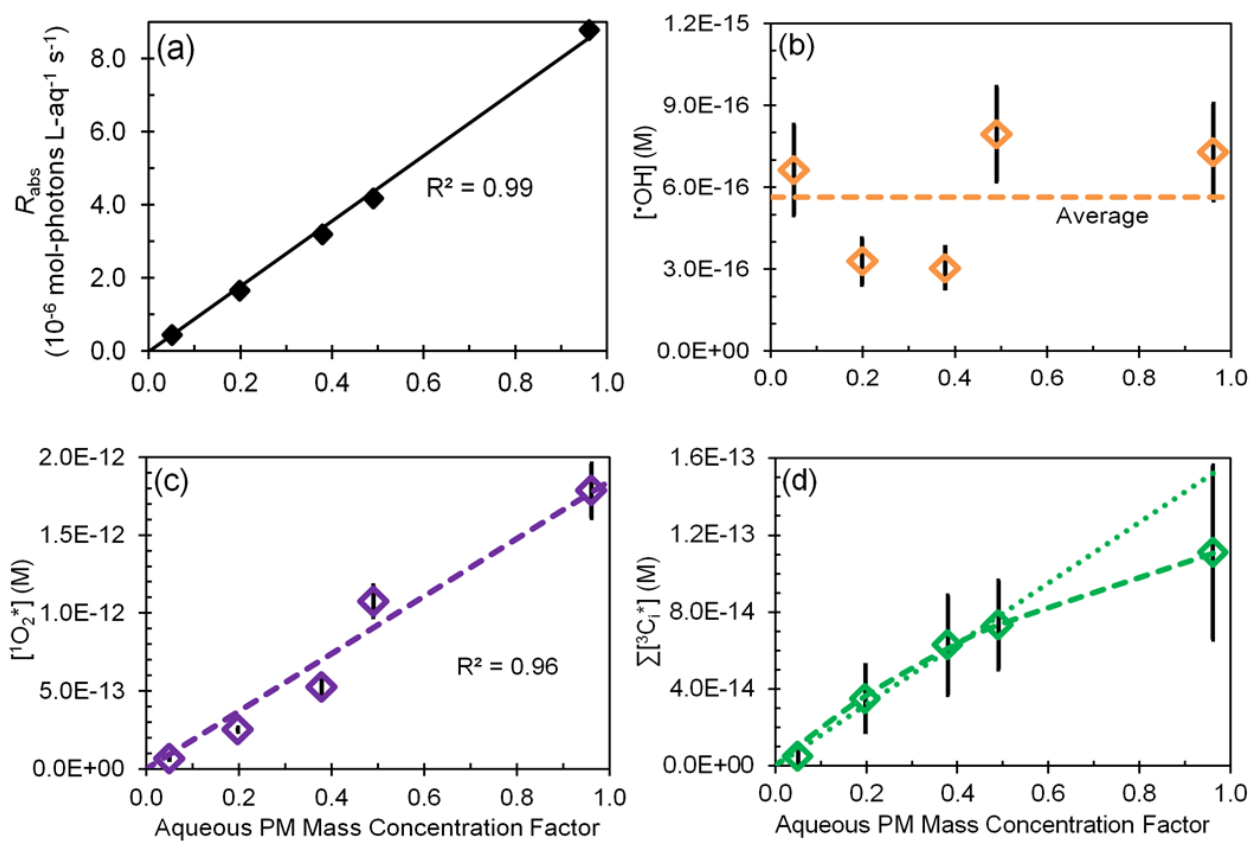
710

711 Figure 2. Measured steady-state concentrations of (a) hydroxyl radical, (b) singlet molecular
 712 oxygen and, (c) oxidizing triplet excited states of organic matter in particle extracts, along with
 713 previous measurements made in Davis fogs collected between 1997-98 and 2011-12 (Anastasio
 714 and McGregor, 2001; Kaur and Anastasio, 2017; Kaur and Anastasio, 2018b). All concentrations
 715 are normalized to Davis midday, winter solstice sunlight. Dilute particle extracts are indicated
 716 with an asterisk. Dashed lines represent sample averages.



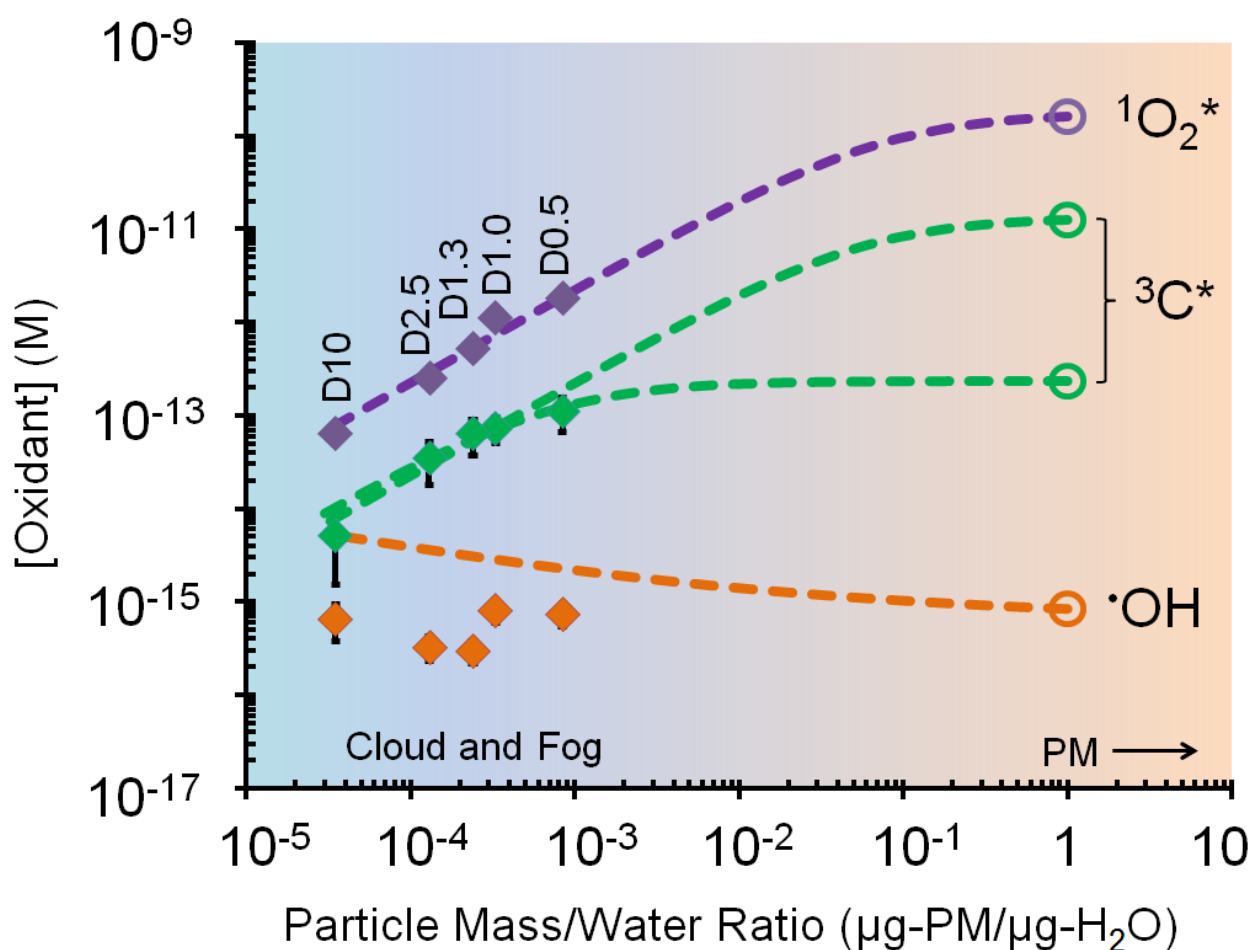
717

718 Figure 3. Correlations between (a) the rate of singlet oxygen photoproduction normalized to
 719 Davis winter solstice sunlight (P_{102^*}), (b) the rate of triplet photoproduction normalized to Davis
 720 winter solstice sunlight (P_{3C^*}) and the rate of light absorption (R_{abs}) between 300 to 450 nm.
 721 Triplet rates for the fog samples were adjusted to account for the small DOC sink for triplets; Eq.
 722 (8). The P/R_{abs} ratios ($\pm 1 \text{ SE}$) listed are unitless and represent the quantum yields.



724

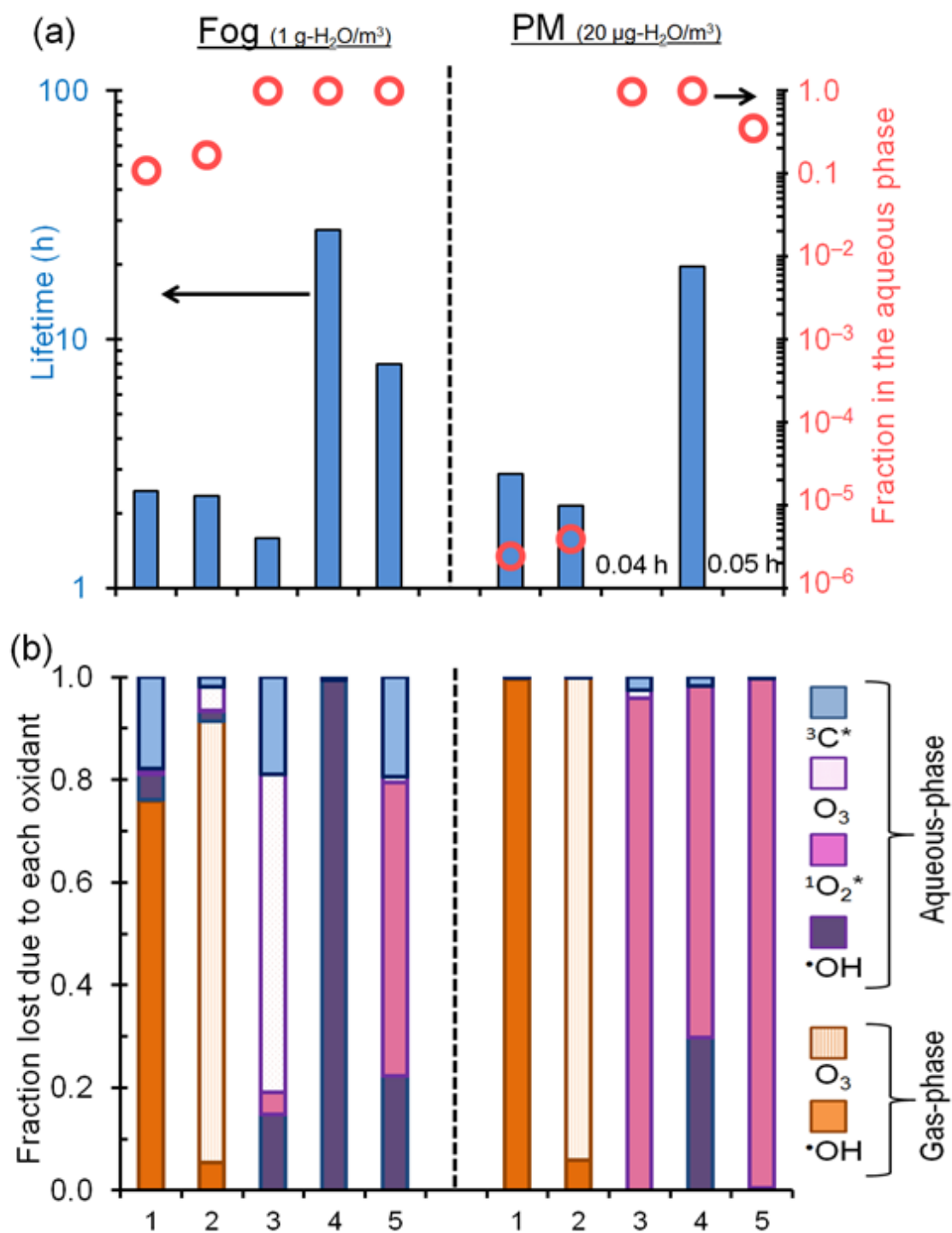
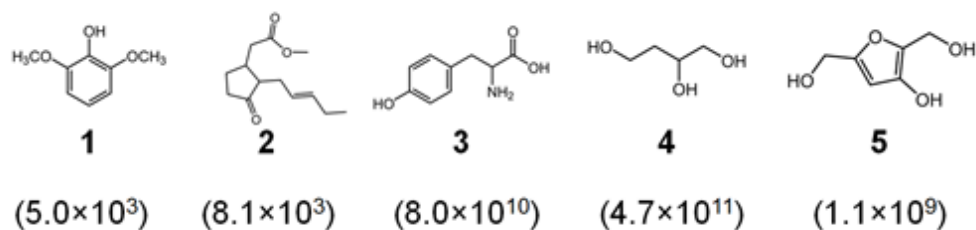
725 Figure 4. Effect of change in aqueous particle mass concentration (i.e., sample dilution) for
 726 sample PME3 on (a) rate of light absorption and the steady-state concentrations of (b) hydroxyl
 727 radical, (c) singlet molecular oxygen and, (d) oxidizing triplet excited states of organic matter.
 728 The last panel shows both linear (dotted) and hyperbolic (dashed) fits to the data. In each plot the
 729 x-axis is a measure of sample dilution, with higher concentration factors corresponding to more
 730 concentrated particle extracts (Eq. (10)).



731

732

733 Figure 5. Dependence of photooxidant concentrations on particle mass / water mass ratio (i.e.,
 734 aqueous particle concentration) in extracts of sample PME3. Solid diamonds are measured
 735 values under experimental dilution conditions (typical for clouds or fogs), while the open circles
 736 are values expected in more concentrated particle liquid water based on the dashed line
 737 extrapolations. For the solid symbols, error bars ($\pm 1\sigma$) are often smaller than the symbols. Data
 738 labels on the diamonds (e.g., D10) represent the water volume used to extract the PME3 filter
 739 square (Sect. 2.5.4). The dashed line extrapolations include the contributions from both aqueous
 740 processes and interactions with the gas phase (Sect. S4). For oxidizing triplets, two extrapolation
 741 scenarios are shown: a best estimate (lower line) and a high estimate (upper line), as described in
 742 Sect. S4 and Table S15.



743

744 Figure 6. Fate of five model organic compounds – (1) syringol, (2) methyl jasmonate, (3)
 745 tyrosine, (4) 1,2,4-butanetriol and (5) 3-hydroxy-2,5-bis(hydroxymethyl)furan – under liquid
 746 water content conditions for fog (left of vertical dashed line; $1 \text{ g-H}_2\text{O} / \text{m}^3\text{-air}$) and PM (right of
 747 line; $20 \text{ } \mu\text{g-H}_2\text{O} / \text{m}^3\text{-air}$). Estimated Henry's law constants for the compounds (in units of M
 748 atm^{-1}) are in parentheses beneath each structure. In panel (a) the columns represent overall
 749 lifetimes of the organics and the open circles represent the fractions in the aqueous phase. Panel

750 (b) shows the fraction of each compound lost via various gas and aqueous pathways. The triplet
751 | contribution in PM is estimated using the lower-bound triplet concentration extrapolation i.e., 1.3
752 $\times 10^{-13}$ M (Fig. 5). Oxidant concentrations and rate constants are in Tables S16 and S17.

753 **References**

- 754 Albinet, A., Minero, C., and Vione, D.: Photochemical generation of reactive species upon
 755 irradiation of rainwater: Negligible photoactivity of dissolved organic matter, *Sci. Total*
 756 *Environ.*, 408, 3367-3373, 2010.
- 757 Anastasio, C., Faust, B. C., and Rao, C. J.: Aromatic carbonyl compounds as aqueous-phase
 758 photochemical sources of hydrogen peroxide in acidic sulfate aerosols, fogs, and clouds
 759 .1. Non-phenolic methoxybenzaldehydes and methoxyacetophenones with reductants
 760 (phenols), *Environ. Sci. Technol.*, 31, 218-232, 1997.
- 761 Anastasio, C., and McGregor, K. G.: Chemistry of fog waters in California's central valley: 1. In
 762 situ photoformation of hydroxyl radical and singlet molecular oxygen, *Atmospheric*
 763 *Environment*, 35, 1079-1089, 2001.
- 764 Anastasio, C., and Jordan, A. L.: Photoformation of hydroxyl radical and hydrogen peroxide in
 765 aerosol particles from Alert, Nunavut: Implications for aerosol and snowpack chemistry
 766 in the Arctic, *Atmos. Environ.*, 38, 1153-1166, 2004.
- 767 Anastasio, C., and Newberg, J. T.: Sources and sinks of hydroxyl radical in sea-salt particles, *J.*
 768 *Geophys. Res.*, 112, D10306, <https://doi.org/10.1029/2006JD008061>, 2007.
- 769 Arakaki, T., and Faust, B. C.: Sources, sinks, and mechanisms of hydroxyl radical ($\cdot\text{OH}$)
 770 photoproduction and consumption in authentic acidic continental cloud waters from
 771 Whiteface Mountain, New York: The role of the Fe (R)(R= II, III) photochemical cycle,
 772 *J. Geophys. Res. Atmos.*, 103, 3487-3504, 1998.
- 773 Arakaki, T., Miyake, T., Shibata, M., and Sakugawa, H.: Photochemical formation and
 774 scavenging of hydroxyl radical in rain and dew waters, *Nippon Kagaku Kaishi*, 5, 335-
 775 340, 1999.
- 776 Arakaki, T., Kuroki, Y., Okada, K., Nakama, Y., Ikota, H., Kinjo, M., Higuchi, T., Uehara, M.,
 777 and Tanahara, A.: Chemical composition and photochemical formation of hydroxyl
 778 radicals in aqueous extracts of aerosol particles collected in Okinawa, Japan, *Atmos.*
 779 *Environ.*, 40, 4764-4774, 2006.
- 780 Arakaki, T., Anastasio, C., Kuroki, Y., Nakajima, H., Okada, K., Kotani, Y., Handa, D., Azechi,
 781 S., Kimura, T., Tsuchi, A., and Miyagi, Y.: A general scavenging rate constant for
 782 reaction of hydroxyl radical with organic carbon in atmospheric waters, *Environ. Sci.*
 783 *Technol.*, 47, 8196-8203, 2013.
- 784 Aregahegn, K. Z., Nozière, B., and George, C.: Organic aerosol formation photo-enhanced by
 785 the formation of secondary photosensitizers in aerosols, *Faraday Discuss.*, 165, 123-134,
 786 2013.
- 787 Bahnmüller, S., von Gunten, U., and Canonica, S.: Sunlight-induced transformation of
 788 sulfadiazine and sulfamethoxazole in surface waters and wastewater effluents, *Water*
 789 *Res.*, 57, 183-192, 2014.
- 790 Bilski, P., Holt, R. N., and Chignell, C. F.: Properties of singlet molecular oxygen $\text{O}_2(1\Delta_g)$ in
 791 binary solvent mixtures of different polarity and proticity, *J. Photochem. Photobiol.*, A,
 792 109, 243-249, 1997.
- 793 Blando, J. D., and Turpin, B. J.: Secondary organic aerosol formation in cloud and fog droplets:
 794 A literature evaluation of plausibility, *Atmos. Environ.*, 34, 1623-1632, 2000.
- 795 Boreen, A. L., Arnold, W. A., and McNeill, K.: Triplet-sensitized photodegradation of sulfa
 796 drugs containing six-membered heterocyclic groups: Identification of an SO_2 extrusion
 797 photoproduct, *Environ. Sci. Technol.*, 39, 3630-3638, 2005.

798 Bower, J. P., and Anastasio, C.: Measuring a 10,000-fold enhancement of singlet molecular
799 oxygen ($^1\text{O}_2^*$) concentration on illuminated ice relative to the corresponding liquid
800 solution, *Atmos. Environ.*, 75, 188-195, 2013.

801 Brezonik, P. L., and Fulkerson-Brekken, J.: Nitrate-induced photolysis in natural waters:
802 Controls on concentrations of hydroxyl radical photo-intermediates by natural scavenging
803 agents, *Environ. Sci. Technol.*, 32, 3004-3010, 1998.

804 Canonica, S., and Hoigné, J.: Enhanced oxidation of methoxy phenols at micromolar
805 concentration photosensitized by dissolved natural organic material, *Chemosphere*, 30,
806 2365-2374, 1995.

807 Canonica, S., Jans, U., Stemmler, K., and Hoigne, J.: Transformation kinetics of phenols in
808 water: Photosensitization by dissolved natural organic material and aromatic ketones,
809 *Environ. Sci. Technol.*, 29, 1822-1831, 1995.

810 Canonica, S., Hellrung, B., and Wirz, J.: Oxidation of phenols by triplet aromatic ketones in
811 aqueous solution, *J. Phys. Chem. A*, 104, 1226-1232, 2000.

812 Canonica, S., Hellrung, B., Müller, P., and Wirz, J.: Aqueous oxidation of phenylurea herbicides
813 by triplet aromatic ketones, *Environ. Sci. Technol.*, 40, 6636-6641, 2006.

814 De Haan, D. O., Corrigan, A. L., Smith, K. W., Stroik, D. R., Turley, J. J., Lee, F. E., Tolbert, M.
815 A., Jimenez, J. L., Cordova, K. E., and Ferrell, G. R.: Secondary organic aerosol-forming
816 reactions of glyoxal with amino acids, *Environ. Sci. Technol.*, 43, 2818-2824, 2009.

817 De Haan, D. O., Hawkins, L. N., Kononenko, J. A., Turley, J. J., Corrigan, A. L., Tolbert, M. A.,
818 and Jimenez, J. L.: Formation of nitrogen-containing oligomers by methylglyoxal and
819 amines in simulated evaporating cloud droplets, *Environ. Sci. Technol.*, 45, 984-991,
820 2010.

821 Dong, M. M., Mezyk, S. P., and Rosario-Ortiz, F. L.: Reactivity of effluent organic matter
822 (EFOM) with hydroxyl radical as a function of molecular weight, *Environ. Sci. Technol.*,
823 44, 5714-5720, 2010.

824 Ervens, B., Turpin, B., and Weber, R.: Secondary organic aerosol formation in cloud droplets
825 and aqueous particles (aqSOA): a review of laboratory, field and model studies, *Atmos.*
826 *Chem. Phys.*, 11, 11069-11102, 2011.

827 Faust, B. C., and Allen, J. M.: Aqueous-phase photochemical sources of peroxy radicals and
828 singlet molecular oxygen in clouds and fog, *J. Geophys. Res. Atmos.*, 97, 12913-12926,
829 1992.

830 Finlayson-Pitts, B. J., and Pitts Jr, J. N.: Chemistry of the upper and lower atmosphere: theory,
831 experiments, and applications, [Academic Press, San Diego](#), 1999.

832 Galbavy, E. S., Ram, K., and Anastasio, C.: 2-Nitrobenzaldehyde as a chemical actinometer for
833 solution and ice photochemistry, *J. Photochem. Photobiol.*, A, 209, 186-192, 2010.

834 Ge, X., Shaw, S. L., and Zhang, Q.: Toward understanding amines and their degradation
835 products from postcombustion CO₂ capture processes with aerosol mass spectrometry,
836 *Environmental Science & Technology*, 48, 5066-5075, 2014.

837 Grebel, J. E., Pignatello, J. J., and Mitch, W. A.: Sorbic acid as a quantitative probe for the
838 formation, scavenging and steady-state concentrations of the triplet-excited state of
839 organic compounds, *Water Res.*, 45, 6535-6544, 2011.

840 Haag, W. R., and Gassman, E.: Singlet oxygen in surface waters—Part I: Furfuryl alcohol as a
841 trapping agent, *Chemosphere*, 13, 631-640, 1984.

842 Haag, W. R., and Hoigné, J.: Singlet oxygen in surface waters .3. Photochemical formation and
843 steady-state concentrations in various types of waters, *Environ. Sci. Technol.*, 20, 341-
844 348, 1986.

845 Hawkins, L. N., Welsh, H. G., and Alexander, M. V.: Evidence for pyrazine-based
846 chromophores in cloud water mimics containing methylglyoxal and ammonium sulfate,
847 Atmospheric Chemistry & Physics, 18, [12413-12431](https://doi.org/10.5194/acp-18-12413-2018), 2018.

848 He, C., Liu, J., Carlton, A., Fan, S., Horowitz, L., Levy, I., and Tao, S.: Evaluation of factors
849 controlling global secondary organic aerosol production from cloud processes, Atmos.
850 Chem. Phys., 13, 1913-1926, 2013.

851 Heald, C. L., Collett Jr, J., Lee, T., Benedict, K., Schwandner, F., Li, Y., Clarisse, L., Hurtmans,
852 D., Van Damme, M., and Clerbaux, C.: Atmospheric ammonia and particulate inorganic
853 nitrogen over the United States, Atmos. Chem. Phys., 12, 10295-10312, 2012.

854 Hecobian, A., Zhang, X., Zheng, M., Frank, N., Edgerton, E. S., and Weber, R. J.: Water-Soluble
855 Organic Aerosol material and the light-absorption characteristics of aqueous extracts
856 measured over the Southeastern United States, Atmos. Chem. Phys., 10, 5965-5977,
857 2010.

858 Herner, J. D., Ying, Q., Aw, J., Gao, O., Chang, D. P., and Kleeman, M. J.: Dominant
859 mechanisms that shape the airborne particle size and composition distribution in central
860 California, Aerosol Sci. Technol., 40, 827-844, 2006.

861 Herrmann, H., Hoffmann, D., Schaefer, T., Brauer, P., and Tilgner, A.: Tropospheric aqueous-
862 phase free-radical chemistry: Radical sources, spectra, reaction kinetics and prediction
863 tools, ChemPhysChem, 11, 3796-3822, 2010a.

864 Herrmann, H., Hoffmann, D., Schaefer, T., Bräuer, P., and Tilgner, A.: Tropospheric aqueous-
865 phase free-radical chemistry: Radical sources, spectra, reaction kinetics and prediction
866 tools, ChemPhysChem, 11, 3796-3822, 2010b.

867 Herrmann, H., Schaefer, T., Tilgner, A., Styler, S. A., Weller, C., Teich, M., and Otto, T.:
868 Tropospheric aqueous-phase chemistry: Kinetics, mechanisms, and its coupling to a
869 changing gas phase, Chem. Rev., 115, 4259-4334, 2015.

870 Hoffer, A., Gelencsér, A., Guyon, P., Kiss, G., Schmid, O., Frank, G., Artaxo, P., and Andreae,
871 M.: Optical properties of humic-like substances (HULIS) in biomass-burning aerosols,
872 Atmos. Chem. Phys., 6, 3563-3570, 2006.

873 Jimenez, J., Canagaratna, M., Donahue, N., Prevot, A., Zhang, Q., Kroll, J. H., DeCarlo, P. F.,
874 Allan, J. D., Coe, H., and Ng, N.: Evolution of organic aerosols in the atmosphere,
875 Science, 326, 1525-1529, 2009.

876 Kaur, R., and Anastasio, C.: Light absorption and the photoformation of hydroxyl radical and
877 singlet oxygen in fog waters, Atmos. Environ., 164, 387-397, 2017.

878 Kaur, R., and Anastasio, C.: Light absorption coefficients of aqueous extracts of wintertime PM
879 collected in Davis, CA, USA., PANGAEA, DOI:
880 <https://doi.pangaea.de/10.1594/PANGAEA.896422>, 2018a.

881 Kaur, R., and Anastasio, C.: First measurements of organic triplet excited states in atmospheric
882 waters, Environ. Sci. Technol., 52, 5218-5226, 2018b.

883 Kirchstetter, T., and Thatcher, T.: Contribution of organic carbon to wood smoke particulate
884 matter absorption of solar radiation, Atmos. Chem. Phys., 12, 6067-6072, 2012.

885 Laskin, A., Laskin, J., and Nizkorodov, S. A.: Chemistry of atmospheric brown carbon, Chem.
886 Rev., 115, 4335-4382, 2015.

887 Latch, D. E., and McNeill, K.: Microheterogeneity of singlet oxygen distributions in irradiated
888 humic acid solutions, Science, 311, 1743-1747, 2006.

889 Lim, H.-J., Carlton, A. G., and Turpin, B. J.: Isoprene forms secondary organic aerosol through
890 cloud processing: Model simulations, Environ. Sci. Technol., 39, 4441-4446, 2005.

891 Lim, Y., Tan, Y., Perri, M., Seitzinger, S., and Turpin, B.: Aqueous chemistry and its role in
892 secondary organic aerosol (SOA) formation, *Atmos. Chem. Phys.*, 10, 10521-10539,
893 2010.

894 Lim, Y., and Turpin, B.: Organic peroxide and OH formation in aerosol and cloud water:
895 laboratory evidence for this aqueous chemistry, *Atmospheric Chemistry & Physics*
896 | *Discussions*, 15, [12867-12877](#), 2015.

897 Tropospheric ultraviolet-visible model (TUV) version 4.1
898 http://cprm.acom.ucar.edu/Models/TUV/Interactive_TUV/, 2002

899 McNeill, K., and Canonica, S.: Triplet state dissolved organic matter in aquatic photochemistry:
900 Reaction mechanisms, substrate scope, and photophysical properties, *Environ. Sci.*
901 *Process. Impact.*, 18, 1381-1399, 2016.

902 Parworth, C. L., Young, D. E., Kim, H., Zhang, X., Cappa, C. D., Collier, S., and Zhang, Q.:
903 Wintertime water-soluble aerosol composition and particle water content in Fresno,
904 California, *J. Geophys. Res. Atmos.*, 122, 3155-3170, 2017.

905 Rossignol, S. p., Aregahegn, K. Z., Tinel, L., Fine, L., Nozière, B., and George, C.: Glyoxal
906 induced atmospheric photosensitized chemistry leading to organic aerosol growth,
907 *Environ. Sci. Technol.*, 48, 3218-3227, 2014.

908 Seinfeld, J. H., and Pandis, S. N.: *Atmospheric chemistry and physics: from air pollution to*
909 | *climate change*, John Wiley & Sons, [Hoboken, New Jersey](#), 2012.

910 Silva, P. J., Liu, D.-Y., Noble, C. A., and Prather, K. A.: Size and chemical characterization of
911 individual particles resulting from biomass burning of local Southern California species,
912 *Environ. Sci. Technol.*, 33, 3068-3076, 1999.

913 Smith, J. D., Sio, V., Yu, L., Zhang, Q., and Anastasio, C.: Secondary organic aerosol production
914 from aqueous reactions of atmospheric phenols with an organic triplet excited state,
915 *Environ. Sci. Technol.*, 48, 1049-1057, 2014.

916 Smith, J. D., Kinney, H., and Anastasio, C.: Aqueous benzene-diols react with an organic triplet
917 excited state and hydroxyl radical to form secondary organic aerosol, *Phys. Chem. Chem.*
918 *Phys.*, 17, 10227-10237, 2015.

919 Sun, H. L., Biedermann, L., and Bond, T. C.: Color of brown carbon: A model for ultraviolet and
920 visible light absorption by organic carbon aerosol, *Geophys. Res. Lett.*, 34, L17813,
921 2007.

922 Thompson, A. M.: The oxidizing capacity of the Earth's atmosphere: Probable past and future
923 changes, *Science*, 256, 1157-1165, 1992.

924 Tong, H., Arangio, A. M., Lakey, P. S., Berkemeier, T., Liu, F., Kampf, C. J., Brune, W. H.,
925 Pöschl, U., and Shiraiwa, M.: Hydroxyl radicals from secondary organic aerosol
926 decomposition in water, *Atmos. Chem. Phys.*, 16, 1761-1771, 2016.

927 Tong, H., Lakey, P. S., Arangio, A. M., Socorro, J., Kampf, C. J., Berkemeier, T., Brune, W. H.,
928 Pöschl, U., and Shiraiwa, M.: Reactive oxygen species formed in aqueous mixtures of
929 secondary organic aerosols and mineral dust influencing cloud chemistry and public
930 health in the Anthropocene, *Faraday Discuss.*, 200, 251-270, 2017.

931 Tratnyek, P. G., and Hoigné, J.: Photo-oxidation of 2,4,6-trimethylphenol in aqueous laboratory
932 solutions and natural waters: Kinetics of reaction with singlet oxygen, *J. Photochem.*
933 *Photobiol.*, A, 84, 153-160, 1994.

934 Tsui, W. G., Rao, Y., Dai, H.-L., and McNeill, V. F.: Modeling photosensitized secondary
935 organic aerosol formation in laboratory and ambient aerosols, *Environ. Sci. Technol.*, 51,
936 7496-7501, 2017.

937 USGS: U.S. Geological Survey. Water Properties - Dissolved Oxygen. Available at
938 <https://water.usgs.gov/edu/dissolvedoxygen.html> [last accessed: January 23, 2018], 2018.

- 939 Varga, B., Kiss, G., Ganszky, I., Gelencsér, A., and Krivacsy, Z.: Isolation of water-soluble
940 organic matter from atmospheric aerosol, *Talanta*, 55, 561-572, 2001.
- 941 Wenk, J., Von Gunten, U., and Canonica, S.: Effect of dissolved organic matter on the
942 transformation of contaminants induced by excited triplet states and the hydroxyl radical,
943 *Environ. Sci. Technol.*, 45, 1334-1340, 2011.
- 944 Wenk, J., Eustis, S. N., McNeill, K., and Canonica, S.: Quenching of excited triplet states by
945 dissolved natural organic matter, *Environ. Sci. Technol.*, 47, 12802-12810, 2013.
- 946 Wilkinson, F., Helman, W. P., and Ross, A. B.: Rate constants for the decay and reactions of the
947 lowest electronically excited singlet-state of molecular-oxygen in solution - an expanded
948 and revised compilation, *J. Phys. Chem. Ref. Data*, 24, 663-1021, 1995.
- 949 Young, D. E., Kim, H., Parworth, C., Zhou, S., Zhang, X., Cappa, C. D., Seco, R., Kim, S., and
950 Zhang, Q.: Influences of emission sources and meteorology on aerosol chemistry in a
951 polluted urban environment: results from DISCOVER-AQ California, *Atmos. Chem.
952 Phys.*, 16, 5427-5451, 2016.
- 953 Yu, L., Smith, J., Laskin, A., Anastasio, C., Laskin, J., and Zhang, Q.: Chemical characterization
954 of SOA formed from aqueous-phase reactions of phenols with the triplet excited state of
955 carbonyl and hydroxyl radical, *Atmos. Chem. Phys.*, 14, 13801-13816, 2014.
- 956 Yu, L., Smith, J., Laskin, A., George, K. M., Anastasio, C., Laskin, J., Dillner, A. M., and
957 Zhang, Q.: Molecular transformations of phenolic SOA during photochemical aging in
958 the aqueous phase: competition among oligomerization, functionalization, and
959 fragmentation, *Atmos. Chem. Phys.*, 16, 4511-4527, 2016.
- 960 Zepp, R. G., Wolfe, N. L., Baughman, G. L., and Hollis, R. C.: Singlet oxygen in natural waters,
961 *Nature*, 267, 421-423, 1977.
- 962 Zepp, R. G., Schlotzhauer, P. F., and Sink, R. M.: Photosensitized transformations involving
963 electronic energy transfer in natural waters: role of humic substances, *Environ. Sci.
964 Technol.*, 19, 74-81, 1985.
- 965 Zhou, H., Yan, S., Lian, L., and Song, W.: Triplet-state Photochemistry of Dissolved Organic
966 Matter: Triplet-state Energy Distribution and Surface Electric Charge Conditions,
967 *Environ. Sci. Technol.*, 53, 2482-2490, 2019.
- 968 Zhou, X., and Mopper, K.: Determination of photochemically produced hydroxyl radicals in
969 seawater and freshwater, *Mar. Chem.*, 30, 71-88, 1990.

970

1 Supporting Information for:

2 **Photooxidants from Brown Carbon and Other Chromophores in**
3 **Illuminated Particle Extracts**

4 Richie Kaur¹, Jacqueline R. Labins¹, Scarlett S. Helbock¹, Wenqing Jiang², Keith J.
5 Bein³, Qi Zhang², Cort Anastasio^{1,*}

6 ¹Department of Land, Air and Water Resources, University of California-Davis, One Shields Avenue,
7 Davis, CA 95616-8627, USA

8 ²Department of Environmental Toxicology, University of California-Davis, One Shields Avenue, Davis,
9 CA 95616-8627, USA

10 ³Center for Health and the Environment, University of California-Davis, One Shields Avenue, Davis, CA
11 95616-8627, USA

12
13 Correspondence to: C. Anastasio (canastasio@ucdavis.edu)

14
15 Originally Submitted to Atmospheric Chemistry and Physics, 2 December 2018

16 Revised and Submitted on **23 April** 2019

Table of Contents

1. Text Sections

17		
18		
19		
20	S1. Hydroxyl radical measurements in PME3 and PME3D extracts.....	<u>35</u>
21	S2. $\cdot\text{OH}$ sink measurements (k'_{OH}) in field blanks FB1 and FB2.....	<u>39</u>
22	S3. Other oxidants in PM extracts.....	<u>42</u>
23	S4. Impacts of mass transport and increasing organic concentration on estimates of aqueous photooxidant concentrations in ambient	
24	particles.....	<u>46</u>
25	S5. Estimating triplet characteristics in particle extract PME3.....	<u>50</u>
26	S6. References.....	<u>53</u>
27		

2. Tables and Figures

28		
29	Table S1. Sample collection details and light absorption of particle extracts.....	<u>4</u>
30	Table S2. Chemical characteristics of particle extracts.....	<u>6</u>
31	Table S3. Hydroxyl radical measurements.....	<u>7</u>
32	Table S4. Contributions of nitrite, nitrate and other sources to $\cdot\text{OH}$ photoproduction.....	<u>9</u>
33	Table S5. Determination of chloride as an $\cdot\text{OH}$ sink, following procedure of Anastasio and Newberg (2007).....	<u>10</u>
34	Table S6. Contributions of nitrite, chloride and organics to k'_{OH}	<u>11</u>
35	Table S7. Singlet oxygen measurements.....	<u>12</u>
36	Table S8. Syringol loss kinetics.....	<u>13</u>
37	Table S9. Methyl jasmonate loss kinetics.....	<u>14</u>
38	Table S10. Second-order rate constants for reactions of syringol and methyl jasmonate with hydroxyl radical, singlet oxygen, and	
39	triplet excited states.....	<u>15</u>
40	Table S11. Characteristics of model triplet species.....	<u>16</u>
41	Table S12. Best triplet matches and best estimate triplet steady-state concentrations.....	<u>17</u>
42	Table S13. Measurements of triplet excited states of organic matter.....	<u>18</u>
43	Table S14. Particle mass to water mass ratios in the PME3 extracts, typical fog drops, and particles.....	<u>20</u>
44	Table S15. Photooxidant concentrations (formed <i>in situ</i>) in PME3D extracts and expected values in ambient particles.....	<u>21</u>
45	Table S16. Gas- and aqueous-phase reaction rate constants for selected organic compounds with the major oxidants.....	<u>22</u>
46	Table S17. Fate of selected organic compounds in fog and particles.....	<u>23</u>
47	Figure S1. $\cdot\text{OH}$ measurement in extract PME5.....	<u>24</u>
48	Figure S2. Singlet oxygen kinetic measurements in extract PME5 diluted 1:1 (volume : volume) with H_2O or D_2O	<u>25</u>
49	Figure S3. Top panel: Light absorbance by fog samples collected during 2011-12 in Davis, CA. Bottom panel: Mass absorption	
50	coefficient of DOC in the Davis fog samples.....	<u>26</u>
51	Figure S4. Correlation between the rate of sunlight absorption (R_{abs}) in the 300-450 nm wavelength range and dissolved organic	
52	carbon (DOC) for the fog samples and particle extracts (PME).....	<u>27</u>

53	Figure S5. (Top) Ratio of pathlength-normalized absorbance for PME and fog samples with highest (black) and median (grey)	
54	absorbances. (Bottom): Ratio of mass absorption coefficients of DOC in PME and fog samples with highest (black) and median (grey)	
55	absorbances.	28
56	Figure S6. (Top) Correlation between the rate of $\cdot\text{OH}$ photoproduction due to sources other than nitrite and nitrate and the	
57	concentration of dissolved organic carbon (DOC). (Bottom) Correlation between apparent pseudo-first order rate constant for loss of	
58	$\cdot\text{OH}$ due to organic sinks (obtained by subtracting inorganic contributions from the measured k'_{OH}) and DOC.....	29
59	Figure S7. Comparison of hydroxyl radical steady-state concentrations formed <i>in situ</i> in various atmospheric waters	30
60	Figure S8. Loss of probes for measuring triplet excited states: syringol (SYR) and methyl jasmonate (MeJA) in extract PME5.....	31
61	Figure S9. Winter-solstice-normalized pseudo-first-order rate constants (k'_{Probe}) for loss of syringol (top panel) and methyl jasmonate	
62	32
63	Figure S10. Dependence of rate of $\cdot\text{OH}$ photoproduction (P_{OH} ; red circles, left y-axis) and rate constant for loss of $\cdot\text{OH}$ due to natural	
64	sinks (k'_{OH} ; blue squares, right y-axis) with PM mass/water mass ratio in three PME3D samples	33
65	Figure S11. Fate of five model organic compounds – syringol, methyl jasmonate, tyrosine, 1,2,4-butanetriol and 3-hydroxy-2,5-	
66	bis(hydroxymethyl)furan – under fog (left of vertical dashed line) and PM (right of dashed line) conditions using an upper-bound	
67	estimate for triplet concentrations in PM.....	34
68	Table S18. Determination of hydroxyl radical steady-state concentrations, [$\cdot\text{OH}$], from results of the MBO experiments.....	37
69	Figure S12. Measured pseudo-first-order rate constant for loss of $\cdot\text{OH}$ due to natural sinks (k'_{OH}) in various solutions using sodium	
70	benzoate/benzoic acid and benzene as $\cdot\text{OH}$ probes.....	40
71	Table S 19. Estimates of the organic sink of $^1\text{O}_2^*$ in aqueous particles at 1 $\mu\text{g-PM}/\mu\text{g-H}_2\text{O}$	48
72	Figure S13. Change in triplet steady-state concentration with dissolved organic carbon concentration in the PME3D extracts.	52
73		

Table S1. Sample collection details and light absorption of particle extracts

Sample ID	Collection Dates	Collection Times ^d	Average hourly PM _{2.5} concentration ^e ($\mu\text{g}/\text{m}^3\text{-air}$)	α_{300} ^f (cm^{-1})	Average Mass of PM extracted ^g	R_{abs} (300-450nm) ^h (10^{-6} mol-photons $\text{L}^{-1} \text{s}^{-1}$)	$f_{\text{Rabs IN}}$ ⁱ	MAC _{DOC} (300 nm) ^j ($10^4 \text{ cm}^2 \text{ g}^{-1}\text{-C}$)	AAE ^k	Light Screening Factor ^l
Particle Extracts										
PME1 ^{*a}	01/06/16 - 01/08/16	17:30 - 07:30 (N)	5.8 (2.1)	0.077	105 (16)	1.7	0.00080	2.6	6.8	0.98
PME2 ^{*a}	12/18/15 - 12/20/15	17:30 - 07:30 (N)	15 (10)	0.100	269 (30)	1.8	0.0059	2.0	7.2	0.97
PME3 ^b	01/26/16 - 01/29/16	10:20 - 09:45 (C)	16 (11)	0.272	328 (19)	4.2	0.0076	1.3	7.9	0.93
PME4 ^b	12/16/15 - 12/18/15	17:30 - 07:30 (N)	20 (8)	0.567	350 (14)	12	0.0031	2.6	6.4	0.85
PME5 ^b	01/10/16 - 01/12/16	17:30 - 07:30 (N)	5.9 (3.4)	0.317	132 (11)	7.4	0.00080	2.6	6.2	0.91
PME6 ^b	01/23/16 - 01/26/16	17:30 - 07:30 (N)	6.8 (2.9)	0.584	174 (14)	13	0.00058	3.0	6.9	0.84
PME3D0.5 ^c				0.556	323 (21)	8.8			7.7	0.87
PME3D1.3 ^c				0.199	315 (23)	3.2	0.0071	1.3	7.6	0.95
PME3D2.5 ^{*a}				0.103	331 (15)	1.7	0.0092	1.3	7.6	0.97
PME3D10 ^c				0.0263	347	0.42	0.0062	1.3	7.6	0.99
Averages ($\pm\sigma$)										
“Standard” (PME3-6)				0.44 (0.16)		9.1 (4.1)	0.0030 (0.0033)	2.4 (0.7)	6.8 (0.7)	
“Dilute” (PME1 [*] -2 [*] ,3D2.5 [*])				0.093 (0.014)		1.7 (0.1)	0.0053 (0.0042)	2.0 (0.6)	7.2 (0.4)	
Davis Fog ^m				0.094 (0.047)		1.8 (0.9)	0.0082 (0.0031)	1.3 (0.1)	6.6 (0.5)	
Test statistic ⁿ				0.021		0.035	0.061	0.013	0.56	
Field Blanks										
FB1 ^a	12/18/15	09:38 - 09:40		0.0025	17.8 (7.6)	0.024				
FB2 ^b	01/20/16	10:08 - 10:10		0.0037	24.9 (9.1)	0.022				

75 ^a Samples extracted in 2.5 mL/filter square and referred to as the “dilute” extracts in the main text.

76 ^b PME3-6 were extracted as 1 mL/filter square and are referred to as “standard” extracts in the main text.

77 ^c PME3D0.5, PME3D1.3 and PME3D10 are extracts of sample PME3 using varying extraction volumes per filter square, namely 0.5 , 1.3 and 10

78 mL, respectively.

79 ^d N = Night-time samples, collected from 17:30 on one day until 07:30 AM the next day; this was done for consecutive days on the same filter. C

80 = Continuous collection for the indicated number of days.

81 ^e Average ($\pm 1\sigma$) hourly PM_{2.5} concentration for each sampling period measured at the UC Davis sampling site by the California Air Resources

82 Board as reported on the iADAM online database (California Air Resources Board, 2018).

83 ^f Base-10 absorbance of the extract (in cm^{-1}) at 300 nm.

84 ^g Average ($\pm 1\sigma$) mass of PM extracted from each filter square for a given sample.

85 ^h Rate of sunlight absorption by each extract in the 300 – 450 nm wavelength range (Eq. (2), main text).

86 ⁱ Fraction of calculated sunlight absorption due to inorganic nitrogen (nitrite and nitrate) in each sample. Equations are in Kaur and Anastasio

87 (2017).

88 ^j Mass absorption coefficient of dissolved organic species at 300 nm for each sample (Eq. (3), main text) in units of $10^4 \text{ cm}^2 \text{ g}^{-1}\text{-C}$.

89 ^k Absorption Angstrom Exponent (AAE), calculated as the negative of the slope of a linear regression of the extract absorbance data between 300
90 and 450 nm versus the log of the wavelength: $\log(\text{Abs}_\lambda) = \log(\text{Abs}_{300}) - \text{AAE} \times \log(\lambda)$, where λ is the wavelength and Abs_λ and Abs_{300} are the
91 absorbance values at λ and 300 nm, respectively.

92 ^l Light-absorption-weighted internal screening factor, calculated as $S_\lambda = \frac{\Sigma[(1-10^{-\alpha_\lambda l}) \times I'_\lambda]}{\Sigma[(2.303 \times \alpha_\lambda l) \times I'_\lambda]}$. In this equation, α_λ is the pathlength-normalized

93 absorbance of the extract at each wavelength, summed for the wavelength range in which light absorption by the extracts was the highest (280-
94 350 nm); l is the pathlength of the quartz tube used for illuminating the extracts (0.4 cm); I'_λ is the actinic flux ($\text{mol-photon L}^{-1} \text{s}^{-1}$) of the
95 illumination system, calculated using the photon count of the illumination system measured using a TIDAS Photo Diode Array Spectrometer
96 and the measured pseudo-first-order rate constant for loss of our chemical actinometer, 2-nitrobenzaldehyde. The numerator represents the
97 actual rate of light absorption by all chromophores in the extract while the denominator is the estimated rate of light absorption in the extract
98 assuming it is low light-absorbing. A value of 1.0 indicates no light screening (Smith et al., 2014; Rehorek and Seidel, 1989).

99 ^m Average values previously measured in Davis fog samples ($n = 4$) (Kaur and Anastasio, 2017).

100 ⁿ Test statistic for comparison of standard PME and Davis fog averages: p -value for a two-tailed t -test for samples of unequal variance. Values
101 below 0.05 are in bold.

102 | **Table S2.** Chemical characteristics of particle extracts

Sample ID	DOC μM-C	[NO ₂] μM	[NO ₃] μM	[SO ₄ ²⁻] μM	[Cl] μM	[HCOO] μM	[NH ₄ ⁺] μM	[Na ⁺] μM	[K ⁺] μM	[Ca ²⁺] μM	[Mg ²⁺] μM
Particle Extracts											
PME1 ^{*a}	562	0.29	113	12.5	15.7	2.1	55.3	82.3	29.9	2.5	0.0
PME2 ^{*a}	900	2.8	884	31.3	19.8	4.1	751	78.9	43.0	8.3	2.3
PME3 ^b	3610	10.2	2520	302	66.3	13.0	2580	343	171	22.1	3.3
PME4 ^b	4090	8.3	3290	91.1	69.6	21.4	2010	317	197	44.1	11.3
PME5 ^b	2350	3.8	375	22.9	36.7	10.9	287	287	76.7	9.8	2.2
PME6 ^b	3720	5.4	432	65.6	77.7	4.9	276	362	97.2	13.0	7.4
PME3D0.5 ^c	7132	18	4820	533	127	27	5052	681	342	53	6.4
PME3D1.3	2760	6.4	1830	216	48.2	10.5	1600	233	105	20.0	1.6
PME3D2.5 ^a	1400	4.1	1250	195	27.3	5.1	816	118	42.6	4.7	1.3
PME3D10	356	1.2	183	28.1	6.9	1.0	177	24.3	11.9	0.0	0.0
Averages (±σ)											
“Standard” (PME3-6)	3440 (760)	6.9 (2.9)	1650 (1480)	120 (124)	62.6 (17.9)	12.5 (6.8)	1290 (1190)	327 (33)	136 (58)	22.2 (15.5)	6.1 (4.1)
“Dilute” (PME1*- 2*,3D2.5*)	953 (419)	2.4 (1.9)	749 (580)	80 (101)	20.9 (5.9)	3.8 (1.5)	541 (420)	93.2 (21.9)	38.5 (7.4)	5.2 (2.9)	1.2 (1.1)
Davis Fog	1240 (560)	3.4 (6.1)	1080 (630)	120 (84)	22.9 (13.0)	5.1 (2.6)	1070 (550)	- ^d	3.5 (1.9)	4.2 (1.1)	1.4 (0.4)
Test statistic ^e	0.0042	0.35	0.51	0.98	0.013	0.11	0.75	-	0.019	0.10	0.11
Field Blanks											
FB1 ^a	78.9	0	4.5	0.8	9.0	1.1	3.1	63.8	8.3	1.4	0.0
FB2 ^b	244	0	1.1	0.4	6.1	9.0	12.3	143.5	10.9	3.4	0.0
MQ	< DL	< DL	< DL	< DL	< DL	< DL	< DL	1.8	< DL	< DL	< DL

103 ^a Samples extracted in 2.5 mL/filter square and referred to as the “dilute” extracts in the main text.

104 ^b Samples extracted in 1mL/filter square and are referred to as “standard” extracts in the main text.

105 ^c DOC and IC values for sample PME3D0.5 were not measured due to a shortage of sample; instead, they were estimated by extrapolating the
106 linear trends between these values and concentration factors for the other PME3 samples, namely, PME3, PME3D1.3, PME3D2.5 and
107 PME3D10.

108 ^d Sodium could not be measured in the 2011 Davis fog samples due to high background sodium content .

109 ^e Test statistic for comparison of standard PME and Davis fog averages: *p*-value for a two-tailed *t*-test for samples of unequal variance. Values
110 below 0.05 are in bold.

111 **Table S3.** Hydroxyl radical measurements

Sample ID	P_{OH}^a $10^{-10} M s^{-1}$	P_{OH}^a $\mu M h^{-1}$	k'_{OH}^b $10^6 s^{-1}$	τ_{OH}^c μs	$[^{\bullet}OH]^d$ $10^{-16} M$	$10^4 \times \Phi_{OH}^f$	$k'_{OH,org} / [DOC]^g$ $10^8 L (mol-C)^{-1} s^{-1}$
Particle Extracts							
PME1*	1.0 (0.1)	0.37 (0.04)	0.63 (0.01)	1.6 (0.1)	1.7 (0.2)	0.62 (0.06)	11.1 (0.2)
PME2*	2.0 (0.2)	0.71 (0.07)	0.44 (0.04)	2.3 (0.2)	4.5 (0.6)	1.1 (0.1)	4.6 (0.4)
PME3	14.7 (0.3)	5.3 (0.1)	<u>1.9 (0.4)</u>	<u>0.54 (0.13)</u>	<u>7.9 (1.9)</u> ^e	3.5 (0.1)	<u>4.9 (1.2)</u>
PME4	14 (2)	5.2 (0.6)	2.3 (0.2)	0.43 (0.03)	6.3 (0.6)	1.2 (0.1)	5.4 (0.4)
PME5	4.6 (0.5)	1.7 (0.2)	1.6 (0.1)	0.62 (0.03)	2.8 (0.3)	0.63 (0.07)	6.8 (0.4)
PME6	13 (3)	4.8 (1.0)	4.0 (0.8)	0.25 (0.05)	3.3 (0.3)	1.1 (0.2)	11 (2)
PME3D0.5					<u>7.3 (1.8)</u> ^e		
PME3D1.3					<u>3.0 (0.8)</u> ^e		
PME3D2.5*	3.1 (0.1)	1.1 (0.02)	<u>0.94 (0.29)</u>	<u>1.1 (0.3)</u>	<u>3.3 (1.0)</u> ^e	1.86 (0.03)	<u>6.4 (2.0)</u>
PME3D10	0.47 (0.04)	0.17 (0.01)	<u>0.071(0.031)</u>	<u>14 (6)</u>	<u>6.6 (2.8)</u> ^e	1.1 (0.1)	<u>1.7 (0.7)</u>
Averages ($\pm\sigma$)							
“Standard” (PME3-6)	12 (5)	4.2 (1.7)	<u>2.5 (1.1)</u>	<u>0.46 (0.16)</u>	<u>5.1 (2.4)</u>	1.6 (1.3)	<u>6.9 (2.6)</u>
“Dilute” (PME1*-2*,3D2.5*)	2.0 (1.0)	0.73 (0.37)	<u>0.67 (0.63)</u>	1.6 (0.6)	<u>3.2 (1.4)</u>	1.2 (0.6)	<u>7.4 (3.4)</u>
Davis Fog	3.5 (1.0)	1.3 (0.3)	0.87 (0.31)	1.2 (0.4)	4.2 (0.7)	2.4 (1.7)	7.5 (3.2)
Test statistic ^h	0.039	0.039	<u>0.058</u>	0.019	<u>0.51</u>	0.47	<u>0.79</u>
Field Blanks ⁱ							
FB1 (dilute)	≤ 0.012	≤ 0.045	0.34 (0.04)	3.0 (0.4)			
FB2 (standard)	≤ 0.012	≤ 0.042	0.27 (0.01)	3.8 (0.2)			

112 Listed uncertainties (in parentheses) are ± 1 standard error from the errors in inverse plot ($1/R_p^*$ vs. $1/[Benzene]$) parameters, except for the
 113 averages ($\pm 1\sigma$)

114 All equations used for these calculations are discussed in Kaur and Anastasio (2017) unless otherwise stated.

115 * Samples extracted in 2.5 mL/filter square and referred to as the “dilute” extracts in the main text.

116 ^a Davis winter solstice-normalized rate of $^{\bullet}OH$ photoproduction.

117 ^b Apparent pseudo-first rate constant for destruction of $^{\bullet}OH$ due to natural sinks .

118 ^c Lifetime of $^{\bullet}OH$, calculated as $1/k'_{OH}$.

119 ^d Winter solstice-normalized steady-state concentration of $^{\bullet}OH$.

120 ^e $^{\bullet}OH$ concentrations in PME3 and PME3D extracts were measured using MBO as a probe, corrected for loss due to quenching by MBO
 121 (discussed in Sect. S1). k'_{OH} for these samples was calculated as $P_{OH} / [^{\bullet}OH]$.

122 ^f Apparent quantum yield of $^{\bullet}OH$ during simulated sunlight illumination, calculated as $\Phi_{OH} = P_{OH} / R_{abs}$.

123 ^g Ratio of $k'_{OH,org}$ (rate constant for loss of $^{\bullet}OH$ due to organics only; Table S6) to the DOC concentration.

124 ^h Test statistic for comparison of standard PME and Davis fog averages: p -value for a two-tailed t -test for samples of unequal variance. Values
125 below 0.05 are in bold.
126 ⁱ Blanks were analyzed by adding 1.5 mM benzene to an aliquot of the blank. Very little phenol formation was observed after 200 minutes of
127 illumination in both blanks, which was used to calculate the upper limit P_{OH} .

128 **Table S4.** Contributions of nitrite, nitrate and other sources to $\cdot\text{OH}$ photoproduction

Sample ID	$f_{\text{POH,NO}_2^-}$ ^a	$f_{\text{POH,NO}_3^-}$ ^b	$f_{\text{POH,Other}}$ ^c
Particle Extracts			
PME1*	0.072 (0.010)	0.15 (0.02)	0.78 (0.02)
PME2*	0.36 (0.05)	0.63 (0.09)	0.011 (0.010)
PME3	0.18 (0.02)	0.24 (0.02)	0.58 (0.03)
PME4	0.15 (0.02)	0.32 (0.05)	0.53 (0.05)
PME5	0.21 (0.03)	0.11 (0.02)	0.67 (0.04)
PME6	0.11 (0.03)	0.046 (0.011)	0.85 (0.03)
PME3D0.5	-	-	-
PME3D1.3	-	-	-
PME3D2.5*	0.35 (0.04)	0.57 (0.06)	0.084 (0.068)
PME3D10	0.67 (0.08)	0.55 (0.07)	-0.22 (0.11) ^d
Averages ($\pm\sigma$)			
“Standard” (PME3-6)	0.16 (0.05)	0.18 (0.12)	0.66 (0.14)
“Dilute” (PME1*- 2*,3D2.5*)	0.26 (0.16)	0.45 (0.26)	0.29 (0.42)
Davis Fog	0.24 (0.40)	0.46 (0.29)	0.41 (0.41)

129 Listed uncertainties (in parentheses) are ± 1 standard error calculated from propagating errors in individual terms, except for the averages ($\pm 1\sigma$).

130 * Samples extracted in 2.5 mL/filter square and referred to as the “dilute” extracts in the main text.

131 ^a Fraction of $\cdot\text{OH}$ photoproduction rate attributable to nitrite. Calculated as $(j_{\text{NO}_2 \rightarrow \text{OH}} \times [\text{NO}_2^-]) / P_{\text{OH}}$ where the numerator is the rate of $\cdot\text{OH}$ photoproduction due
 132 to nitrite ($P_{\text{OH,NO}_2}$), and is the product of the aqueous photolysis rate constant under Davis winter-solstice sunlight, $j_{\text{NO}_2 \rightarrow \text{OH}} = 2.6 \times 10^{-5} \text{ s}^{-1}$ (Anastasio and
 133 McGregor, 2001), and the molar concentration of NO_2^- in each sample.

134 ^b Fraction $\cdot\text{OH}$ photoproduction rate attributable to nitrate. Calculated using an equation analogous to $f_{\text{POH,NO}_2^-}$, using aqueous nitrate photolysis rate constant,
 135 $j_{\text{NO}_3 \rightarrow \text{OH}} = 1.4 \times 10^{-7} \text{ s}^{-1}$ (Anastasio and McGregor, 2001) and molar concentration of NO_3^- in each sample.

136 ^c Fraction of $\cdot\text{OH}$ photoproduction due to non-nitrite and -nitrate sources; calculated as $(P_{\text{OH}} - P_{\text{OH,NO}_2^-} - P_{\text{OH,NO}_3^-}) / P_{\text{OH}}$.

137 ^d $f_{\text{POH,other}}$ is negative for PME3D10 indicating that the total rate of $\cdot\text{OH}$ photoproduction is over-predicted using the measured molar NO_2^- and NO_3^-
 138 concentrations.

139 **Table S5.** Determination of chloride as an $\cdot\text{OH}$ sink, following procedure of Anastasio and Newberg (2007)

Sample ID	Measured $k'_{\text{OH}}{}^c$ s^{-1}	$[\text{Cl}^-]{}^d$ M	$[\text{H}^+]{}^e$ M	$f_{\text{Cl}^- \text{re-formed}}{}^f$	$k'_{\text{OH,Cl}^-}{}^g$ s^{-1}	$f_{k_{\text{OH,Cl}^-}}{}^h$
PME1* ^a	6.3E+05	1.6E-05	6.31E-05	0.9997828	1.5E+01	2.3E-05
PME2* ^a	4.4E+05	2.0E-05	6.31E-05	0.99978	1.8E+01	4.2E-05
PME3	<u>1.9E+06</u>	6.6E-05	6.31E-05	0.99978	6.2E+01	<u>3.3E-05</u>
PME4	2.3E+06	7.0E-05	6.31E-05	0.99978	6.5E+01	2.8E-05
PME5	1.6E+06	3.7E-05	6.31E-05	0.999783	3.4E+01	2.1E-05
PME6	4.0E+06	7.8E-05	6.31E-05	0.99978	7.3E+01	1.8E-05
PME3D2.5* ^a	<u>9.4E+05</u>	2.7E-05	6.31E-05	0.99978	2.5E+01	<u>2.7E-05</u>
PME3D10 ^b	<u>7.1E+04</u>	6.9E-06	6.31E-05	0.999783	6.4E+00	<u>9.0E-05</u>

140 ^a Samples PME1*, PME2*, PME3D2.5 were extracted in 2.5 mL Milli-Q per filter square, and are referred to as “dilute extracts” in the main text.

141 ^b PME3D10 was extracted in 10 mL Milli-Q per filter square.

142 ^c Measured pseudo-first order rate constant for loss of $\cdot\text{OH}$.

143 ^d Measured chloride concentrations in the extracts.

144 ^e Hydrogen ion concentration. Since the extracts were acidified to pH 4.2, this value is constant across all extracts.

145 ^f Fraction of Cl^- reacting with $\cdot\text{OH}$ that ends up back as Cl^- and $\cdot\text{OH}$. Values are calculated based on the reactions 1-4 below and the equation f_{Cl^-}

146 $\text{re-formed} = k_4 / ((k_2 \times [\text{Cl}^-]) + (k_3 \times [\text{H}^+]) + k_4)$

147 ^g Rate constant for loss of $\cdot\text{OH}$ due to Cl^- based on the fraction of reformed Cl^- , calculated as $k'_{\text{OH,Cl}^-} = (1 - f_{\text{Cl}^- \text{re-formed}}) \times k_1$

148 ^h Fraction of measured k'_{OH} due to chloride.

149

150 (1) $\cdot\text{OH} + \text{Cl}^- \rightarrow \text{HOCl}^-$ $k_1 = 4.3\text{E}+09 \text{ M}^{-1}\text{s}^{-1}$

151 (2) $\text{HOCl}^- + \text{Cl}^- \rightarrow \cdot\text{Cl}_2^- + \text{OH}^-$, $k_2 = 1.0\text{E}+04 \text{ M}^{-1}\text{s}^{-1}$

152 (3) $\text{HOCl}^- + \text{H}^+ \rightarrow \text{Cl}^\cdot + \text{H}_2\text{O}$, $k_3 = 2.1\text{E}+10 \text{ M}^{-1}\text{s}^{-1}$

153 (4) $\text{HOCl}^- \rightarrow \text{Cl}^- + \cdot\text{OH}$, $k_4 = 6.4\text{E}+09 \text{ M}^{-1}\text{s}^{-1}$

154 **Table S6.** Contributions of nitrite, chloride and organics to k'_{OH}

Sample ID	Measured k'_{OH} ^c s ⁻¹	k'_{OH,NO_2^-} ^d s ⁻¹	k'_{OH,Cl^-} ^e s ⁻¹	$k'_{OH,org}$ ^f s ⁻¹	$f_{k_{OH,NO_2^-}}$ ^g	$f_{k_{OH,org}}$ ¹⁵⁵ _{hi}
PME1* ^a	6.3E+05	2.9E+03	1.5E+01	6.2E+05	0.0046	1.0
PME2* ^a	4.4E+05	2.7E+04	1.8E+01	4.1E+05	0.063	0.94
PME3	1.9E+06	1.0E+05	6.2E+01	1.8E+06	0.055	0.95
PME4	2.3E+06	8.3E+04	6.5E+01	2.2E+06	0.036	0.96
PME5	1.6E+06	3.8E+04	3.4E+01	1.6E+06	0.023	0.98
PME6	4.0E+06	5.4E+04	7.3E+01	4.0E+06	0.013	0.99
PME3D2.5* ^a	9.4E+05	4.1E+04	2.5E+01	9.0E+05	0.044	0.96
PME3D10 ^b	7.1E+04	1.2E+04	6.4E+00	5.9E+04	0.16	0.83

156 ^a Samples PME1*, PME2*, and PME3D2.5* were extracted in 2.5 mL Milli-Q per filter square, and are referred to as “dilute extracts” in the main
157 text.

158 ^b PME3D10 was extracted in 10 mL Milli-Q per filter square. All other extracts were extracted in 1.0 mL Milli-Q per filter square (standard
159 extracts).

160 ^c Measured pseudo-first order rate constant for loss of $\bullet OH$ (Table S3).

161 ^d Pseudo-first order rate constant for loss of $\bullet OH$ due to nitrite. Value is calculated as $k'_{OH,NO_2^-} = (k_{OH+NO_2^-} \times [NO_2^-])$ where $k_{OH+NO_2^-} = 1.1 \times 10^{10} M^{-1} s^{-1}$ (Barker et al., 1970).
162

163 ^e Pseudo-first order rate constant for loss of $\bullet OH$ due to chloride. Value is calculated using the reaction between $\bullet OH$ and Cl^- corrected for the
164 fraction of the initial product $HOCl^{\bullet}$ that fragments to reform $\bullet OH$ and Cl^- , as discussed in Table S5 and Anastasio and Newberg (2007).

165 ^f Calculated pseudo-first-order rate constant for loss of $\bullet OH$ due to organics, determined by subtracting the contribution of nitrite from the
166 measured k'_{OH} . Contributions to k'_{OH} from common inorganic ions, including sulfate, nitrate, chloride, bicarbonate/carbonate (see footnote *h*
167 below), and ammonium are negligible.

168 ^g Fraction of measured k'_{OH} due to nitrite.

169 ^h Fraction of measured $\bullet OH$ sink due to organic species, estimated by subtracting the contributions due to nitrite from the measured value of k'_{OH} .

170 ⁱ The upper bound of the fraction of the measured k'_{OH} due to bicarbonate (HCO_3^-) and carbonate (CO_3^{2-}) was calculated to be 1.1×10^{-6} based on
171 using the sample pH of 4.2 and assuming equilibrium with 400 ppm of atmospheric CO_2 . This fraction was calculated based on the CO_2
172 equilibria 1-3 below (Seinfeld and Pandis, 2012), $k_{OH+HCO_3^-} = 1 \times 10^7 M^{-1} s^{-1}$, and $k_{OH+CO_3^{2-}} = 4 \times 10^8 M^{-1} s^{-1}$ (Buxton et al., 1988b).

173 (1) $CO_2 \leftrightarrow CO_2 \cdot H_2O (aq)$, $K_{H^*} = 3.4E-02 M atm^{-1}$ (Physical Henry's law constant)

174 (2) $CO_2 \cdot H_2O (aq) \leftrightarrow H^+ + HCO_3^-$, $K_{a1} = 4.3E-07 M$ ($pK_{a1} = 6.3$)

175 (3) $HCO_3^- \leftrightarrow H^+ + CO_3^{2-}$, $K_{a2} = 4.7E-11 M$ ($pK_{a2} = 10.3$)

176 Thus, the contributions of HCO_3^- and CO_3^{2-} to measured k'_{OH} in all PME samples should be negligible.

Table S7. Singlet oxygen measurements

Sample ID	$P_{1O_2^*}$ ^a 10^{-7} M s^{-1}	$P_{1O_2^*}$ ^a $\mu\text{M h}^{-1}$	$[^1O_2^*]$ ^b 10^{-12} M	$f_{\text{FFA},1O_2}$ ^c	$10^2 \times \Phi_{1O_2^*}$ ^d
Particle Extracts					
PME1*	0.36 (0.04)	131 (15)	0.16 (0.02)	0.51 (0.08)	2.2 (0.2)
PME2*	0.68 (0.06)	246 (20)	0.31 (0.03)	0.72 (0.07)	3.8 (0.3)
PME3	2.4 (0.2)	851 (81)	1.1 (0.1)	1.1 (0.1)	5.7 (0.5)
PME4	4.2 (0.4)	1515 (135)	1.9 (0.2)	1.0 (0.1)	3.4 (0.3)
PME5	2.8 (0.2)	1000 (59)	1.3 (0.1)	1.2 (0.1)	3.8 (0.2)
PME6	4.8 (0.3)	1719 (114)	2.2 (0.1)	1.1 (0.1)	3.8 (0.3)
PME3D0.5	3.9 (0.4)	1413 (138)	1.8 (0.2)	0.79 (0.10)	4.5 (0.4)
PME3D1.3	1.1 (0.1)	414 (40)	0.52 (0.05)	0.68 (0.07)	3.6 (0.3)
PME3D2.5*	0.55 (0.03)	198 (11)	0.25 (0.01)	0.61 (0.04)	3.3 (0.2)
PME3D10	0.14 (0.02)	50.8 (6.0)	0.064 (0.008)	0.59 (0.09)	3.3 (0.4)
Average ($\pm\sigma$)					
“Standard” (PME3-6)	3.5 (1.1)	1271 (412)	1.6 (0.5)	1.1 (0.1)	4.2 (1.0)
“Dilute” (PME1*-2*,3D2.5*)	0.53 (0.16)	192 (58)	0.24 (0.07)	0.61 (0.11)	3.1 (0.8)
Davis Fog	0.51 (0.14)	183 (49)	0.23 (0.06)	1.4 (0.8)	3.8 (3.1)
Test statistic ^f	0.0064	0.0064	0.0064		0.98
Field Blanks ^e					
FB1 (dilute)	≤ 0.076	≤ 27	≤ 0.0034		
FB2 (standard)	≤ 0.069	≤ 25	≤ 0.0031		

178

Listed uncertainties are ± 1 standard error unless otherwise stated.

179

All equations involved in the technique are discussed in Kaur and Anastasio (2017).

180

* Samples extracted in 2.5 mL/filter square and referred to as the “dilute” extracts in the main text.

181

^a Davis winter solstice-normalized rate of $^1O_2^*$ formation.

182

^b Davis winter solstice-normalized steady-state concentration of $^1O_2^*$.

183

^c Fraction of probe FFA lost due to $^1O_2^*$.

184

^d Apparent quantum yield of $^1O_2^*$, calculated as $\Phi_{1O_2^*} = P_{1O_2^*} / R_{\text{abs}}$.

185

^e Blanks were analyzed by measuring FFA loss in undiluted blanks. This is an upper bound determined by ascribing all FFA loss to $^1O_2^*$.

186

^f Test statistic for comparison of standard PME and Davis fog averages: p -value for a two-tailed t -test for samples of unequal variance. Values below 0.05 are in bold.

187

188 **Table S8.** Syringol loss kinetics

Sample ID	k'_{SYR}^a 10^{-5} s^{-1}	τ_{SYR}^b h	$k'_{\text{SYR,OH}}^c$ 10^{-5} s^{-1}	$k'_{\text{SYR,1O2}}^d$ 10^{-5} s^{-1}	$k'_{\text{SYR,3C}^*}^e$ 10^{-5} s^{-1}	$f_{\text{SYR,3C}^*}^f$
Particle Extracts						
PME1*	12 (1)	2.3 (0.3)	0.43 (0.04)	0.59 (0.07)	11 (1)	0.92 (0.15)
PME2*	14 (2)	2.0 (0.3)	1.2 (0.1)	1.1 (0.09)	11 (2)	0.83 (0.17)
PME3	33 (1)	0.85 (0.03)	<u>2.1 (0.5)</u>	3.9 (0.4)	27 (1)	<u>0.82</u> (0.06)
PME4	69 (8)	0.40 (0.04)	1.6 (0.2)	6.9 (0.6)	61 (8)	0.88 (0.15)
PME5	35 (2)	0.80 (0.04)	0.74 (0.07)	4.5 (0.3)	29 (2)	0.85 (0.06)
PME6	37 (3)	0.74 (0.05)	0.85 (0.09)	7.8 (0.5)	24 (3)	0.77 (0.09)
PME3D0.5	48 (3)	0.58 (0.04)	<u>1.9 (0.5)</u>	6.4 (0.6)	40 (3)	<u>0.83</u> (0.08)
PME3D1.3	26 (2)	1.1 (0.1)	<u>0.78 (0.21)</u>	1.9 (0.2)	<u>24</u> (2)	0.90 (0.11)
PME3D2.5*	15 (2)	1.9 (0.3)	<u>0.86 (0.26)</u>	0.90 (0.05)	13 (2)	<u>0.88</u> (0.19)
PME3D10	3.6 (0.4)	7.7 (0.8)	<u>1.7 (0.7)</u>	0.23 (0.03)	<u>1.6 (0.8)</u>	<u>0.46 (0.24)</u>
Average ($\pm\sigma$)						
“Standard” (PME3-6)	43 (17)	0.70 (0.20)	<u>1.3 (0.7)</u>	5.8 (1.9)	36 (16)	0.83 (0.05)
“Dilute” (PME1*- 2*,3D2.5*)	14 (1)	2.0 (0.2)	<u>0.82 (0.37)</u>	0.87 (0.26)	12 (1)	0.88 (0.04)
Davis Fog	16 (11)	2.4 (1.4)	1.1 (0.2)	0.83 (0.22)	14 (11)	0.85 (0.06)
Test statistic ^g	0.040					
Field Blanks						
FB1 (dilute)	1.3 (0.2)	22 (3)				
FB2 (standard)	0.95 (0.07)	29 (2)				

189 Listed uncertainties are ± 1 standard error unless otherwise stated.

190 Bimolecular rate constants are given in Table S10.

191 * Samples extracted in 2.5 mL/filter square and referred to as the “dilute” extracts in the main text.

192 ^a Davis winter-solstice-normalized value of the measured pseudo-first-order rate constant for loss of syringol (SYR).

193 ^b Lifetime of syringol, calculated as $1/k'_{\text{SYR}}$.

194 ^c Pseudo-first-order rate constant for loss of SYR due to hydroxyl radical, calculated as $k'_{\text{SYR,OH}} = k_{\text{SYR+OH}} \times [\text{OH}]$.

195 ^d Pseudo-first-order rate constant for loss of SYR due to singlet oxygen, calculated as $k'_{\text{SYR,1O2}} = k_{\text{SYR+1O2}} \times [^1\text{O}_2^*]$.

196 ^e Pseudo-first-order rate constant for loss of SYR due to triplet excited states, calculated as $k'_{\text{SYR,3C}^*} = k'_{\text{SYR}} - (k'_{\text{SYR,OH}} + k'_{\text{SYR,1O2}})$.

197 ^f Fraction of SYR loss due to triplets, calculated as $k'_{\text{SYR,3C}^*} / k'_{\text{SYR}}$.

198 ^g Test statistic for comparison of standard PME and Davis fog averages: p -value for a two-tailed t -test for samples of unequal variance. Values below 0.05 are in
199 bold.

Table S9. Methyl jasmonate loss kinetics

Sample ID	k'_{MeJA}^a 10^{-5} s^{-1}	τ_{MeJA}^b h	$k'_{\text{MeJA,OH}}^c$ 10^{-5} s^{-1}	$k'_{\text{MeJA,1O2}}^d$ 10^{-5} s^{-1}	$k'_{\text{MeJA,3C}^*}^e$ 10^{-5} s^{-1}	$f_{\text{MeJA,3C}^*}^f$
Particle Extracts						
PME1*	0.98 (0.13)	28 (4)	0.11 (0.01)	0.099 (0.010)	0.77 (0.13)	0.79 (0.17)
PME2*	1.1 (0.1)	26 (1)	0.30 (0.04)	0.19 (0.02)	0.59 (0.07)	0.55 (0.07)
PME3	2.4 (0.2)	12 (1)	0.53 (0.13)	0.64 (0.06)	1.2 (0.2)	0.51 (0.10)
PME4	3.5 (0.4)	7.9 (0.8)	0.42 (0.04)	1.1 (0.1)	2.0 (0.4)	0.56 (0.12)
PME5	1.7 (0.2)	16 (2)	0.19 (0.02)	0.76 (0.04)	0.79 (0.18)	0.45 (0.11)
PME6	2.7 (0.2)	10 (1)	0.22 (0.02)	1.3 (0.1)	1.2 (0.2)	0.44 (0.08)
PME3D0.5	4.7 (0.5)	5.9 (0.7)	0.49 (0.12)	1.1 (0.1)	3.1 (0.6)	0.67 (0.14)
PME3D1.3	2.6 (0.2)	11 (1)	0.20 (0.05)	0.31 (0.03)	2.1 (0.3)	0.80 (0.12)
PME3D2.5*	1.8 (0.2)	16 (2)	0.22 (0.07)	0.15 (0.01)	1.4 (0.2)	0.79 (0.15)
PME3D10	0.67 (0.09)	42 (5)	0.44 (0.19)	0.038 (0.005)	0.19 (0.21)	0.28 (0.31)
Average ($\pm\sigma$)						
“Standard” (PME3-6)	2.6 (0.7)	11 (3)	0.34 (0.16)	0.96 (0.31)	1.3 (0.5)	0.49 (0.05)
“Dilute” (PME1*- 2*,3D2.5*)	1.3 (0.4)	23 (7)	0.21 (0.10)	0.15 (0.04)	0.92 (0.42)	0.71 (0.14)
Davis Fog	0.90 (0.12)	31 (4)	0.28 (0.05)	0.14 (0.04)	0.48 (0.17)	0.53 (0.13)
Test statistic ^g	0.018					
Field Blanks						
FB1 (dilute)	0.17 (0.2)	160 (18)				
FB2 (standard)	0.27 (0.08)	104 (31)				

201 Listed uncertainties are ± 1 standard error unless otherwise stated.

202 Bimolecular rate constants are given in Table S10.

203 * Samples extracted in 2.5 mL/filter square and referred to as the “dilute” extracts in the main text.

204 ^a Davis winter-solstice-normalized measured pseudo-first-order rate constant for loss of methyl jasmonate (MeJA).

205 ^b Lifetime of methyl jasmonate, calculated as $1/k'_{\text{MeJA}}$.

206 ^c Pseudo-first-order rate constant for loss of MeJA due to hydroxyl radical, calculated as $k'_{\text{MeJA,OH}} = k_{\text{MeJA+OH}} \times [\text{OH}\cdot]$.

207 ^d Pseudo-first-order rate constant for loss of MeJA due to singlet oxygen, calculated as $k'_{\text{MeJA,1O2}} = k_{\text{MeJA+1O2}} \times [^1\text{O}_2^*]$.

208 ^e Pseudo-first-order rate constant for loss of MeJA due to triplet excited states, calculated as $k'_{\text{MeJA,3C}^*} = k'_{\text{MeJA}} - (k'_{\text{MeJA,OH}} + k'_{\text{MeJA,1O2}})$.

209 ^f Fraction of MeJA loss due to triplets, calculated as $k'_{\text{MeJA,3C}^*} / k'_{\text{MeJA}}$.

210 ^g Test statistic for comparison of standard PME and Davis fog averages: p -value for a two-tailed t -test for samples of unequal variance. Values below 0.05 are in
211 bold.

212 | **Table S10.** Second-order rate constants for reactions of syringol and methyl jasmonate with hydroxyl radical, singlet oxygen, and triplet
 213 excited states

Oxidants	$k_{\text{SYR+Oxidant}}$ $10^9 \text{ M}^{-1} \text{ s}^{-1}$	Reference	$k_{\text{MeJA+Oxidant}}$ $10^8 \text{ M}^{-1} \text{ s}^{-1}$	Reference	
$\cdot\text{OH}$	26	O'Neill and Steenken (1977)	67 (± 3)	Richards-Henderson et al. (2014a)	
$^1\text{O}_2^*$	0.0036	Tratnyek and Hoigne (1991a)	0.0060 (± 0.0007)	Richards-Henderson et al. (2014b)	
Model Triplets ($^3\text{C}^*$)					$k_{\text{SYR+}^3\text{C}^*} / k_{\text{MeJA+}^3\text{C}^*}$ ^a
$^3\text{2AN}^*$	1.9 (± 0.1)	Kaur and Anastasio (2018)	0.19 (± 0.07)	Kaur and Anastasio (2018)	100 (± 37)
$^3\text{3MAP}^*$	3.8 (± 0.6)	Kaur and Anastasio (2018)	1.2 (± 0.3)	Richards-Henderson et al. (2014b)	32 (± 9)
$^3\text{DMB}^*$	3.5 (± 0.8)	Smith et al. (2015)	4.1 (± 1.6)	Richards-Henderson et al. (2014b)	8.5 (± 3.8)
$^3\text{BP}^*$	8.5 (± 1.6)	Kaur and Anastasio (2018)	51 (± 9)	Kaur and Anastasio (2018)	1.7 (± 0.4)

214 Listed uncertainties are ± 1 standard error.

215 ^a Ratio of the bimolecular rate constants for reaction of a given model triplet with syringol (SYR) and methyl jasmonate (MeJA).

216 **Table S11.** Characteristics of model triplet species

Model Triplet	E_T^a (kJ mol ⁻¹)	$E^{0*}({}^3C^*/C^{\cdot-})^b$ (V)	$k_{O_2+{}^3C^*}^c$ (10 ⁹) M ⁻¹ s ⁻¹	f_Δ^d
³ 2AN*	249	1.10	2.5	0.81 (C ₆ H ₆)
³ 3MAP*	303	1.64	3.3	0.33 (C ₆ H ₆)
³ DMB*	298 (estimated) ^e	-	-	< 0.61 (MeOH) (estimated) ^e
³ BP*	288	1.67	2.6	0.35 (C ₆ H ₆)

217 All values from Canonica et al.(Cannonica et al., 2000) and Wilkinson et. al.(Wilkinson et al., 1993)

218 ^a Triplet state energy (T₁→ S₀).

219 ^b One-electron reduction potential for the triplet/triplet radical anion pair.

220 ^c Bimolecular rate constant for quenching of triplet by molecular O₂. To calculate rates of triplet photoformation (described in the main text), an
221 average value of 2.8 (± 0.4) × 10⁹ M⁻¹s⁻¹ is used.

222 ^d Yield of singlet oxygen from quenching of model triplet species by O₂. The solvent used in the determination is indicated in parentheses. Including
223 the upper-bound value of 0.61 for ³DMB* (discussed in footnote *e*), the average value of f_Δ for the model triplets is 0.53 (± 0.23).

224 ^e Since the E_T and f_Δ values for ³DMB* are not available, values for benzaldehyde (Hunter, 1970; Wilkinson et al., 1993) are used as estimates. The f_Δ
225 value is an upper-bound estimate.

226

227 **Table S12.** Best triplet matches and best estimate triplet steady-state concentrations

Sample ID	$k'_{\text{SYR},3\text{C}^*} / k'_{\text{MeJA},3\text{C}^*}$ ^a	Mole-fractions of Best Triplet Matches ^b				Bimolecular rate constants ($\text{M}^{-1} \text{s}^{-1}$) $\chi_{3\text{C}1^*} \times k_{\text{Probe}+3\text{C}1^*} + \chi_{3\text{C}2^*} \times k_{\text{Probe}+3\text{C}2^*}$ ^c			Triplet Steady-State Concentration (10^{-14} M)		
		³ 2AN*	³ 3MAP*	³ DMB*	³ BP*	SYR	MeJA	SYR/MeJA Ratio	$\Sigma[{}^3\text{C}_i^*]_{\text{SYR}}$ ^d	$\Sigma[{}^3\text{C}_i^*]_{\text{MeJA}}$ ^e	$\Sigma[{}^3\text{C}_i^*]$ ($\pm 1\text{S.E.}$) Best Estimate ^{f,g}
PME1*	15 (3)		0.55	0.45		3.7E+09	2.5E+08	15	3.1	3.1	3.1 (1.2)
PME2*	20 (4)		0.76	0.24		3.7E+09	1.9E+08	20	3.1	3.1	3.1 (1.0)
PME3	20 (4)		0.77	0.23		3.7E+09	1.9E+08	20	7.3	7.3	7.3 (2.3)
PME4	30 (7)		0.98	0.02		3.8E+09	1.3E+08	30	16	16	16 (5)
PME5	37 (8)	0.34	0.66			3.2E+09	8.5E+07	37	9.3	9.3	9.3 (3.1)
PME6	24 (4)		0.86	0.14		3.8E+09	1.6E+08	24	7.7	7.7	7.7 (2.2)
PME3D0.5	12 (2)		0.41	0.59		3.6E+09	2.9E+08	12	11	11	11 (5)
PME3D1.3	12 (2)		0.38	0.62		3.6E+09	3.0E+08	12	6.3	6.3	6.3 (2.6)
PME3D2.5*	10 (3)		0.22	0.78		3.6E+09	3.5E+08	10	3.5	3.5	3.5 (1.7)
PME3D10	7.9 (7.6)			0.99	0.01	3.5E+09	4.5E+08	7.9	0.51	0.51	0.51 (0.36)

228 Uncertainties in parentheses are ± 1 standard error.

229 Details of the technique are discussed in Kaur and Anastasio (2018).

230 * Samples extracted in 2.5 mL/filter square and referred to as the “dilute” extracts in the main text.

231 ^a Ratio of measured values of $k'_{\text{Probe},3\text{C}^*}$ in a given particle extract

232 ^b Mole fractions of model triplets whose $k_{\text{Probe}+3\text{C}^* \text{Model}}$ ratio lies closest to the $k'_{\text{Probe},3\text{C}^*}$ ratio in each sample.

233 ^c Mole-fraction-weighted bimolecular rate constants for both probes.

234 ^d Triplet steady-state concentration calculated from syringol loss as $k'_{\text{SYR},3\text{C}^*} / (\chi_{3\text{C}1^*} k_{\text{SYR}+3\text{C}1^*} + \chi_{3\text{C}2^*} k_{\text{SYR}+3\text{C}2^*})$

235 ^e Triplet steady-state concentration calculated from methyl jasmonate loss as $k'_{\text{MeJA},3\text{C}^*} / (\chi_{3\text{C}1^*} k_{\text{MeJA}+3\text{C}1^*} + \chi_{3\text{C}2^*} k_{\text{MeJA}+3\text{C}2^*})$

236 ^f Best estimate steady-state concentration calculated as the average of the $\Sigma[{}^3\text{C}_i^*]_{\text{SYR}}$ and $\Sigma[{}^3\text{C}_i^*]_{\text{MeJA}}$.

237 ^g Uncertainties in parentheses are ± 1 SE propagated from the errors of $k'_{\text{SYR},3\text{C}^*}$ and $k'_{\text{MeJA},3\text{C}^*}$ and the mole-fraction-weighted bimolecular rate constants. Values are
238 shown in Tables S8 and S9.

239 **Table S13.** Measurements of triplet excited states of organic matter

Sample ID	$\Sigma[{}^3\text{C}_i^*]$ Best Estimate ^a 10^{-14} M	$P_{3\text{C}^*}$ ^b 10^{-7} M s ⁻¹	$P_{3\text{C}^*}$ ^b $\mu\text{M h}^{-1}$	$10^2 \times \Phi_{3\text{C}^*}$ ^c	$\frac{\Phi_{3\text{C}^*}}{(\Phi_{1\text{O}_2^*}/f_\Delta)}$ ^d *	$\frac{\Sigma[{}^3\text{C}_i^*]}{[{}^1\text{O}_2^*]}$ ^e
Particle Extracts						
PME1*	3.1 (1.2)	0.30 (0.13)	109 (48)	1.8 (0.8)	0.44 (0.20)	0.19 (0.07)
PME2*	3.1 (1.0)	0.34 (0.13)	122 (47)	1.9 (0.7)	0.26 (0.10)	0.10 (0.03)
PME3	7.3 (2.3)	1.5 (0.6)	534 (204)	3.6 (1.4)	0.33 (0.13)	0.068 (0.022)
PME4	16 (5)	3.5 (1.4)	1260 (501)	2.8 (1.1)	0.44 (0.18)	0.083 (0.029)
PME5	9.3 (3.1)	1.5 (0.6)	534 (211)	2.0 (0.8)	0.28 (0.11)	0.074 (0.025)
PME6	7.7 (2.2)	1.6 (0.6)	568 (206)	1.3 (0.5)	0.18 (0.06)	0.035 (0.011)
PME3D0.5	11 (5)	3.6 (1.6)	1286 (593)	4.1 (1.9)	0.48 (0.23)	0.062 (0.026)
PME3D1.3	6.3 (2.6)	1.1 (0.5)	393 (182)	3.4 (1.6)	0.50 (0.24)	0.12 (0.05)
PME3D2.5*	3.5 (1.7)	0.44 (0.24)	160 (86)	2.7 (1.5)	0.43 (0.23)	0.14 (0.07)
PME3D10	0.51 (0.36)	0.0047 (0.0034)	17 (12)	1.1 (0.8)	0.18 (0.13)	0.079 (0.057)
Averages ($\pm\sigma$)						
“Standard” (PME3-6)	10 (4)	2.0 (1.0)	723 (355)	2.4 (1.0)	0.31 (0.11)	0.065 (0.021)
“Dilute” (PME1*- 2*,3D2.5*)	3.2 (0.2)	0.36 (0.01)	130 (26)	2.1 (0.5)	0.38 (0.10)	0.14 (0.04)
Davis Fog	5.4 (6.3)	0.59 (0.60)	212 (216)	5.8 (8.6)	0.55 (0.44)	0.21 (0.20)
Test statistic ^f	0.27	0.059	0.059	0.49	0.35	0.25

240 Listed uncertainties are ± 1 standard error.

241 * Samples extracted in 2.5 mL/filter square and referred to as the “dilute” extracts in the main text.

242 ^a Best estimate of oxidizing triplets steady-state concentration, calculated as the average of the $\Sigma[{}^3\text{C}_i^*]_{\text{SYR}}$ and $\Sigma[{}^3\text{C}_i^*]_{\text{MeJA}}$ values, as shown in Table S12.

243 ^b Davis winter solstice-normalized rate of triplet photoproduction, calculated as $P_{3\text{C}^*} = \Sigma[{}^3\text{C}_i^*] \times (k_{3\text{C}^*+\text{O}_2} \times [\text{O}_2] + (k_{\text{rxn}} + k_{\text{Q}})[\text{DOC}])$ (Eq. (8), main text).

244 ^c Quantum yield for formation of oxidizing organic triplet excited states, calculated as $\Phi_{3\text{C}^*} = P_{3\text{C}^*} / R_{\text{abs}}$.

245 ^d Fraction of the total triplet pool that can oxidize our probes, i.e., that are “oxidizing triplets”. This is estimated as the ratio of the quantum yields for oxidizing
 246 triplets and singlet oxygen (Table S7) divided by the average yield of ${}^1\text{O}_2^*$ ($f_\Delta = 0.53$; Table S11) from ${}^3\text{C}^*$ via energy transfer. The denominator, $\Phi_{1\text{O}_2^*}/f_\Delta$, is an
 247 estimate of the quantum yield for formation of energy-transfer triplets that can make singlet molecular oxygen, a pool that likely includes essentially all organic
 248 triplet states.

249 ^e Ratio of the Davis-winter-normalized steady-state triplet and singlet oxygen concentrations.

250 ^f Test statistic for comparison of standard PME and Davis fog averages: *p*-value for a two-tailed *t*-test for samples of unequal variance. Values below 0.05 are in
251 bold.

252 **Table S14.** Particle mass to water mass ratios in the PME3 extracts, typical fog drops, and particles

Sample ID	Number of filter squares extracted	Volume of Milli-Q water per filter square (mL) ^a	Aqueous PM mass concentration factor (CF) ^b	Average PM mass extracted per filter square (μg) ^c	Total PM mass extracted (μg) ^d	Total volume of extract (mL) ^e	PM mass / water mass (μg-PM / μg-H ₂ O) ^f
PME3D10	1	10	0.05	347	347	10	3.5E-05
PME3D2.5	12	2.5	0.20	331 (15)	3977	30	1.3E-04
PME3D1.3	8	1.3	0.38	315 (23)	2520	10	2.4E-04
PME3D1 or “PME3”	12	1.0	0.49	328 (19)	3932	12	3.3E-04
PME3D0.5	26	0.5	0.96	323 (21)	10979	13	8.4E-04
Cloud/Fog drop							(1 – 5)E-04 ^g
Particles							≥ 1 ^h

253 ^a Volume of water used to extract each 2 × 2 cm square piece of the filter sheet.

254 ^b PM mass concentration factor in the extract (Eq. (10), main text).

255 ^c Average (± 1σ) mass extracted from the filter squares for each dilution.

256 ^d Total mass extracted per extract. For each extract, the filter pieces used in the extraction were weighed pre- and post-extraction using a Mettler Toledo XP2U ultra-microbalance (error ± 2 μg). The PM mass extracted is the difference between pre- and post-extraction weights.

258 ^e Total volume of extract = number of filter pieces extracted × water volume per filter square.

259 ^f PM mass-to-water mass ratio, calculated as total [solute](#) mass extracted / total volume of extract.

260 ^g For fog drops, we estimate that PM mass/water mass ratios are in the range of (1 – 5) × 10⁻⁴ μg-PM/μg-H₂O based on a typical PM mass of 31 μg m⁻³-air in California’s Central Valley, as measured by Young et al. (2016), and assuming a range for the liquid water content (LWC) of 0.06 to 0.3 g-H₂O m⁻³-air (Hess et al., 1998).

263 ^h Based on measurements of particle mass [concentration](#) (Young et al. (2016)) and [estimated](#) particle water (Parworth et al., 2017) in California’s Central Valley during winter, the calculated range of PM mass to water mass ratios is 0.79 – 50. From this range, we use a value of 1 to represent typical PM conditions.

264

265 **Table S15.** Photooxidant concentrations (formed *in situ*) in PME3D extracts and expected values in ambient particles

Sample ID	Aqueous PM Mass Concentration Factor (CF) ^a	PM Mass /Water Mass (μg-PM/μg-H ₂ O) ^b	[•OH] (M)	[¹ O ₂ *] (M)	Σ[³ C _i *] (M)
PME3D10	0.05	3.5E-05	<u>6.7E-16</u>	6.4E-14	<u>5.1E-15</u>
PME3D2.5*	0.20	1.3E-04	<u>3.4E-16</u>	2.5E-13	<u>3.5E-14</u>
PME3D1.3	0.38	2.4E-04	<u>3.2E-16</u>	5.2E-13	<u>6.3E-14</u>
PME3D1	0.49	3.3E-04	<u>8.5E-16</u>	1.1E-12	7.3E-14
PME3D0.5	0.96	8.4E-04	<u>8.3E-16</u>	1.8E-12	1.1E-13
Ambient Particles		1.0	<u>8.4E-16</u> ^c	<u>1.6E-10</u> ^d	<u>2.3E-13</u> ^e <u>1.3E-11</u> ^f

266 ^a Aqueous PM mass concentration factor (Eq. (10), main text).

267 ^b PM mass/water mass ratio (Table S14).

268 ^c Expected *in situ* [•OH] concentration in ambient PM (in the absence of partitioning of •OH from the gas phase), determined as the average of the five measurements
 269 in PME3D extracts and corrected for quenching by probe MBO (Sect. S1.1). Including mass transport of •OH(g) to the drops will increase the aqueous
 270 concentration by approximately 30%, as discussed in the text.

271 ^d Expected [¹O₂*] concentration in ambient PM; see section S4.

272 ^e Best estimate for the Σ[³C_i*] concentration in ambient PM, obtained by plotting Σ[³C_i*] against the PM mass/water mass ratio, fitting the data to the equation y =
 273 ax/(1+bx); parameters a = 3.08 × 10⁻¹⁰ M and b = 1.31 × 10³ were obtained using Excel. The curve was then extrapolated to a PM mass/water mass ratio of 1.0 μg-
 274 PM/μg-H₂O.

275 ^f High estimate for the Σ[³C_i*] concentration in ambient PM, obtained by fitting Σ[³C_i*] against PM mass/water mass ratio with the equation y = ax/(1+bx);
 276 parameters a = 2.26 × 10⁻¹⁰ M and b = 17.0 were obtained using Excel. The curve was then extrapolated to a PM mass/water mass ratio of 1.0 μg-PM/μg-H₂O.

277

278 **Table S16.** Gas- and aqueous-phase reaction rate constants for selected organic compounds with the major oxidants

#	Organic Compound	Gas-phase rate constant, $k_{\text{ORG+Ox(g)}}$ ($\text{cm}^3 \text{mlc}^{-1} \text{s}^{-1}$)				Aqueous-phase rate constants, $k_{\text{ORG+Ox(aq)}}$ ($\text{M}^{-1} \text{s}^{-1}$)							
		$\bullet\text{OH(g)}$	Ref.	$\text{O}_3(\text{g})$	Ref.	$\bullet\text{OH(aq)}$	Ref.	$^1\text{O}_2^*(\text{aq})$	Ref.	$\text{O}_3(\text{aq})$	Ref.	$^3\text{C}^*(\text{aq})^a$	Ref.
1	Syringol	9.6E-11	(Lauraguais et al., 2012)	4.0E-19 ^b	(Zein et al., 2015)	2.6E+10	(O'Neill and Steenken, 1977)	3.6E+07	(Tratnyek and Hoigne, 1991b)	1.3E+04 ^c	(Hoigné and Bader, 1983)	3.7E+09	(Kaur and Anastasio, 2018), (Smith et al., 2015)
2	Methyl jasmonate	7.8E-12 ^d	(Meylan and Howard, 1993)	1.7E-16 ^d	(Meylan and Howard, 1993)	6.7E+09	(Richards-Henderson et al., 2014a)	6.0E+06	(Richards-Henderson et al., 2014b)	1.0E+05 ^e	(Richards-Henderson et al., 2014b)	2.7E+08	(Kaur and Anastasio, 2018)
3	Tyrosine	2.8E-11 ^f	(Rinke and Zetzsch, 1984)	4.7E-19 ^g	(Atkinson et al., 1982)	1.3E+10	(Solar et al., 1984)	3.8E+07	(Bertolotti et al., 1991)	3.3E+05 (pH 4.2)	(McGregor and Anastasio, 2001)	6.6E+08 ^h	(Canonica et al., 2000)
4	1,2,4-Butanetriol	8.5E-12 ⁱ	(Atkinson et al., 2006)	1.0E-20 ^j	(Atkinson et al., 2006)	5.0E+09 ^k	(Anbar et al., 1966)	6.0E+04 ^l	(Wilkinson et al., 1995)	2 ^m	(Hoigné and Bader, 1983)	1.1E+06 ⁿ	(Tetreau et al., 1972)
5	3-Hydroxy-2,5-bis(hydroxymethyl) furan	4.0E-11 ^o	(Atkinson et al., 1983)	2.4E-18 ^o	(Atkinson et al., 1983)	3.9E+09 ^p	(Lilie, 1971)	1.0E+08 ^q	(Wilkinson et al., 1995)	1.2E+03 ^r	(Andreev, 2012)	1.4E+08 ^s	(Kaur and Anastasio, 2018)

279 References for the measured rate constants are indicated. Values indicated are at 298 K wherever available. In cases where no measurements were found, rate
 280 constants for structurally similar compounds are used as proxies; references for those are provided, and discussed in the following footnotes.

281 ^a For triplets, we use an average of rate constants for ³MAP* and ³DMB*.

282 ^b Second-order rate constant for the gas-phase reaction of O₃ with guaiacol (2-methoxyphenol).

283 ^c Second-order rate constant for the aqueous reaction of O₃ with phenol is used as a proxy, with a ten-fold enhancement based on the measured ratio of phenol and
 284 syringol rate constants for reaction with ³DMB* (discussed in the SI of Kaur and Anastasio (2018)).

285 ^d Average of cis- and trans-methyl jasmonate rate constants with hydroxyl radical and ozone.

286 ^e Estimated by Richards-Henderson et al. (2014b) using a structurally similar compound.

287 ^f Second-order rate constant for the aqueous-phase reaction of O₃ with phenol.

288 ^g Second-order rate constant for the aqueous-phase reaction of O₃ with 3-methylphenol.

289 ^h Second-order rate constant for aqueous-phase reaction of tyrosine with 3'-methoxyacetophenone.

290 ⁱ Second-order rate constant for gas-phase reaction of $\bullet\text{OH}$ with 1-butanol.

291 ^j Second-order rate constant for gas-phase reaction of O₃ with pinonaldehyde.

292 ^k Second-order rate constant for aqueous-phase reaction of $\bullet\text{OH}$ with 1,6-hexanediol.

293 ^l Second-order rate constant for aqueous-phase reaction of ¹O₂* with 2-butanol.

294 ^m Second-order rate constant for aqueous-phase reaction of O₃ with 2-propanol.

295 ⁿ Second-order rate constant for aqueous-phase reaction of ³DMB* with 2-propanol.

296 ^o Second-order rate constant for gas-phase reaction of $\bullet\text{OH}$ and O₃ with furan.

297 ^p Second-order rate constant for aqueous-phase reaction of $\bullet\text{OH}$ with furan.

298 ^q Second-order rate constant for aqueous-phase reaction of ¹O₂* with furan, adjusted by multiplying with 0.5 based on effect of changing substituents.

299 ^r Second-order rate constant for aqueous-phase reaction of O₃ with furan in glacial acetic acid.

300 ^s Average of the second-order rate constant for aqueous-phase reaction of ³MAP* and ³DMB* with methyl jasmonate is used as a proxy, adjusted by multiplying with
 301 0.5 based on effect of changing substituents observed for rate constant of furan with ¹O₂*.

302 **Table S17.** Fate of selected organic compounds in fog and particles

#	Organic Compound	K_H^a (M atm ⁻¹)	f_{aq}^b	Overall		Percent of loss due to each oxidant ^e					
				k'_{ORG}^c (s ⁻¹)	τ_{ORG}^d (h)	•OH(g)	O ₃ (g)	•OH(aq)	¹ O ₂ *(aq)	O ₃ (aq)	³ C*(aq)
Fog											
1	Syringol	5.0E+03	0.11	1.1E-04	2.5	76	0	5	1	0	18
2	Methyl jasmonate	8.1E+03	0.17	1.2E-04	2.3	5	86	2	0	5	2
3	Tyrosine	8.0E+10	1.0	1.8E-04	1.6	0	0	15	4	62	19
4	1,2,4-Butanetriol	4.7E+11	1.0	1.0E-05	28	0	0	99	0	0	0
5	3-Hydroxy-2,5-bis(hydroxymethyl) furan	1.1E+09	1.0	3.5E-05	7.9	0	0	22	57	1	19
PM (Best-fit [³C*] scenario)											
1	Syringol	5.0E+03	2.4E-06	9.6E-05	2.9	100	0	0	0	0	0
2	Methyl jasmonate	8.1E+03	4.0E-06	1.3E-04	2.1	6	94	0	0	0	0
3	Tyrosine	8.0E+10	0.98	6.3E-03	0.044	0	0	0	96	2	2
4	1,2,4-Butanetriol	4.7E+11	1.0	1.4E-05	20	0	0	30	68	0	2
5	3-Hydroxy-2,5-bis(hydroxymethyl) furan	1.1E+09	0.35	5.7E-03	0.049	0.5	0	0	99	0.0	0.2
PM (High estimate [³C*] scenario)											
1	Syringol	5.0E+03	2.4E-06	9.6E-05	2.9	98	0	0	0	0	1
2	Methyl jasmonate	8.1E+03	4.0E-06	1.3E-04	2.1	6	94	0	0	0	0
3	Tyrosine	8.0E+10	0.98	1.4E-02	0.020	0	0	0	42	1	57
4	1,2,4-Butanetriol	4.7E+11	1.0	2.6E-05	10.5	0	0	16	37	0	47
5	3-Hydroxy-2,5-bis(hydroxymethyl) furan	1.1E+09	0.35	6.3E-03	0.044	0.4	0	0	90	0	9

303 For fog, a liquid water content of 1×10^{-6} L-aq / L-air is assumed.

304 For PM, a liquid water content of 2×10^{-11} L-aq / L-air is assumed, based on typical wintertime Central Valley conditions (Parworth et al., 2017).

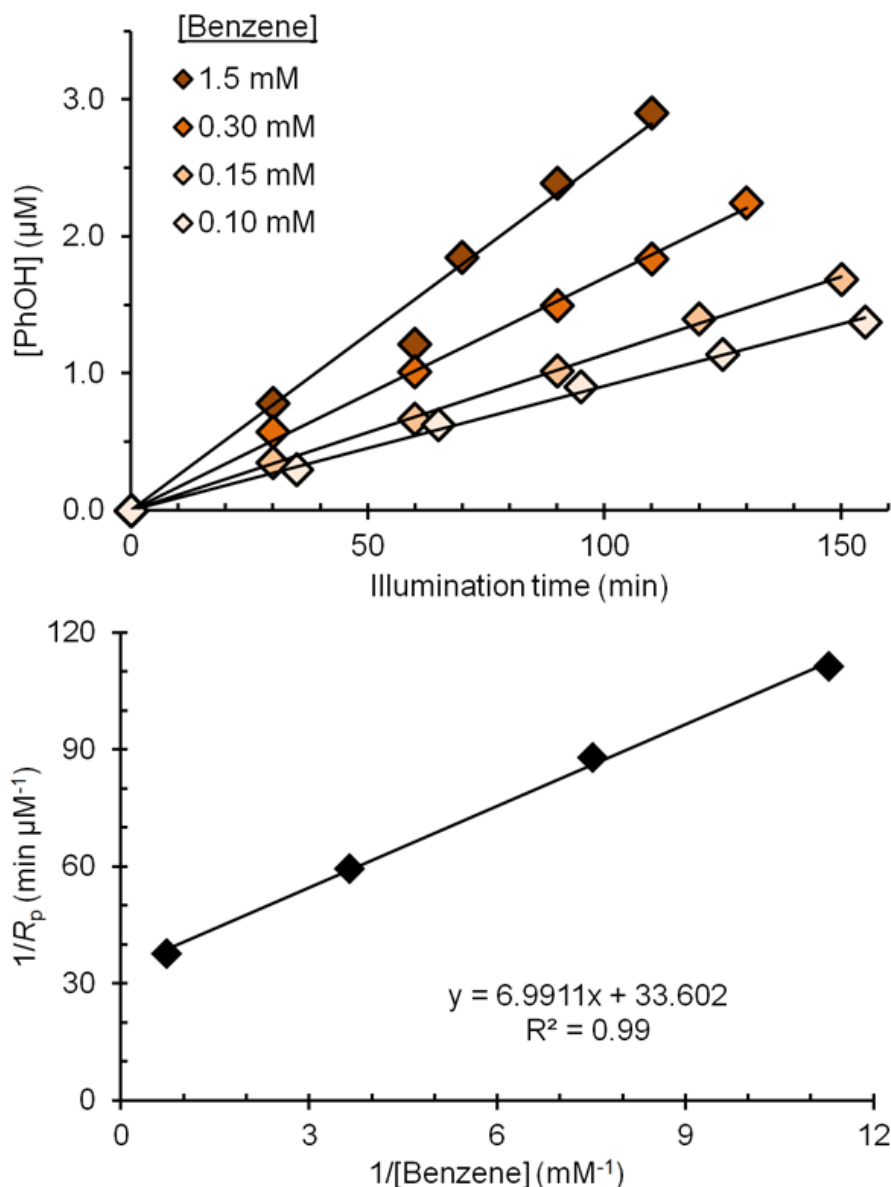
305 ^a Henry's law constant estimated using EPISuite version 4.11 (USEPA, 2012). For methyl jasmonate, measured value from Vempati (2014).

306 ^b Fraction of organic compound present in the aqueous-phase, calculated as $f_{aq} = 1/(1+1/(K_H \times L \times R \times T))$, where K_H is the Henry's law constant, L is the liquid water content, R is the gas constant (0.082 L atm K⁻¹ mol⁻¹), and $T = 298$ K.

307 ^c Total pseudo-first order rate constant for loss of organic compound, calculated as $k'_{ORG} = \Sigma(f_{aq} \times k'_{ORG,Ox(aq)} + (1-f_{aq}) \times k'_{ORG,Ox(g)})$. $k'_{ORG,Ox(g)}$ and $k'_{ORG,Ox(aq)}$ are by
 308 calculated by multiplying the bimolecular reaction rate constant (Table S16) with the corresponding steady-state concentration of oxidant: [[•]OH(g)] = 1×10^6
 309 molecules cm⁻³, [O₃(g)] = 30 ppbv = 7.4×10^{11} molecules cm⁻³, [[•]OH(aq)] = 2×10^{-15} M (includes gas-to-aqueous partitioning; Kaur and Anastasio (2017) and
 310 this study), [O₃(aq)] = 3.3×10^{-10} M (based on equilibrium with 30 ppbv O₃(g) and $K_H = 1.1 \times 10^{-2}$ M atm⁻¹; Seinfeld and Pandis (2012)), [¹O₂*(aq)] = 2×10^{-13} M
 311 in fog (average in Davis fog; Kaur and Anastasio (2017)), and 1.5×10^{-10} M in PM (estimate in PM after accounting for evaporative loss and loss due to organic
 312 sinks at higher DOC concentrations; Sect. S5). In case of the triplets, in fog [³C*(aq)] = 5×10^{-14} M (average in Davis fog; Kaur and Anastasio (2018)); in PM
 313 both the **best-fit and high-estimate** concentrations obtained via extrapolation (Table S15) are considered, i.e., [³C*(aq)] = 2.3×10^{-13} M and 1.3×10^{-11} M,
 314 respectively.

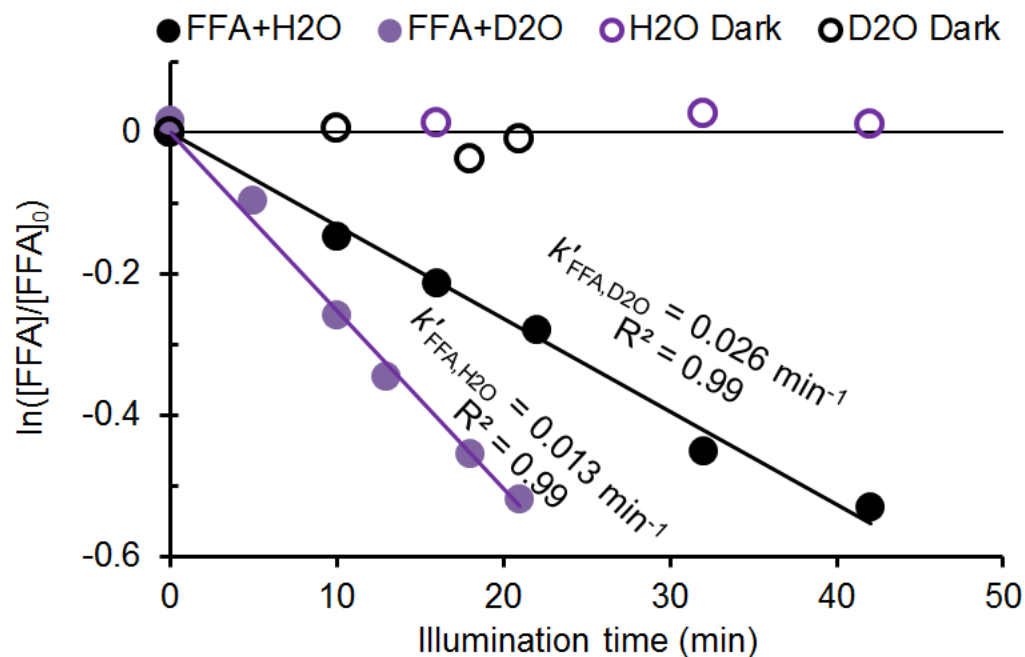
315 ^d Overall lifetime of organic compound, calculated as $1/k'_{ORG}$.

316 ^e Percent of organic compound lost due to each pathway, calculated as $(f_{aq} \times k'_{ORG,Ox(aq)})/k'_{ORG}$ for aqueous pathways and $((1-f_{aq}) \times k'_{ORG,Ox(g)})/k'_{ORG}$ for gas-phase
 317 processes. The sum of all pathways for a given compound is sometimes not equal to 100% because of rounding.
 318
 319



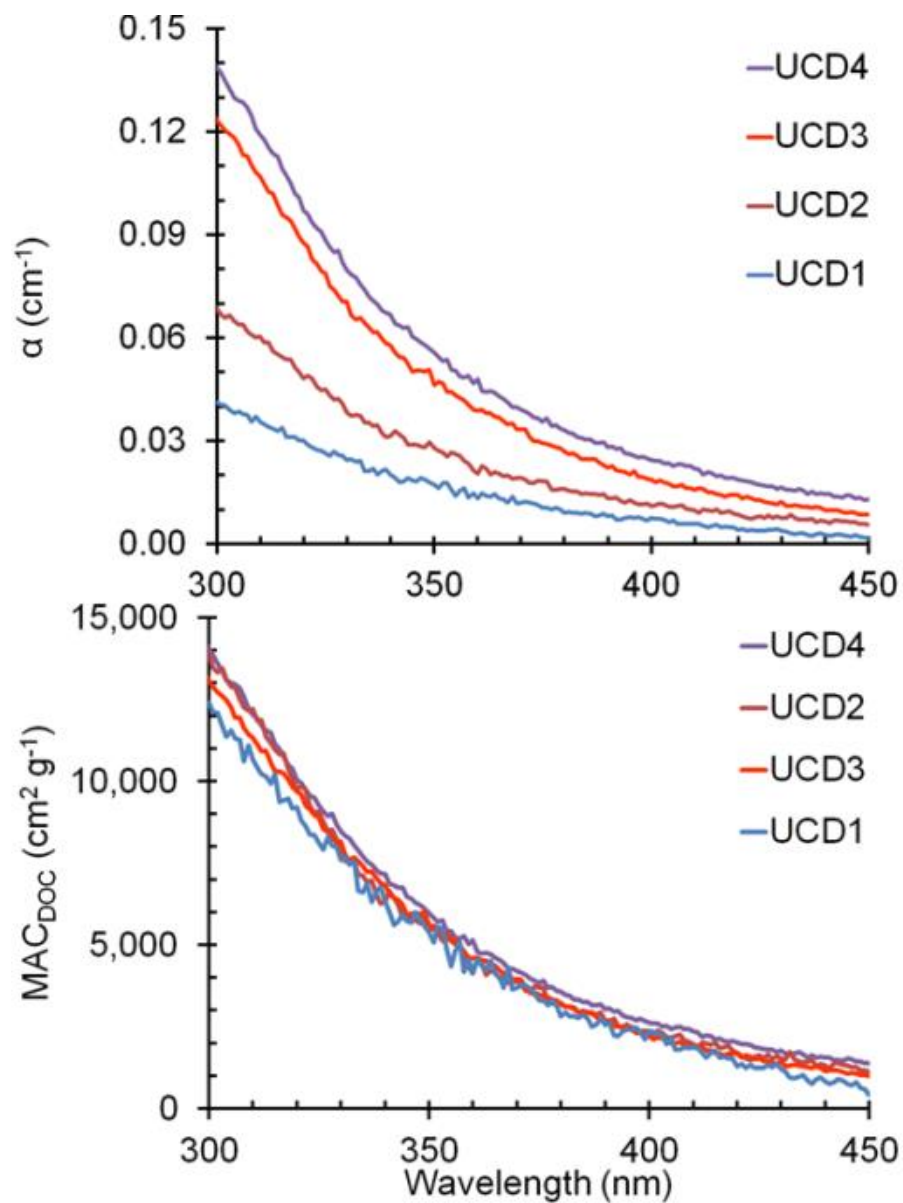
320
 321 | **Figure S1.** $\cdot\text{OH}$ measurement in extract PME5. Top Panel: Photoformation of phenol in four
 322 aliquots of the extract spiked with varying benzene concentrations (0.10 to 1.5 mM). The rates of
 323 phenol formation, R_p , were determined as the slopes of the linear fits for each of the four data
 324 sets. Bottom: "Inverse" plot, i.e., the inverse of R_p vs. the inverse of the benzene concentration.
 325 The slope and y-intercept from this plot are used to calculate P_{OH} , $[\cdot\text{OH}]$, and k'_{OH} using
 326 equations described in Kaur and Anastasio (2017). $\cdot\text{OH}$ results for all particle extracts are
 327 tabulated in Table S3.

328



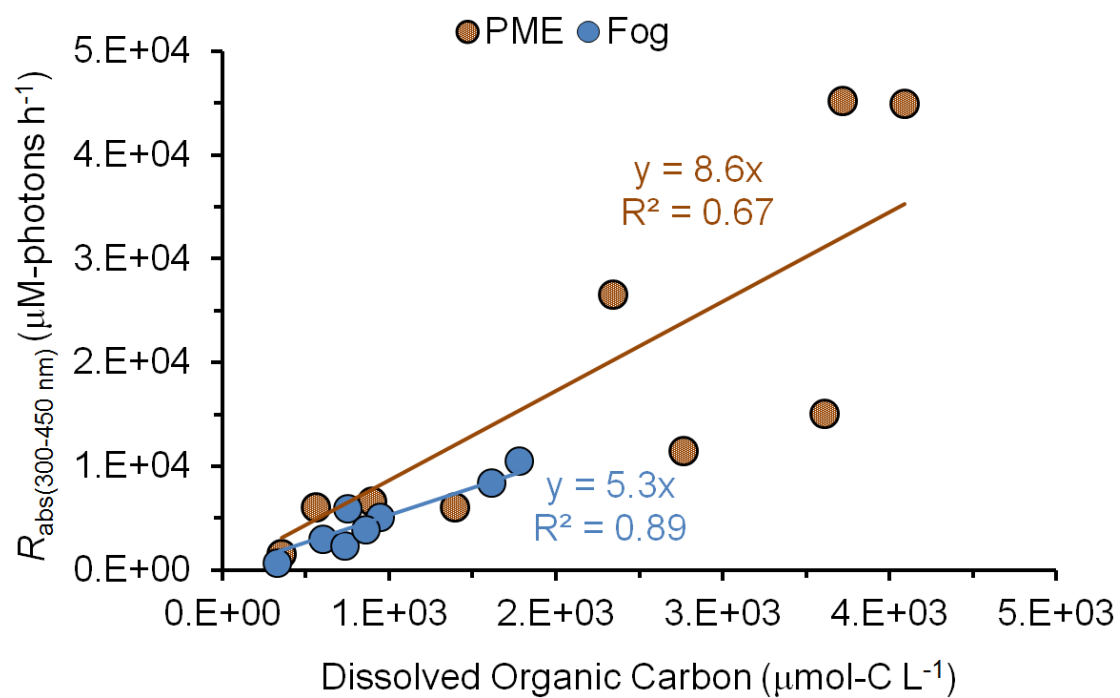
329
 330 **Figure S2.** Singlet oxygen kinetic measurements in extract PME5 diluted 1:1 (volume : volume)
 331 with H₂O or D₂O. Data show the change in probe concentration (furfuryl alcohol, FFA) with
 332 illumination time. Closed symbols are illuminated samples while open symbols represent dark
 333 controls. Equations for calculating ¹O₂* steady-state concentrations and rates of photoproduction
 334 are described in Kaur and Anastasio (2017).

335



336

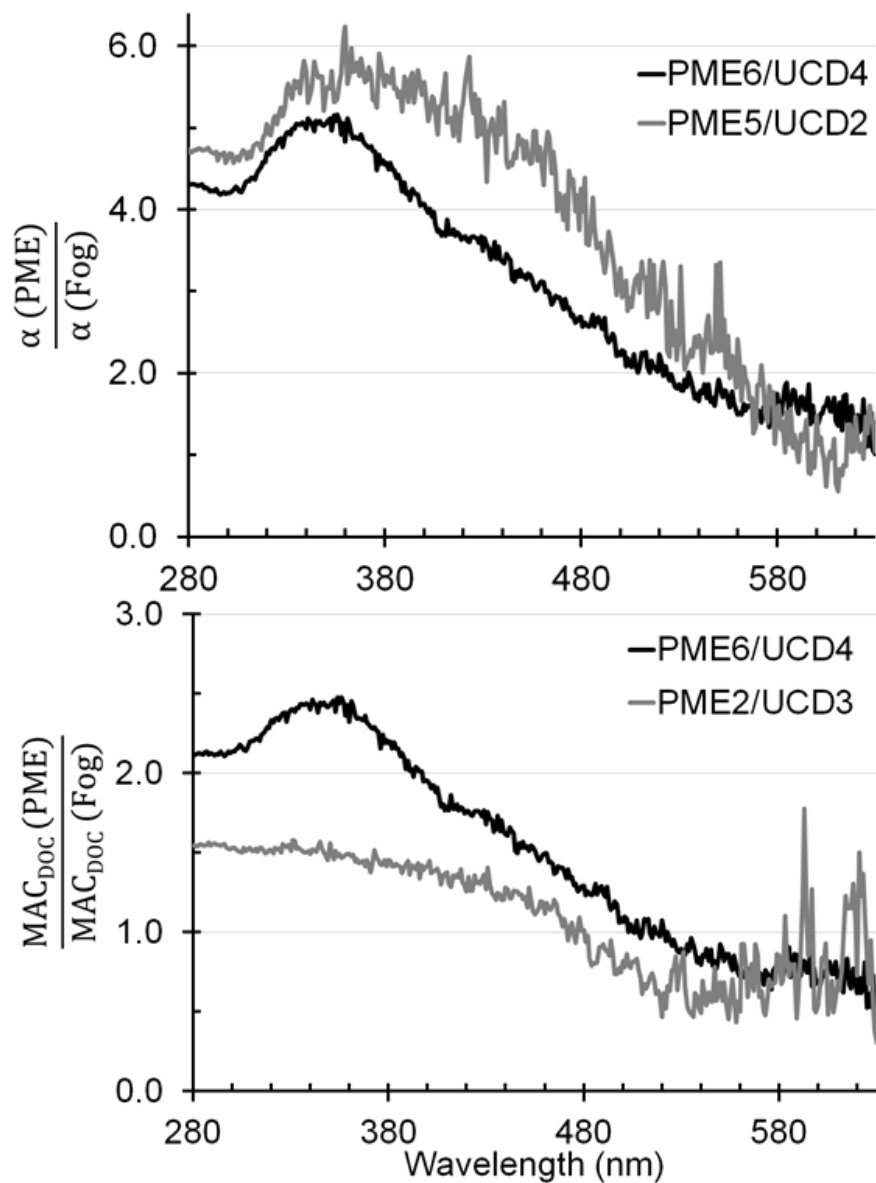
337 **Figure S3.** Top panel: Light absorbance by fog samples collected during 2011-12 in Davis, CA.
338 The legend shows the sample identities, arranged from the highest absorbing (top) to lowest
339 absorbing (bottom) at 300 nm. Bottom panel: Mass absorption coefficient of DOC in the Davis
340 fog samples. All data from Kaur and Anastasio (2017).



341

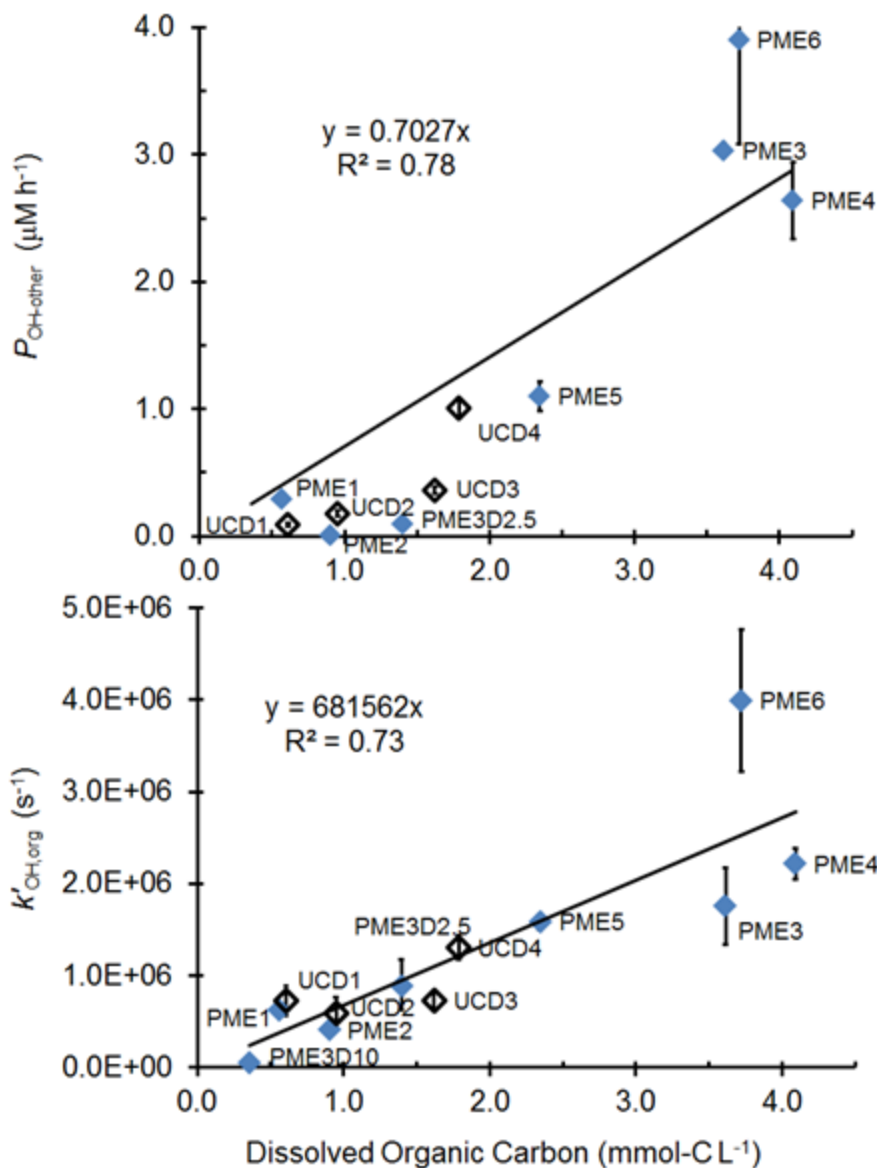
342 **Figure S4.** Correlation between the rate of sunlight absorption (R_{abs}) in the 300-450 nm
 343 wavelength range and dissolved organic carbon (DOC) for the fog samples (data from Kaur and
 344 Anastasio (2017)) and particle extracts (PME) (this work). Values for PME in this plot are
 345 summarized in Table S1.

346



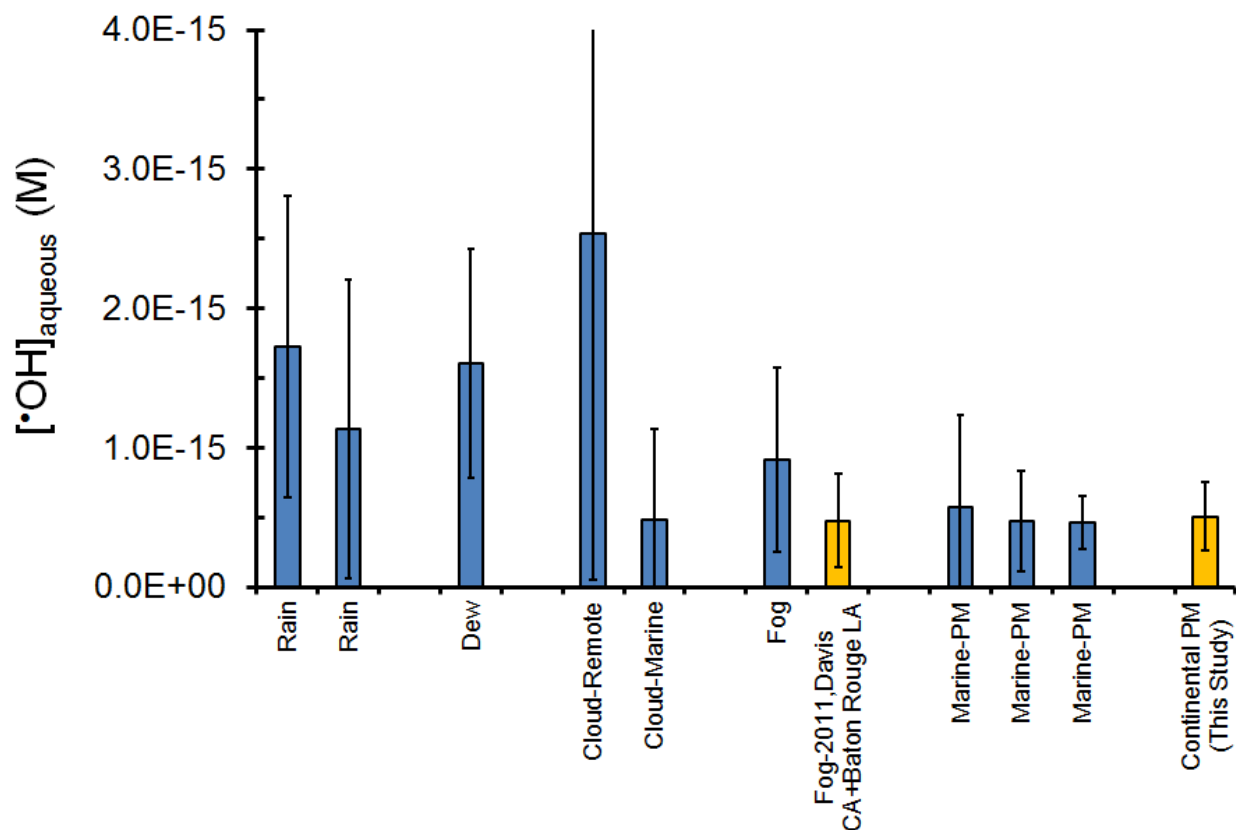
347

348 **Figure S5.** (Top) Ratio of pathlength-normalized absorbance for PME and fog samples with
 349 highest (black) and median (grey) absorbances. (Bottom): Ratio of mass absorption coefficients
 350 of DOC in PME and fog samples with highest (black) and median (grey) absorbances.



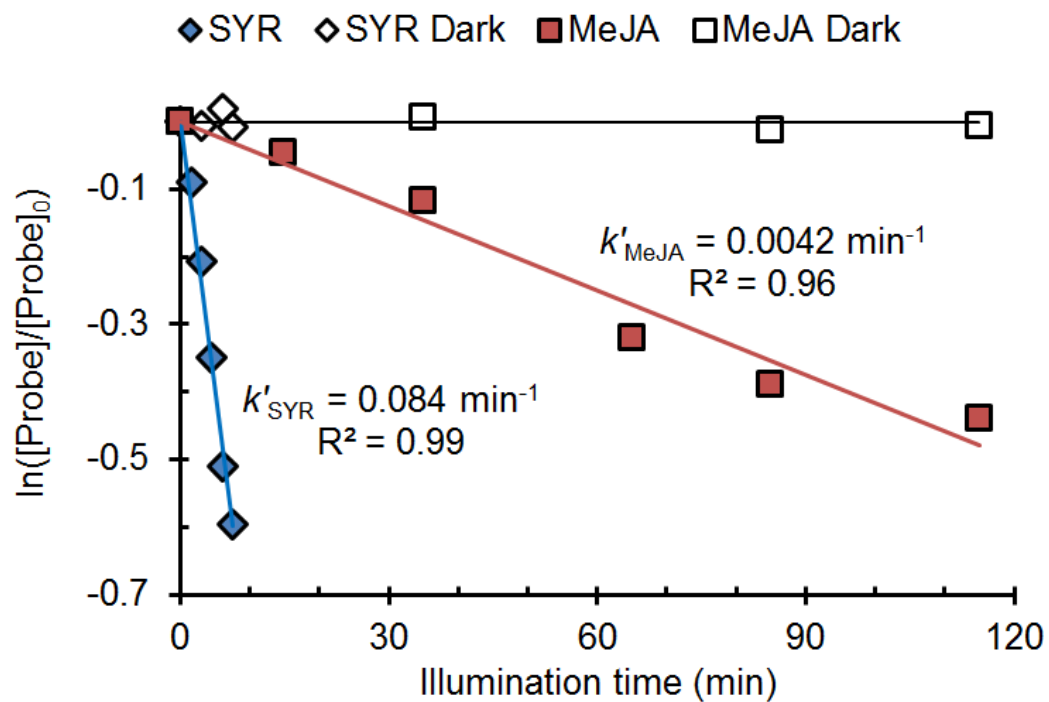
351
 352 **Figure S6.** (Top) Correlation between the rate of $\cdot\text{OH}$ photoproduction due to sources other than
 353 nitrite and nitrate and the concentration of dissolved organic carbon (DOC). While the R^2 value
 354 for this correlation is relatively high, this is largely driven by the highest three points: most of the
 355 data are poorly fit by the regression line. (Bottom) Correlation between apparent pseudo-first
 356 order rate constant for loss of $\cdot\text{OH}$ due to organic sinks (obtained by subtracting inorganic
 357 contributions from the measured k'_{OH}) and DOC. Data include measurements in particle extracts
 358 (measured in this work) and in Davis fogs (Kaur and Anastasio, 2017).

359



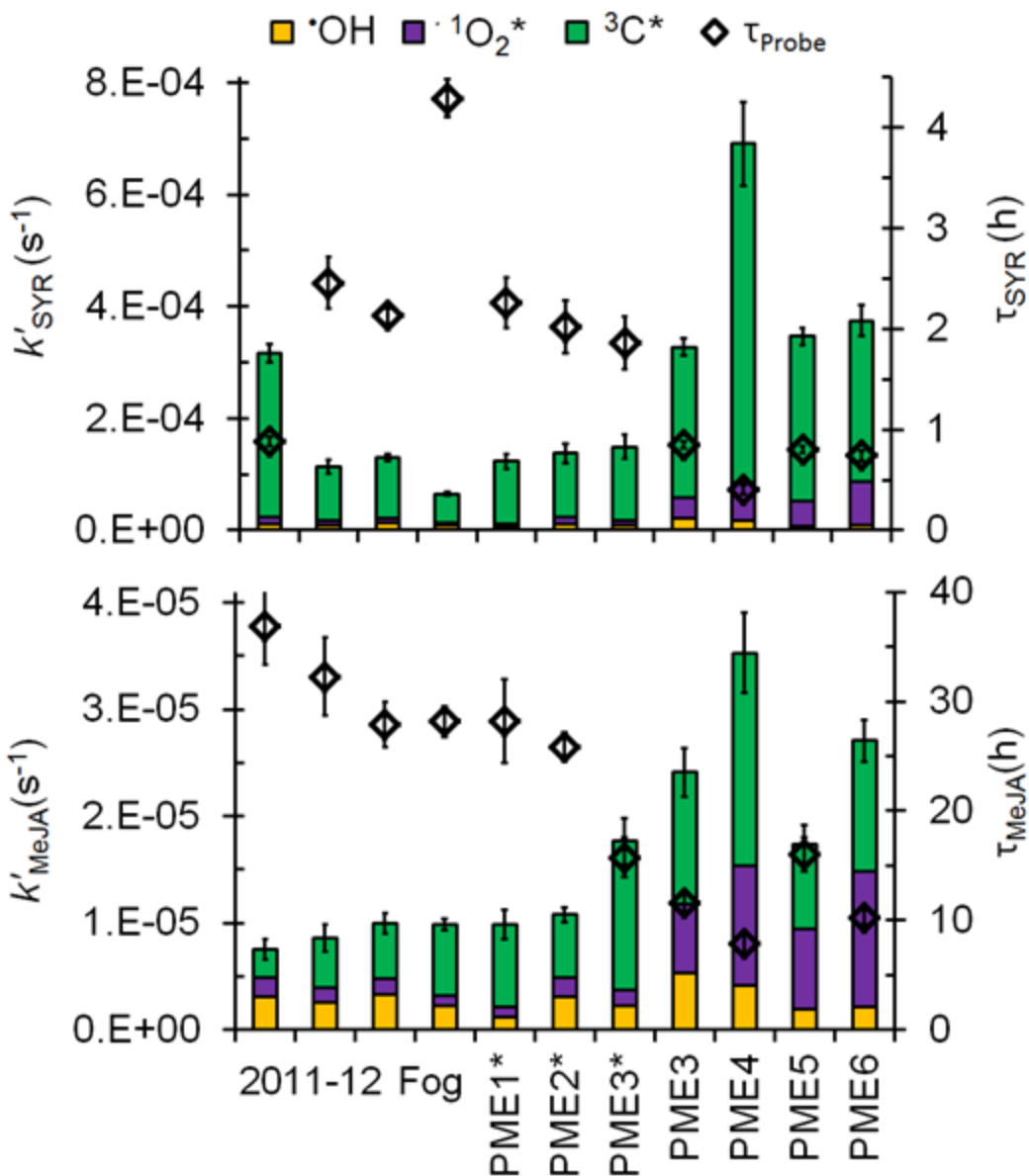
360

361 **Figure S7.** Comparison of hydroxyl radical steady-state concentrations formed *in situ* (i.e., not
 362 including mass transport of •OH from the gas phase) measured in various atmospheric waters, as
 363 summarized in Arakaki et al. (2013) (blue bars) and including (in yellow bars) our recent data for
 364 fog (Kaur and Anastasio, 2017) and current data for PM. Error bars are $\pm 1\sigma$, calculated from the
 365 variability in values used to calculate the mean for a given study.



366

367 **Figure S8.** Loss of probes for measuring triplet excited states: syringol (SYR) and methyl
 368 jasmonate (MeJA) in extract PME5. Closed symbols are illuminated samples while open
 369 symbols represent dark controls.

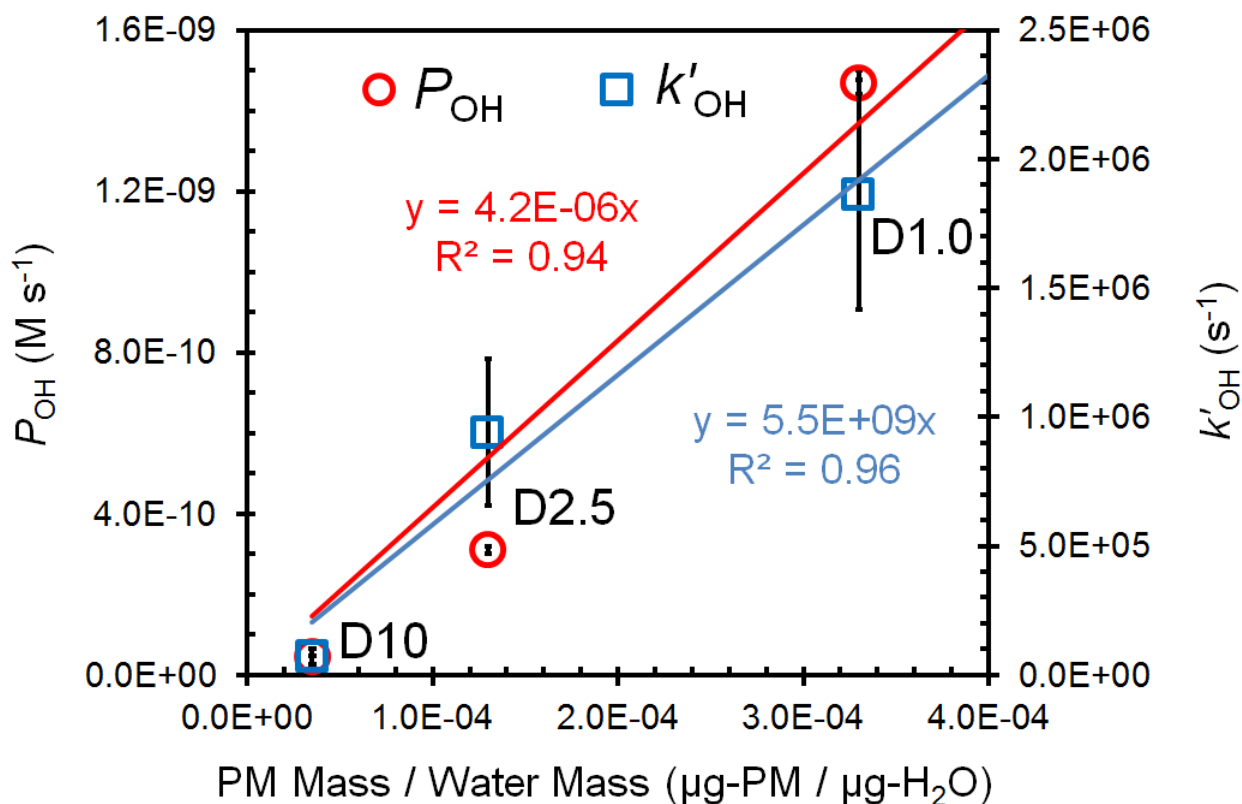


370

371 **Figure S9.** Winter-solstice-normalized pseudo-first-order rate constants (k'_{Probe}) for loss of
 372 syringol (top panel) and methyl jasmonate (bottom panel). The bar representing each rate
 373 constant is colored to represent the contributions of hydroxyl radical (yellow), singlet molecular
 374 oxygen (purple) and triplet excited states (green) to probe loss. The Davis winter-solstice lifetime
 375 of each probe (τ_{Probe} , black diamonds) is shown on the right y-axes. The first four bars represent
 376 probe data from wintertime fog waters collected in Davis (Kaur and Anastasio, 2018)

377

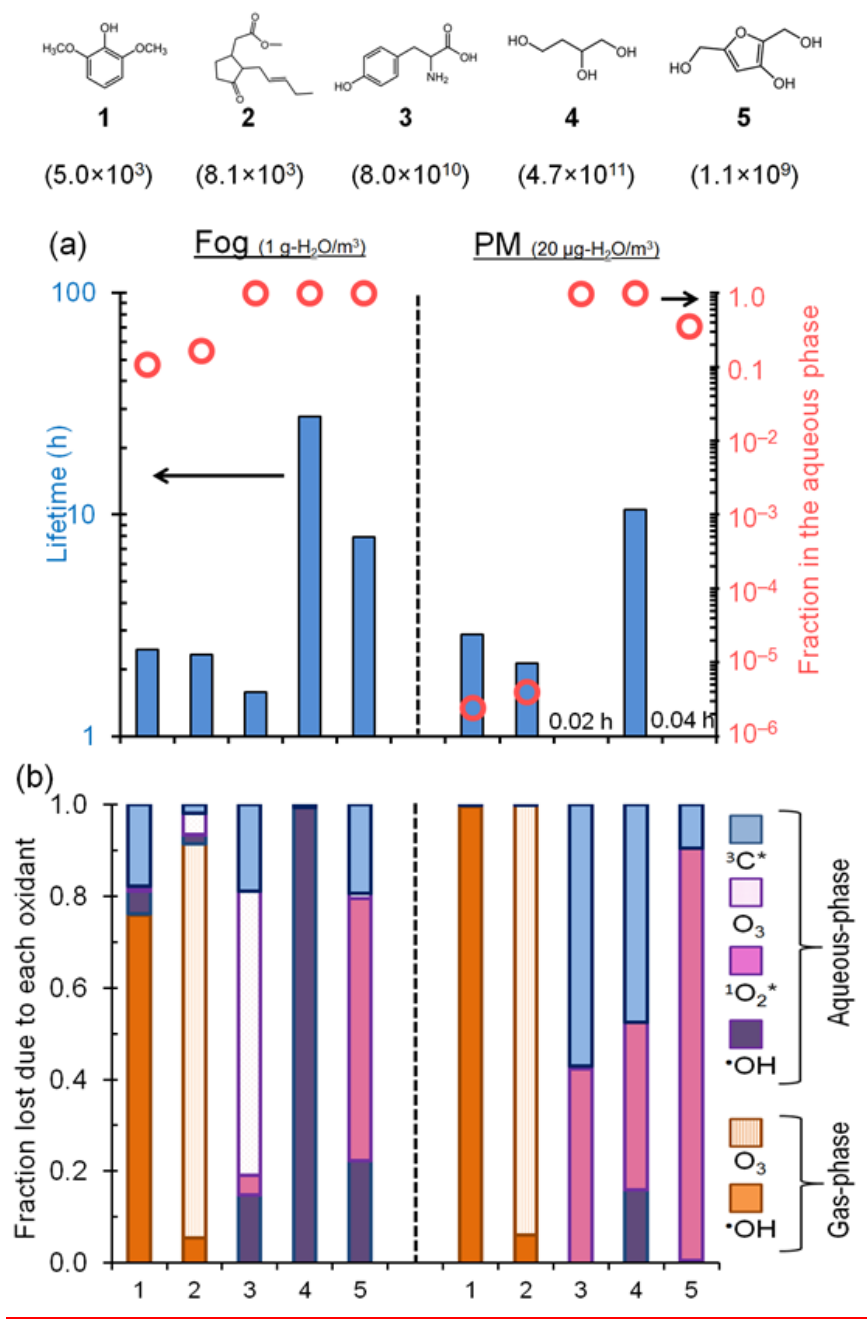
378



379

380 **Figure S10.** Dependence of rate of $\cdot\text{OH}$ photoproduction (P_{OH} ; red circles, left y-axis) and rate
 381 constant for loss of $\cdot\text{OH}$ due to natural sinks (k'_{OH} ; blue squares, right y-axis) with PM
 382 mass/water mass ratio in three PME3D samples. ($\cdot\text{OH}$ kinetic measurements were not made in
 383 the other two PME3D samples.) Measurements of $\cdot\text{OH}$ kinetics in the PME3D samples are
 384 discussed in Section S1 and shown in Table S3. Using the slopes of the linear relationships to
 385 extrapolate P_{OH} and k'_{OH} to values under ambient particle conditions (1 $\mu\text{g-PM}/\mu\text{g-H}_2\text{O}$) gives
 386 $P_{\text{OH}} = 4.2 \times 10^{-6} \text{ M s}^{-1}$ and $k'_{\text{OH}} = 5.5 \times 10^9 \text{ s}^{-1}$. Error bars represent ± 1 standard error and are
 387 too small to be visible for P_{OH} .

388



389

390 **Figure S11.** Fate of five model organic compounds – syringol, methyl jasmonate, tyrosine,
 391 1,2,4-butanetriol and 3-hydroxy-2,5-bis(hydroxymethyl)furan – under fog (left of vertical dashed
 392 line) and PM (right of dashed line) conditions using an upper-bound estimate for triplet
 393 concentrations in PM. Estimated Henry's law constants for the compounds (in units of M atm^{-1})
 394 are in parentheses beneath each structure. Panel (a): the blue columns represent overall lifetimes
 395 of the organics via both gas and aqueous-phase loss processes, and the red open circles represent
 396 the fractions present in fog or aqueous PM. (b) Fraction of each compound lost via each
 397 pathway. The aqueous triplet concentration in PM is $1.5 \times 10^{-10} \text{ M}$ (Table S15, Fig. 5, main text).
 398 All oxidant concentrations and rate constant data are shown in Tables S16 and S17.

399 S1. Hydroxyl radical measurements in PME3 and PME3D extracts

400 S1.1: Determining $\cdot\text{OH}$ steady-state concentrations ($[\cdot\text{OH}]$)

401 Typically, for $\cdot\text{OH}$ measurements we used benzene as the probe. Since benzene is volatile, we
402 performed the illumination in 5 mL sealed quartz cuvettes (instead of quartz tubes) fully filled
403 with extract, only withdrawing 100 μL for analysis at each time point to minimize loss of
404 benzene due to volatilization into the headspace. However, for the PME3D extracts, where we
405 had limited sample volume, we could not fully fill the 5 mL cuvettes. Due to this limitation, for
406 the PME3D samples we monitored the loss of 2-methyl-3-buten-2-ol (MBO) to determine $\cdot\text{OH}$
407 concentrations, then separately measured the production rate of $\cdot\text{OH}$ using benzene (for the three
408 dilutions with sufficient volume), and combined these two measures to determine the $\cdot\text{OH}$ sink.

409
410 There are three main reasons we chose MBO as a probe: 1) it is less volatile than benzene in
411 water, 2) its rate constants with the major photooxidants (i.e. $\cdot\text{OH}$, $^1\text{O}_2^*$ and $^3\text{C}_i^*$) are known, and
412 3) its reaction with $\cdot\text{OH}$ is much faster than with $^1\text{O}_2^*$ and $^3\text{C}_i^*$ (see below). Fresh MBO stock
413 was made one day prior to each experiment. 1.0 mL of acidified (pH 4.2) PME3D extract was
414 spiked to 75 μM MBO, capped and illuminated with simulated sunlight in a quartz tube of 4 mm
415 pathlength. [Unfortunately, we later realized that this relatively high concentration of MBO was
416 sometimes a significant sink for \$\cdot\text{OH}\$ in our PME3 extracts, thus suppressing the apparent steady-
417 state concentration of hydroxyl radical. We are able to approximately correct for this error using
418 an MBO Correction Factor, which is described below.](#)

419
420 Throughout the illumination period, MBO loss was measured with HPLC-UV (eluent of 20%
421 acetonitrile: 80% Milli-Q water, flow rate of 0.6 mL/min, detection wavelength of 200 nm and
422 column temperature of 35°C). The pseudo-first-order rate constant for loss of MBO (k'_{MBO} ; s^{-1})
423 was obtained as the negative of the slope of the plot of $\ln([\text{MBO}]/[\text{MBO}]_0)$ versus time, then
424 normalized to Davis-winter-solstice light using an analog of Eq. (4) in the main text. Because
425 MBO is not a specific probe for $\cdot\text{OH}$, its loss in each sample is the sum of all its loss pathways:

$$426 \quad k'_{\text{MBO}} = k_{\text{MBO}+\text{OH}} [\cdot\text{OH}] + k_{\text{MBO}+^1\text{O}_2^*} [^1\text{O}_2^*] + \Sigma(k_{\text{MBO}+^3\text{C}_i^*} [^3\text{C}_i^*]) + j_{\text{MBO}} \quad (\text{S1})$$

427 where $[\cdot\text{OH}]$, $[^1\text{O}_2^*]$ and $\Sigma[^3\text{C}_i^*]$ are the steady-state concentrations of the photooxidants. The
428 variables $k_{\text{MBO}+\text{OH}}$ ($7.4 (\pm 0.5) \times 10^9 \text{ M}^{-1} \text{ s}^{-1}$; (Richards-Henderson et al., 2014b)), $k_{\text{MBO}+^1\text{O}_2^*}$ (7.0
429 $(\pm 1.0) \times 10^5 \text{ M}^{-1} \text{ s}^{-1}$; (Richards-Henderson et al., 2014b)) and $k_{\text{MBO}+^3\text{C}_i^*}$ (discussed below) are the

430 second-order rate constants for reactions of MBO. j_{MBO} is the rate constant for direct
431 photodegradation of the probe and is negligible for our illumination times ($2.7 \times 10^{-7} \text{ s}^{-1}$).

432
433 Eq. (S1) has two unknown quantities: 1) $[\cdot\text{OH}]$ and 2) the loss of MBO due to triplets, i.e.,
434 $\Sigma(k_{\text{MBO}+3\text{Ci}^*}[\cdot\text{C}_i^*])$. To get $[\cdot\text{OH}]$, we first estimated MBO loss due to triplets ($\Sigma(k_{\text{MBO}+3\text{Ci}^*}[\cdot\text{C}_i^*])$)
435 by using two assumptions about the triplets. Our first assumption is that all loss of the triplet
436 probe syringol is due to $^3\text{C}^*$ and $^1\text{O}_2^*$, i.e., $\cdot\text{OH}$ is a negligible oxidant for SYR, based on our
437 measurements in the other samples, PME1-6, where the fraction of SYR lost due to $^3\text{C}^*$ and $^1\text{O}_2^*$
438 (combined) is 91 to 98% (Table S8). While we did measure the loss of methyl jasmonate in the
439 PME3D samples, we only used syringol loss to determine $\cdot\text{OH}$ concentrations since our first
440 assumption listed above is not valid for MeJA, i.e., we cannot assume that all loss of MeJA is
441 due to $^3\text{C}^*$ and $^1\text{O}_2^*$ since $\cdot\text{OH}$ is a significant sink for MeJA (Table S9).

442
443 The loss of syringol in the PME3D extracts is the sum of its loss due to $\cdot\text{OH}$, $^1\text{O}_2^*$ and $^3\text{C}^*$:

444
445
$$k'_{\text{SYR}} = k_{\text{SYR}+\text{OH}} [\cdot\text{OH}] + k_{\text{SYR}+^1\text{O}_2^*} [^1\text{O}_2^*] + \Sigma(k_{\text{SYR}+3\text{C}_i^*} [^3\text{C}_i^*]) \quad (\text{S2})$$

446
447 Direct photodegradation of syringol is negligible, and the contributions of other oxidants have
448 been previously determined to be small (Section 2.5.3, main text). Based on our first assumption,
449 $k_{\text{SYR}+\text{OH}} [\cdot\text{OH}]$ is much smaller than the sum of the other two terms on the right-hand side of Eq.
450 (S2) and this equation can be simplified to:

451
452
$$k'_{\text{SYR}} \approx k_{\text{SYR}+^1\text{O}_2^*} [^1\text{O}_2^*] + \Sigma(k_{\text{SYR}+3\text{C}_i^*} [^3\text{C}_i^*]) \quad (\text{S3})$$

453
454 Our second assumption is that the reactivity of the triplet mixture in the PM extracts most closely
455 resembles a binary mixture of the model triplets $^3\text{MAP}^*$ and $^3\text{DMB}^*$ — since these are the best
456 triplet matches obtained for majority of the particle extracts (Table S11). For simplicity, we use a
457 1:1 mixture of the two model triplets. Thus, for $k_{\text{SYR}+3\text{C}_i^*}$ we used a triplet-syringol rate constant
458 ($\pm \sigma$) of $3.7 (\pm 0.2) \times 10^9 \text{ M}^{-1} \text{ s}^{-1}$, which is the average of $k_{\text{SYR}+3\text{MAP}^*}$ and $k_{\text{SYR}+3\text{DMB}^*}$ (Table S10)
459 in Eq. (S3) to obtain the triplet steady-state concentration:

460

$$\Sigma[{}^3\text{C}_i^*] = \frac{k'_{\text{SYR}} - (k_{\text{SYR}+1\text{O}_2^*} [{}^1\text{O}_2^*])}{k_{\text{SYR}+3\text{C}_i^*}} \quad (\text{S4})$$

Using the measured singlet oxygen concentration, $[{}^1\text{O}_2^*]$, for each PME3 dilution we determine $\Sigma[{}^3\text{C}_i^*]$ in Eq. (S4), which we then plug into Eq. (S1), along with $k_{\text{MBO}+3\text{C}_i^*} = 3.4 (\pm 0.4) \times 10^7 \text{ M}^{-1} \text{ s}^{-1}$, the average of $k_{\text{MBO}+33\text{MAP}^*}$ and $k_{\text{MBO}+3\text{DMB}^*}$ (Richards-Henderson et al. (2014b)), to obtain the first iteration of $[{}^\bullet\text{OH}]$:

$$[{}^\bullet\text{OH}] = \frac{k'_{\text{MBO}} - k_{\text{MBO}+1\text{O}_2^*} [{}^1\text{O}_2^*] - \Sigma(k_{\text{MBO}+3\text{C}_i^*} [{}^3\text{C}_i^*])}{k_{\text{MBO}+3\text{C}_i^*}} \quad (\text{S5})$$

We then remove the first assumption and plug these $[{}^\bullet\text{OH}]$ values into Eq. (S2) to get a second set of $\Sigma[{}^3\text{C}_i^*]$ values, which we use in Eq. (S1) to obtain the second iteration of $[{}^\bullet\text{OH}]$. We continue this iterative process until the $[{}^\bullet\text{OH}]$ values change by less than 0.01% (Table S18).

Table S18. [Determination of hydroxyl radical steady-state concentrations, \$\[{}^\bullet\text{OH}\]\$, from results of the MBO experiments](#)

Sample ID	[OH] from Iterations, 10^{-16} M				MBO Correction Factor	1/S_λ	Final [{}^\bullet\text{OH}] 10^{-16} M
	Iteration 1	Iteration 2	Iteration 3	Iteration 4			
PME3D0.5	5.54 (1.87)	5.72 (1.93)	5.73 (1.93)	5.73 (1.39)	1.10	1.15	7.3 (1.8)
PME3D1	5.74 (1.91)	5.93 (1.97)	5.94 (1.97)	5.94 (1.40)	1.24	1.07	7.9 (1.9)
PME3D1.3	2.23 (0.76)	2.31 (0.77)	2.31 (0.79)	2.31 (0.57)	1.27	1.05	3.0 (0.8)
PME3D2.5*	2.19 (0.75)	2.26 (0.77)	2.26 (0.77)	2.26 (0.57)	1.43	1.03	3.3 (1.0)
PME3D10	1.89 (0.68)	1.95 (0.70)	1.95 (0.70)	1.95 (0.54)	3.31	1.01	6.6 (2.8)

Uncertainties in parentheses are ± 1 standard error.

479 We then made two corrections to the fourth (and final) iteration values. The first, and largest,
480 correction was to account for the scavenging of $\cdot\text{OH}$ by MBO by multiplying by an “MBO
481 Correction Factor”. This correction factor is the sum of the pseudo-first-order rate constants for
482 MBO and natural scavengers divided by the pseudo-first-order rate constant for natural
483 scavengers. As shown in Table S18, this correction increases as the sample gets more dilute:
484 values range from a modest 1.10 in the most concentrated extract to a very large 3.31 in the most
485 dilute extract. The second correction was to divide by the light screening factor, S_λ (Table S1 and
486 Sect. 2.5.1 of main text) to account for light absorption in our container; since the light screening
487 factors are close to 1 (i.e., 0.87 – 0.99), these corrections are relatively small. The standard errors
488 on the final $\cdot\text{OH}$ concentrations account for both the experimental uncertainty as well as the
489 uncertainty associated with the MBO correction factor.

490 **S1.2: Rate of $\cdot\text{OH}$ photoproduction (P_{OH})**

491 Similar to the other extracts, in the PME3 samples we used benzene as the probe measure $\cdot\text{OH}$
492 photoformation (Kaur and Anastasio, 2017; Anastasio and McGregor, 2001; Zhou and Mopper,
493 1990). A 5.0 mL aliquot of extract was acidified to pH 4.2 (± 0.2) and spiked with 1500 μM
494 benzene, which should scavenge essentially all $\cdot\text{OH}$. The solution was illuminated in a capped,
495 sealed quartz cuvette with a 1 cm pathlength (Sect. 2.5.1 in main text). In all cases, phenol
496 concentration increased linearly with time, and the rate of phenol formation (R_p) was obtained as
497 the slope of the plot of phenol concentration versus time. We then plotted $1/R_p$ versus
498 $1/[\text{Benzene}]$ and the intercept of that plot gave the experimentally measured rate of $\cdot\text{OH}$
499 photoproduction ($P_{\text{OH,EXP}}$) (Zhou and Mopper, 1990). Measured rates of $\cdot\text{OH}$ formation were
500 normalized to the rate expected under midday Davis, CA winter-solstice sunlight (P_{OH}) based on
501 2-nitrobenzaldehyde (2NB) actinometry:

$$502 \quad P_{\text{OH}} = P_{\text{OH,EXP}} \times \frac{j_{2\text{NB,WIN}}}{j_{2\text{NB,EXP}}} \quad (\text{S6})$$

503 where $j_{2\text{NB,WIN}}$ is the rate constant for loss of 2NB measured at midday near the winter solstice in
504 Davis (0.0070 s^{-1} ; Anastasio and McGregor, (2001)), and $j_{2\text{NB,EXP}}$ is the measured rate constant
505 for loss of 2NB on the day of the experiment. Due to the volume requirements of this technique,
506 we were only able to measure P_{OH} in three extracts – PME3, PME3D2.5* and PME3D10.

507

508 **S1.3 Rate constant for loss of $\cdot\text{OH}$ due to natural sinks (k'_{OH})**

509 In the PME3 samples we calculated the pseudo-first-order rate constant for loss of $\cdot\text{OH}$ due to
510 natural sinks by dividing the measured rate of $\cdot\text{OH}$ photoproduction determined with benzene
511 (Sect. S1.2) by the measured $\cdot\text{OH}$ steady-state concentration determined with MBO (Sect. S1.1):

$$512 \quad k'_{\text{OH}} = \frac{P_{\text{OH}}}{[\cdot\text{OH}]} \quad (\text{S7})$$

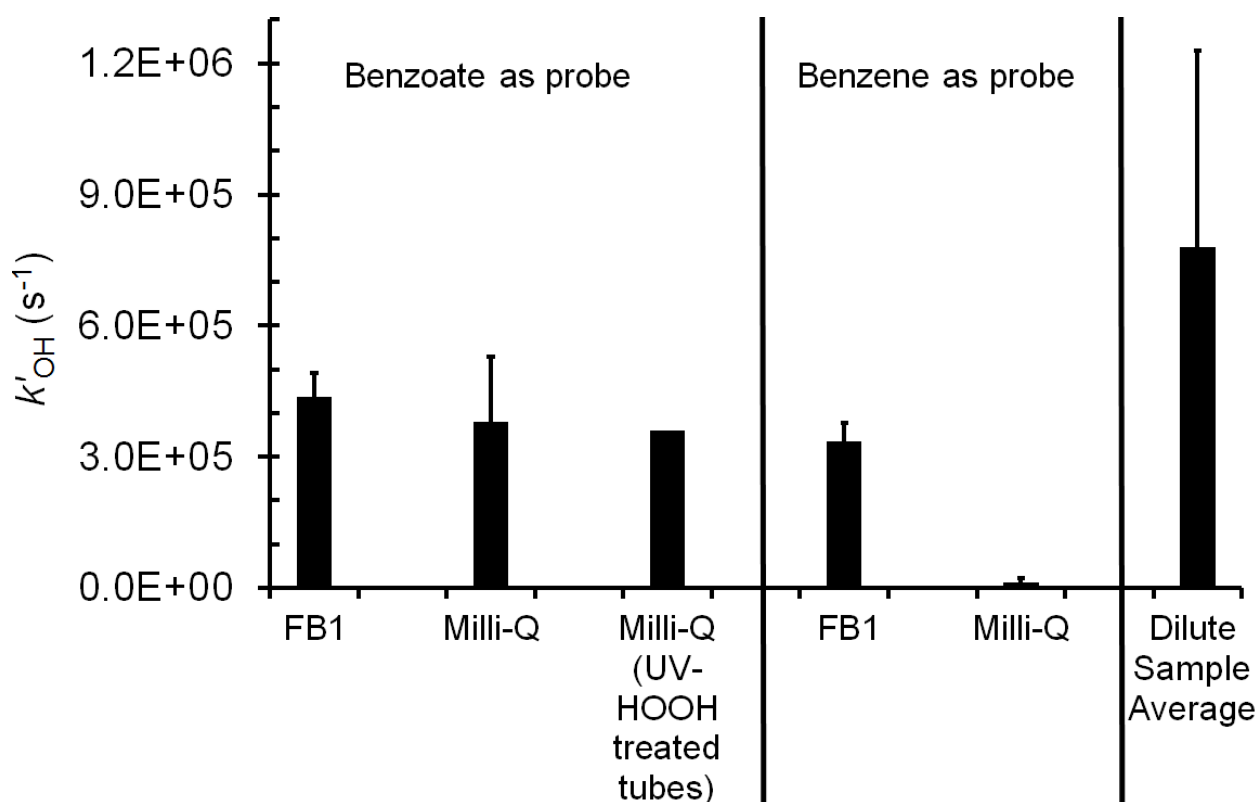
513 **S2. $\cdot\text{OH}$ sink measurements (k'_{OH}) in field blanks FB1 and FB2**

514 We also measured the rate constant for loss of $\cdot\text{OH}$ due to natural sinks (k'_{OH}) in field blank FB1,
515 which was extracted under the “dilute conditions”, i.e. each 2×2 cm filter square was extracted
516 in 2.5 mL Milli-Q.

517
518 In the early stages of this project, we used benzoate as an $\cdot\text{OH}$ probe (Anastasio and McGregor,
519 2001), which reacts with $\cdot\text{OH}$ to form m-hydroxybenzoic acid, m-HBA (and other products),
520 which was quantified using UV-HPLC. Four 5.0 mL aliquots of extract were spiked with 100–
521 1500 μM of sodium benzoate/benzoic acid solution (20 mM) at pH 4.2. Since P_{OH} in FB1 was
522 below our detection limit (Table S3), we added 200 μM hydrogen peroxide as an $\cdot\text{OH}$ source to
523 each aliquot in order to measure the $\cdot\text{OH}$ sinks. Aliquots were illuminated in capped quartz tubes
524 with a 0.4 cm pathlength (Sect. 2.3 main text). The formation of m-HBA was linear in all cases,
525 and the slope of the plot of [m-HBA] versus time in each aliquot is the rate of m-HBA formation
526 (R_{P} , $\mu\text{M min}^{-1}$). Similar to the benzene technique, we then plotted $1/R_{\text{P}}$ versus $1/[\text{benzoate}]$, used
527 the slope and y-intercept of the inverse plot to obtain P_{OH} , k'_{OH} and $[\cdot\text{OH}]$, which were
528 normalized to Davis midday solstice sunlight conditions. k'_{OH} measured using benzoate was 4.4
529 $(\pm 0.5) \times 10^5 \text{ s}^{-1}$, and represented 56% of the dilute sample average (PME1*, PME2*,
530 PME3D2.5). Because this is high, we ran a number of tests to identify the source of the
531 background $\cdot\text{OH}$ sinks in FB1, starting with measuring k'_{OH} in two Milli-Q solutions containing
532 only HOOH and probe stocks to identify whether these were the source of contamination. k'_{OH} in
533 Milli-Q was nearly as high as in FB1: even after rigorously cleaning the quartz tubes using a
534 UV+HOOH treatment (Chen et al., 2016), k'_{OH} was not lowered appreciably (Fig. S12). Since at
535 this point, it appeared that the probe chemicals (sodium benzoate and benzoic acid) could be
536 contaminated, we decided to switch to benzene as the $\cdot\text{OH}$ probe.

537

538 The experimental procedure for the benzene technique is very similar to the benzoate technique,
 539 except that the aliquots of FB1 were acidified to pH 4.2 (± 0.2) using 10 mM sulfuric acid. While
 540 the k'_{OH} value using benzene was slightly lower than the benzoate case ($3.4 (\pm 0.4) \times 10^5 s^{-1}$), it
 541 still represented 43% of the PM sample average. We then performed the benzene technique in
 542 Milli-Q water: the resulting k'_{OH} of $1.2 (\pm 0.1) \times 10^4 s^{-1}$ was more than 10 times lower than the
 543 other measurements, typical of solutions without any background organic contamination (Chen
 544 et al., 2016). This was the lowest k'_{OH} measured in our trials so, we chose to proceed with
 545 benzene as the probe for measuring $\cdot OH$ in the particle extracts.



546
 547 **Figure S12.** Measured pseudo-first-order rate constant for loss of $\cdot OH$ due to natural sinks (k'_{OH})
 548 in various solutions using sodium benzoate/benzoic acid and benzene as $\cdot OH$ probes. Samples
 549 labeled “Milli-Q” contain only probe and HOOH. Samples labeled “FB1” are measurements in
 550 the extract solution of Field Blank 1. “Dilute Sample Average” is the average of the k'_{OH}
 551 measurements in PME1*, PME2* and PME3D2.5* (Table S3).

552
 553 We next determined k'_{OH} in FB2 with benzene under standard extract conditions (1 mL Milli-Q
 554 per filter square). However, the resulting value of $2.7 (\pm 0.1) \times 10^5 s^{-1}$ is not much lower than the
 555 value in (more dilute) FB1 determined with benzoate and is 20 times higher than the Milli-Q
 556 value. But because the k'_{OH} value in the standard extracts (PME3D1-PME6) is high (Table S3),

557 the corresponding FB2 value is only 11% of the standard sample average. One plausible
558 contributing factor to the high k'_{OH} in the field blanks is that organic matter is coming off the
559 filter material during extraction; we see this in the DOC measurements for both field blanks
560 (Table S2). For future studies, we recommend first evaluating a few different types of particle
561 filters by making background k'_{OH} measurements and then picking the filters that introduce the
562 least contamination.

563 We did not adjust values of k'_{OH} measured in the particle extracts for the field blank rate
564 constants. If we had adjusted them, $\bullet\text{OH}$ concentrations would have increased by 50% in the
565 “dilute” extracts and by 10% in the standard extracts. However, the concentrations would still be
566 similar to fog. Additionally, this adjustment would have no effect on the extrapolation to ambient
567 PM conditions, since $[\bullet\text{OH}]$ in all PME3D extracts would go up equally.

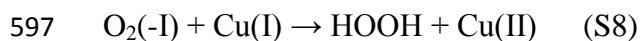
568 **S3. Other oxidants in PM extracts**

569 Since the probes we use for triplet determination do not react with only triplets (Eq. (5), main
570 text), we account for the contributions of $^1\text{O}_2^*$ and $\bullet\text{OH}$ to probe loss. However, it is also
571 possible that other oxidants (that we do not measure) are also contributing to triplet probe loss.
572 Here we examine this possibility for triplet probe loss in the PM extracts. In our previous
573 measurements of photooxidants in fog water (Kaur and Anastasio, 2018), we estimated the
574 importance of hydroperoxyl radical/superoxide radical anion ($\text{HO}_2\bullet/\bullet\text{O}_2^-$), ozone (O_3), carbonate
575 radical ($\bullet\text{CO}_3^-$) and hydrogen ion/hydrated electron ($\text{H}\bullet(\text{aq})/\text{e}^-(\text{aq})$) and found that these species
576 in total contributed less than 7 % to the average measured syringol loss. To do this calculation
577 for our PM extracts, we estimate the steady-state concentrations of these oxidants in the
578 illuminated extracts and, using reaction rate constants available in literature, calculate a pseudo-
579 first-order rate constant for their reaction with syringol. We then compare that to the average (\pm
580 σ) measured syringol loss in the standard extracts, $k'_{\text{SYR}} = 3.9 (\pm 1.3) \times 10^{-4} \text{ s}^{-1}$. As we noted in
581 our previous paper, there are insufficient rate constants in the literature for reactions of methyl
582 jasmonate in order to estimate its potential loss to other oxidants.

583 **Hydroperoxyl Radical / Superoxide Radical Anion ($\text{O}_2(-\text{I})$)**

584 Hydroperoxyl radical and superoxide radical anion (i.e., $\text{O}_2(-\text{I})$) are a conjugate acid-base pair;
585 the $\text{p}K_a$ of $\text{HO}_2\bullet$ is 4.75 ± 0.08 (Bielski et al., 1985). Since the pH of our extracts was adjusted to
586 ambient particle pH of 4.2 (Parworth et al., 2017), the mole fractions of $\text{HO}_2\bullet$ and $\bullet\text{O}_2^-$ in the
587 extracts are 0.78 and 0.22, respectively. There are no rate constants available for reaction of
588 either species with syringol (2,6-dimethoxyphenol) so we use the fastest reported rate constants
589 for reactions of similar compounds with $\bullet\text{O}_2^-$ and $\text{HO}_2\bullet$. For substituted phenols, the rate
590 constant for reaction of $\bullet\text{O}_2^-$ with guaiacol (2-methoxyphenol) is $2.5 \times 10^3 \text{ M}^{-1}\text{s}^{-1}$ (Yasuhisa et
591 al., 1993); for $\text{HO}_2\bullet$, the rate constant with catechol (1,2-benzenediol) is $4.7 \times 10^4 \text{ M}^{-1}\text{s}^{-1}$
592 (Bielski, 1983). At pH 4.2, the mole-fraction weighted rate constant, used as the proxy for
593 $k_{\text{SYR}+\text{O}_2(-\text{I})}$, is $3.7 \times 10^4 \text{ M}^{-1}\text{s}^{-1}$.

594 To estimate $\text{O}_2(-\text{I})$ concentrations in the extracts, we use previously measured rates of HOOH
595 formation in illuminated fog waters from California's Central Valley since these two oxidants
596 are intimately connected (Deguillaume et al., 2004; Anastasio, 1994):



598 The maximum measured production rate of HOOH, P_{HOOH} , in illuminated Central Valley fogs is
599 $3 \mu M h^{-1}$ ($8.3 \times 10^{-10} M s^{-1}$; Anastasio (1994)). We expect that P_{HOOH} in particle extracts will be
600 higher than fog, so we use an enhancement factor based on the observed increase in singlet
601 oxygen concentrations in the standard extracts, which is a factor of seven higher than Davis fog
602 average (Table S7). The reaction rate constants for $\cdot O_2^-$ and $HO_2\cdot$ reacting with Cu(I) are $9.4 \times$
603 $10^9 M^{-1} s^{-1}$ (Piechowski et al., 1993) and $3.5 \times 10^9 M^{-1} s^{-1}$ (Berdnikov, 1973), respectively,
604 which gives an overall, mole-fraction-weighted reaction rate constant, $k_{O_2(-I)+Cu(I)}$, of $4.8 \times 10^9 M^{-1}$
605 s^{-1} . We assume that the Cu(I) concentration is similar to that of $O_2(-I)$ (e.g., $[Cu(I)] \approx 1$ nM in
606 the daytime urban cloud scenario of Deguillaume et al. (2004)). Solving the rate equation for S8
607 with these inputs gives an $O_2(-I)$ steady-state concentration of $1.1 \times 10^{-9} M$. At this
608 concentration, the estimated loss rate constant for syringol due to $O_2(-I)$, $k'_{SYR,O_2(-I)}$ is 4.1×10^{-5}
609 s^{-1} , which would account for 11 % of the average observed syringol loss. This suggests that
610 superoxide is a minor sink for syringol in our samples, although it does appear to be more
611 significant in particle extracts than fog.

612 **Ozone (O_3)**

613 Based on the Henry's law constant for ozone at 25°C ($K_H = 1.1 \times 10^{-2} M atm^{-1}$ (Seinfeld and
614 Pandis, 2012) and assuming a gas-phase mixing ratio for O_3 of 30 ppbv, gives an initial aqueous-
615 phase concentration of ozone in our samples of $3.3 \times 10^{-10} M$. The actual concentration is likely
616 lower since our samples are capped during illumination. The bimolecular rate constant for
617 reaction of ozone with syringol is not available in the literature, so we estimate the rate constant
618 by using the value for phenol ($k_{PhOH+O_3} = 1.3 \times 10^3 M^{-1} s^{-1}$) (Hoigné and Bader, 1983) with an
619 enhancement factor of 10 based on the measured ratio of phenol and syringol rate constants for
620 reaction with $^3DMB^*$ (Smith et al., 2015). Under these assumptions, ozone is a very minor sink
621 for syringol in the fog samples ($k'_{SYR,O_3} = 4.3 \times 10^{-6} s^{-1}$), accounting for 1% of the average
622 measured syringol loss.

623 **Carbonate Radical ($\cdot CO_3^-$)**

624 The carbonate radical is formed mainly from the reactions of bicarbonate (HCO_3^-) and carbonate
625 (CO_3^{2-}) ions with $\cdot OH$ and triplet CDOM species. Although DOM components are likely

626 important sinks for $\bullet\text{CO}_3^-$, this quenching is poorly understood (Canonica et al., 2005; Vione et
627 al., 2014; Huang and Mabury, 2000). There are no published measurements of $\bullet\text{CO}_3^-$ in
628 atmospheric waters, so we use the typical steady-state concentration measured in surface waters
629 of 2×10^{-14} M determined using N,N-dimethylaniline as a probe (Huang and Mabury, 2000;
630 Zeng and Arnold, 2012). There are concerns that aniline probes overestimate $\bullet\text{CO}_3^-$ since they
631 also react rapidly with triplets (Rosario-Ortiz and Canonica, 2016), so we treat this as an upper-
632 bound estimate. We do not apply an enhancement factor in this case since DOM appears to play
633 the dual role of source and sink. While $\bullet\text{CO}_3^-$ reacts rapidly with electron-rich phenolates (i.e., a
634 deprotonated phenol), at pH 4.2 syringol is in the neutral, less reactive form. There are no rate
635 constants available for $\bullet\text{CO}_3^-$ reacting with methoxyphenols, so we assume the value with SYR
636 is 10 times higher than that with phenol ($4.9 \times 10^6 \text{ M}^{-1}\text{s}^{-1}$; Chen et al. (1975)). This results in a
637 pseudo-first-order rate constant for loss of SYR due to carbonate radical of $1 \times 10^{-6} \text{ s}^{-1}$, which
638 represents a negligible 0.3% of the average measured syringol loss rate constant in our standard
639 PM extracts.

640 **Hydrogen Ion / Aquated Electron ($\text{H}^\bullet_{(\text{aq})}/\text{e}^-_{(\text{aq})}$)**

641 Hydrogen ion (H^\bullet) and aquated electron ($\text{e}^-_{(\text{aq})}$) can be formed during irradiation or illumination
642 of dissolved organic matter in natural waters; these exist as a conjugate acid-base pair with a $\text{p}K_a$
643 of 9.6 (Kozmér et al., 2014; Buxton et al., 1988a). In our extracts at pH 4.2, the predominant
644 species would be $\text{H}^\bullet_{(\text{aq})}$. Zepp et al. (1987) determined an average steady-state concentration of
645 $\text{e}^-_{(\text{aq})}$ in sunlight-illuminated lake waters to be 1.2×10^{-17} M. Similar to $^1\text{O}_2^*$, since DOM is the
646 main source of $\text{e}^-_{(\text{aq})}$, we assume an enhancement factor of seven in the steady-state
647 concentration of $\text{e}^-_{(\text{aq})}$. As an upper bound, we assume the H^\bullet concentration to be equal to this.
648 The rate constant for syringol reacting with H^\bullet is not known. Using the average rate constant for
649 methoxyphenol, $2.1 \times 10^9 \text{ M}^{-1}\text{s}^{-1}$ (O'Neill et al., 1975; Neta and Schuler, 1972), the pseudo-
650 first-order rate constant for loss of SYR due to hydrogen ion is $1.7 \times 10^{-7} \text{ s}^{-1}$, which would
651 account for only 0.04% of the average observed syringol loss.

652 **Combined Contributions from Other Oxidants**

653 Based on our upper-bound estimates, the total rate constant for loss of syringol due to $\text{HO}_2^\bullet/\bullet\text{O}_2^-$,
654 O_3 , $\bullet\text{CO}_3^-$ and $\text{H}^\bullet_{(\text{aq})}/\text{e}^-_{(\text{aq})}$ is $\sim 4.6 \times 10^{-5} \text{ s}^{-1}$, which is only 12% of the average measured

655 syringol loss rate constant. Since this is small, our assumption that the loss of syringol is mainly
656 due to $\cdot\text{OH}$, $^1\text{O}_2^*$ and $^3\text{C}^*$ (Eq. (6), main text) seems valid.

657 **S4. Impacts of mass transport and increasing organic concentration on estimates of**
658 **aqueous photooxidant concentrations in ambient particles**

659 The steady-state concentration of an oxidant reflects the balance between its rate of formation
660 (P_{OX}) and first-order rate constant for loss ($k'_{OX} = 1 / \tau_{OX}$):

661
662 $[OX] = P_{OX} / k'_{OX}$ (S9)

663
664 where k'_{OX} is the sum of all the pseudo-first-order sinks of the oxidant. We can use our oxidant
665 measurements for the dilution series of sample PME3 to estimate how the aqueous formation rate
666 and rate constant for loss vary with solute concentration. But extrapolating these results to
667 particle liquid water conditions requires accounting for additional factors, such as mass transport.
668 Here we combine our aqueous measurements with estimates of these other factors to better
669 estimate oxidant concentrations from dilute fog or cloud drop conditions (i.e., a PM solute
670 mass/water mass ratio of 3×10^{-5} $\mu\text{g-PM}/\mu\text{g-H}_2\text{O}$) to a particle liquid water condition ($1 \mu\text{g-}$
671 PM/ $\mu\text{g-H}_2\text{O}$). We roughly estimate the gas-phase influence using a simplified case assuming a
672 temperature of 298 K, total pressure of 1 atm, an aqueous particle radius (R_p) of $0.5 \mu\text{m}$ at a PM
673 mass/water mass ratio of $1 \mu\text{g-PM}/\mu\text{g-H}_2\text{O}$, and a constant particle/drop density of 1 g cm^{-3} .

674
675 In the case of hydroxyl radical, based on our current measurements and previous work (Arakaki
676 et al., 2013; Anastasio and Newberg, 2007), the concentrations of the major aqueous sources
677 (nitrate, nitrite, and unknown species) and sinks (organic compounds) both scale linearly with
678 PM aqueous mass concentration, indicating that [$\cdot\text{OH}$] should be independent of dilution.
679 However, this does not consider the influence of the gas phase. The extremely short lifetime of
680 $\cdot\text{OH}$ in the particles ($1/k'_{OH} \sim 2 \times 10^{-10}$ s) indicates that this oxidant will not be at Henry's law
681 equilibrium and that the gas phase will be a source of $\cdot\text{OH}$. We estimate the rate of this gas-phase
682 mass transport to the particles (P_{MT}) using the Fuchs-Sutugin transition regime formula (Seinfeld
683 and Pandis, 2012) with an estimated gas-phase $\cdot\text{OH}$ concentration of 1×10^6 molecules cm^{-3} and
684 a mass accommodation coefficient of 1. Under these conditions the drop-volume-normalized
685 rate of $\cdot\text{OH}$ gas-to-particle transport increases from $7.7 \times 10^{-10} \text{ M s}^{-1}$ in dilute drops ($3 \times 10^{-5} \mu\text{g-}$
686 PM/ $\mu\text{g-H}_2\text{O}$) to $4.2 \times 10^{-7} \text{ M s}^{-1}$ under particle conditions ($1 \mu\text{g-PM}/\mu\text{g-H}_2\text{O}$). Over this same
687 range, the aqueous photoformation of $\cdot\text{OH}$ increases even more strongly, from $1.3 \times 10^{-10} \text{ M s}^{-1}$
688 to $4.2 \times 10^{-6} \text{ M s}^{-1}$, respectively. Thus the contribution of gas-phase mass transport to the overall

689 ·OH formation rate decreases as the drops become more concentrated, dropping from 86% in the
690 dilute drops to 9% in the particle condition. Considering both the aqueous- and gas-phase
691 sources of ·OH to the particles, we estimate the steady-state concentration at any dilution using
692

$$693 \quad [{}^{\bullet}\text{OH}(\text{aq})] = (P_{\text{OH}} + P_{\text{MT}})/k'_{\text{OH}} \quad (\text{S10})$$

694

695 These overall steady-state concentrations range from 5.4×10^{-15} M in the dilute drop condition to
696 8.4×10^{-16} M in the particle condition, as shown by the solid orange line in Figure 5.
697

698 In the case of singlet molecular oxygen, there is little gas-phase data, but past estimates
699 suggested concentrations on the order of 1×10^8 molecules cm^{-3} (Demerjian, 1974). At Henry's
700 law equilibrium, this gas-phase concentration corresponds to an aqueous concentration of 5×10^{-14}
701 M (using the Henry's law constant for ground state O_2 , 1.3×10^{-3} M atm^{-1} at 298 K; Seinfeld
702 and Pandis (2012)). This estimated aqueous concentration is somewhat smaller than our
703 measured concentrations in dilute extracts (Table S7), which are approximately as concentrated
704 as fog/cloud drops, and many orders of magnitude lower than our extrapolated particle
705 concentrations. Thus the net effect of mass transport will be to move ${}^1\text{O}_2^*$ from the particles to
706 the gas phase. As an upper bound, the fastest step in evaporation of ${}^1\text{O}_2^*$ is likely liquid-phase
707 diffusion, which has a characteristic time (Seinfeld and Pandis, 2012) of
708

$$709 \quad \tau_{\text{LD}} = R_p^2 / (\pi^2 \times D_{\text{aq}}) \quad (\text{S11})$$

710

711 where D_{aq} is the aqueous diffusion coefficient, approximately 1×10^{-5} $\text{cm}^2 \text{s}^{-1}$ if we assume an
712 aqueous particle. Calculated liquid-phase diffusion lifetimes range from 3×10^{-5} s for particles
713 ($1 \mu\text{g-PM}/\mu\text{g-H}_2\text{O}$ and an assumed radius of $0.5 \mu\text{m}$) to 0.02 s for dilute drops (3×10^{-5} $\mu\text{g-}$
714 $\text{PM}/\mu\text{g-H}_2\text{O}$, which corresponds to a radius of $13 \mu\text{m}$). The inverse of τ_{LD} is the approximate
715 first-order rate constant for liquid-phase diffusion, k'_{LD} ; values range from 60 s in dilute drops to
716 $4 \times 10^4 \text{ s}^{-1}$ in particles. These values are low compared to the first-order rate constant for
717 deactivation of ${}^1\text{O}_2^*$ in water ($k'_{\text{H}_2\text{O}} = 2.2 \times 10^5 \text{ s}^{-1}$; Bilski et al. (1997)), indicating that
718 evaporation is a minor sink.
719

720 Under cloud and fog drop conditions (and in our PM extracts) deactivation by water is the major
 721 sink for singlet oxygen, but under the more concentrated conditions of aqueous particles, organic
 722 compounds might also be important. To very roughly estimate this organic sink, we multiply our
 723 average DOC concentration in PM extracts (3.4 mM-C; Table S2) by a factor of 1000 to
 724 extrapolate to ambient PM conditions and assume all of this material is soluble, resulting in an
 725 aqueous concentration of particulate organics of 3.4 M-C. If each organic molecule has an
 726 average of 6 C atoms (i.e., the average is the same as levoglucosan), this corresponds to a water-
 727 soluble organic [molecule](#) concentration of 0.56 [mol-compounds L⁻¹](#). We apportion this total
 728 concentration based on the emissions measurements of Jen et al. (2019), where water-soluble
 729 organics in biomass burning emissions are roughly 50% sugars, 25% phenols, and 25% organic
 730 nitrogen. Table S19 below shows the resulting estimated particle concentrations, along with an
 731 estimated average rate constant for each class based on the compilation by Wilkinson et al.
 732 (1995). Summing the contributions from each compound class we estimate a total pseudo-first
 733 order rate constant for loss of ¹O₂* by soluble organics in the particles [\(at 1 μg-PM/μg-H₂O\)](#) of
 734 $2.8 \times 10^6 \text{ s}^{-1}$. [We linearly scale this sink, \$k'_{\text{ORG}}\$, by the PM mass/water mass ratio of the drops](#)
 735 [and particles to address dilution effects; e.g., for particles with 0.1 μg-PM/μg-H₂O, \$k'_{\text{ORG}} = 2.8 \times\$](#)
 736 [10⁵ s⁻¹.](#)

737 **Table S 19.** Estimates of the organic sink of ¹O₂* in aqueous particles [at 1 μg-PM/μg-H₂O](#)

Compound Class	Dissolved Concentration (M)	2 nd -order Rate Constant Range (M ⁻¹ s ⁻¹)	Assumed 2 nd -order k (M ⁻¹ s ⁻¹)	k'_{ORG} (s ⁻¹)
Sugars	0.28	10 ⁴	10 ⁴	2800
Phenols	0.14	10 ⁶ - 10 ⁷	10 ⁷	1.4 × 10 ⁶
Organic Nitrogen	0.14	10 ³ - 10 ⁹	10 ⁷	1.4 × 10 ⁶

738
 739 The resulting estimate for the steady-state concentration of ¹O₂* in [drops and](#) particles is

740
 741
$$[{}^1\text{O}_2^*] = P_{\text{IO}_2^*} / (k'_{\text{H}_2\text{O}} + k'_{\text{LD}} + k'_{\text{ORG}}) \quad (\text{S12})$$

742
 743 where the numerator, i.e., the rate of ¹O₂* photoformation [increases with increasing solute](#)
 744 [concentration according to the linear regression of our PME3D values \(with the y-intercept fixed](#)

745 at zero): $P_{1O_2^*} = 5.0 \times 10^{-4} \text{ M s}^{-1}/(\mu\text{g-PM}/\mu\text{g-water})$. This gives rates of singlet oxygen formation
746 that range from $1.5 \times 10^{-8} \text{ M s}^{-1}$ in dilute drops to $5.0 \times 10^{-4} \text{ M s}^{-1}$ for our standard particle
747 condition. The denominator of Eq. S12 is $2.2 \times 10^5 \text{ s}^{-1}$ in dilute drops and remains at this value
748 until the particle concentration reaches $10^{-3} \mu\text{g-PM}/\mu\text{g-water}$, at which point it increases because
749 of the increasingly concentrated organic sinks. At the particle condition of $1 \mu\text{g-PM}/\mu\text{g-H}_2\text{O}$, the
750 denominator is $3.1 \times 10^6 \text{ s}^{-1}$ and organic sinks account for 92% of $^1O_2^*$ loss. Calculated values of
751 $[^1O_2^*]$ range from $6.7 \times 10^{-14} \text{ M}$ in dilute drops to $1.6 \times 10^{-10} \text{ M}$ for the particle liquid water
752 condition.

753
754 For triplet excited states we fit our experimental data to a hyperbolic fit:

$$755 \quad [^3C^*] = \frac{a [m_{PM}/m_{H_2O}]}{1 + b [m_{PM}/m_{H_2O}]} \quad (\text{S13})$$

756 where m_{PM}/m_{H_2O} is the PM mass/water mass ratio, the numerator represents the formation of
757 triplets and the denominator represents the sinks. We fit our experimental data to this equation in
758 Excel in two ways: (1) a best fit, where the hyperbolic equation parameters were tuned to
759 minimize the regression error, and (2) a high estimate fit, where the parameters were tuned so
760 that the regression line passed near the top of the error bar for the most concentrated sample
761 extract (PME3D0.5). The parameters for these two fits are: (1) $a = 3.08 \times 10^{-10} \text{ M}$ and $b = 1.31 \times$
762 10^3 , and (2) $a = 2.26 \times 10^{-10} \text{ M}$ and $b = 17.0$. We did not include the data point for PME3D10
763 when determining the regression fits (but do show it in the plots) because of the larger
764 uncertainty in its triplet concentration, a result of the significant $\cdot\text{OH}$ perturbation by MBO in
765 this most dilute sample. Our interpretation of the curvature in these regression fits (Figure 5) is
766 that as the solutions get more concentrated, organics become the major triplet sink, causing
767 $[^3C^*]$ to plateau at higher PM mass/water mass ratios; we estimate the size of this organic sink in
768 the next section. Thus, these fits should account for the organic sinks that will be important under
769 particle conditions.

770
771 To a first approximation, we expect that mass transport will have no significant impact on the
772 concentrations of triplets. Since most of the BrC precursors for $^3C^*$ are likely in the particle
773 phase (rather than the gas phase) we expect that gas-phase concentrations of triplets are relatively
774 small and that the gas phase is not a significant source of triplets to the particles. We also expect
775 that evaporation of triplets is minor since their lifetimes are relatively short ($1 \mu\text{s}$ based just on

776 O₂ as a sink) and their gas-particle partitioning (like that of their BrC precursors) is strongly
777 tilted toward the particle phase. Thus we assume that the particle concentration of triplets is
778 relatively unaffected by mass transport. ~~As for potential organic sinks of ³C*, the curvature~~
779 ~~shown in Figures 4 and 5 is likely due to organics becoming major sinks in the more~~
780 ~~concentrated PM extracts; this is accounted for in our hyperbolic fit. However, it is also possible~~
781 ~~that the curvature is noise and that the ³C* concentration in particles is much higher than~~
782 ~~extrapolated using the hyperbolic fit in Figure 5; we explore both of these scenarios in the main~~
783 ~~text.~~

785 S5. Estimating triplet characteristics in particle extract PME3

786 We can use our measurements of triplet steady-state concentrations in the PME3 dilution series
787 to derive the first-order rate constant for triplet formation and the overall rate constant for triplet
788 reaction and quenching by DOC. The rate of triplet formation (P_{3C^*}) from the photoexcitation of
789 chromophores 'C' in the extracts can be expressed as:

$$791 \quad P_{3C^*} = j_{\text{abs}} \times \Phi_{\text{ISC}} \times [C] \quad (\text{S14})$$

792
793 where j_{abs} is the rate constant for light absorption (s^{-1}) by C and Φ_{ISC} is the intersystem crossing
794 quantum yield, i.e., the fraction of the first excited single state, S₁, that forms the lowest triplet
795 excited state, T₁. Assuming the chromophore concentration is a fraction f (mole-chromophore
796 mole-C⁻¹) of the DOC concentration (mole-C L⁻¹), the rate of triplet formation can be expressed
797 as

$$799 \quad P_{3C^*} = j_{\text{abs}} \times \Phi_{\text{ISC}} \times f \times [\text{DOC}] \quad (\text{S15})$$

801 The rate constant for loss of the triplet (k'_{3C^*} ; s^{-1}) in an extract is the sum of all its loss pathways:

$$803 \quad k'_{3C^*} = k_{3C^*+O_2} [O_2] + k_{\text{rxn}} [\text{DOC}] + k_{\text{Q}} [\text{DOC}] \quad (\text{S16})$$

805 where $k_{3C^*+O_2}$ is the bimolecular rate constant for O₂ quenching (we use the average value for the
806 three model triplets with measurements, $2.8 (\pm 0.4) \times 10^9 \text{ M}^{-1} \text{ s}^{-1}$; Table S11); [O₂] is the

807 dissolved oxygen concentration (284 μM at 20 $^{\circ}\text{C}$) (USGS, 2018); k_{rxn} ($\text{M}^{-1}\text{s}^{-1}$) is the rate
 808 constant for reaction of triplet with dissolved organics; and k_{Q} ($\text{M}^{-1}\text{s}^{-1}$) is the rate constant for
 809 the non-reactive quenching of triplet by DOC (Smith et al., 2014).

810 Assuming steady state, the triplet concentration is the ratio of its rate of photoproduction and its
 811 rate constant for loss:

$$812 \quad [{}^3\text{C}^*] = \frac{P_3\text{C}^*}{k'_{3\text{C}^*}} = \frac{j_{\text{abs}} \times \Phi_{\text{ISC}} \times f \times [\text{DOC}]}{k_{3\text{C}^*+\text{O}_2} [\text{O}_2] + (k_{\text{rxn}} + k_{\text{Q}}) [\text{DOC}]} \quad (\text{S17})$$

813 This can be re-written as

$$814 \quad [{}^3\text{C}^*] = \frac{\left(\frac{j_{\text{abs}} \times \Phi_{\text{ISC}} \times f}{k_{3\text{C}^*+\text{O}_2} [\text{O}_2]}\right) \times [\text{DOC}]}{1 + \left(\frac{k_{\text{rxn}} + k_{\text{Q}}}{k_{3\text{C}^*+\text{O}_2} [\text{O}_2]}\right) \times [\text{DOC}]} \quad (\text{S18})$$

815 We then fit our triplet steady-state concentration measurements in the PME3D extracts to the
 816 following two-parameter equation:

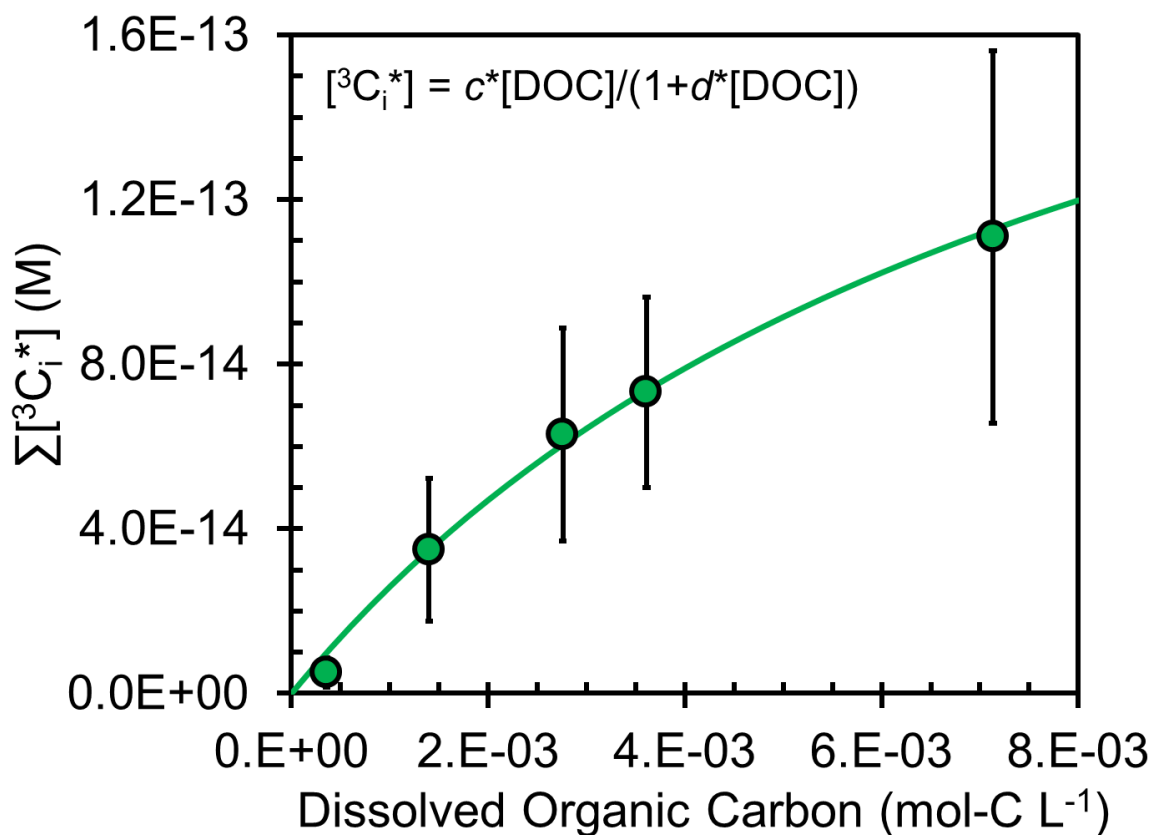
$$817 \quad [{}^3\text{C}^*] = \frac{c [\text{DOC}]}{1 + d [\text{DOC}]} \quad (\text{S19})$$

818 The regression fit is shown in Fig. S13; the parameters for the fit obtained using [Excel](#) are $c =$
 819 2.9×10^{-11} and $d = 117 \text{ M}^{-1}$; [we did not include the data point for PME3D10 in determining the](#)
 820 [regression fit because of the larger uncertainty in its triplet concentration, a result of the](#)
 821 [significant probe perturbation in this most dilute sample](#). Using the [regression](#) parameters, we
 822 calculate that the rate constant for triplet formation, i.e., $j_{\text{abs}} \times \Phi_{\text{ISC}} \times f$, is $2.3 (\pm 0.3) \times 10^{-5} \text{ s}^{-1}$
 823 and the sum of the reaction and quenching rate constants for the triplets by DOC, i.e., $k_{\text{rxn}} + k_{\text{Q}}$, is
 824 $9.3 (\pm 1.3) \times 10^7 \text{ L mol}^{-1} \text{ s}^{-1}$.

825

826

827



828

829

830 **Figure S13.** Change in triplet steady-state concentration with dissolved organic carbon
 831 concentration in the PME3D extracts. Error bars represent ± 1 standard error in measured triplet
 832 concentrations (Table S13). [The regression line is a fit of Equation S19 to the experimental data](#)
 833 [in Excel, yielding parameter estimates of \$c = 2.90 \times 10^{-11}\$ and \$d = 117 \text{ M}^{-1}\$.](#) [The PME3D10 point](#)
 834 [was not included in the regression fit \(although is shown on the plot\) because of issues with too-](#)
 835 [high probe concentrations in the \$\cdot\text{OH}\$ determination.](#) The DOC value for sample PME3D0.5
 836 (which had very limited volume) is estimated based on results for the other four dilutions and
 837 given in Table S2.

838 **S6. References**

- 839 Anastasio, C.: Aqueous phase photochemical formation of hydrogen peroxide in authentic
840 atmospheric waters and model compound solutions, Ph.D. Dissertation, Duke University,
841 1994.
- 842 Anastasio, C., and McGregor, K. G.: Chemistry of fog waters in California's central valley: 1. In
843 situ photoformation of hydroxyl radical and singlet molecular oxygen, *Atmospheric*
844 *Environment*, 35, 1079-1089, 2001.
- 845 Anastasio, C., and Newberg, J. T.: Sources and sinks of hydroxyl radical in sea-salt particles, *J.*
846 *Geophys. Res.*, 112, D10306, 2007.
- 847 Anbar, M., Meyerstein, D., and Neta, P.: Reactivity of aliphatic compounds towards hydroxyl
848 radicals, *Journal of the Chemical Society B: Physical Organic*, 742-747, 1966.
- 849 Andreev, P. Y.: Reaction of ozone with five-membered hetarenes in a liquid phase, *Russ. J.*
850 *Appl. Chem.*, 85, 1395-1398, 2012.
- 851 Arakaki, T., Anastasio, C., Kuroki, Y., Nakajima, H., Okada, K., Kotani, Y., Handa, D., Azechi,
852 S., Kimura, T., Tshako, A., and Miyagi, Y.: A general scavenging rate constant for
853 reaction of hydroxyl radical with organic carbon in atmospheric waters, *Environ. Sci.*
854 *Technol.*, 47, 8196-8203, 2013.
- 855 Atkinson, R., Aschmann, S. M., Fitz, D. R., Winer, A. M., and Pitts, J. N.: Rate constants for the
856 gas-phase reactions of O₃ with selected organics at 296 K, *Int. J. Chem. Kinet.*, 14, 13-
857 18, 1982.
- 858 Atkinson, R., Aschmann, S. M., and Carter, W. P.: Kinetics of the reactions of O₃ and OH
859 radicals with furan and thiophene at 298±2 K, *Int. J. Chem. Kinet.*, 15, 51-61, 1983.
- 860 Atkinson, R., Baulch, D., Cox, R., Crowley, J., Hampson, R., Hynes, R., Jenkin, M., Rossi, M.,
861 Troe, J., and Subcommittee, I.: Evaluated kinetic and photochemical data for atmospheric
862 chemistry: Volume II—gas phase reactions of organic species, *Atmos. Chem. Phys.*, 6,
863 3625-4055, 2006.
- 864 Barker, G., Fowles, P., and Stringer, B.: Pulse radiolytic induced transient electrical conductance
865 in liquid solutions. Part 2.—radiolysis of aqueous solutions of NO₃⁻, NO₂⁻ and Fe(CN)₆³⁻,
866 *J. Chem. Soc. Faraday Trans.*, 66, 1509-1519, 1970.
- 867 Berdnikov, V.: Catalytic activity of the hydrated copper ion in the decomposition of hydrogen
868 peroxide, *Russ. J. Phys. Chem.*, 47, 1060-1062, 1973.
- 869 Bertolotti, S. G., García, N. A., and Argüello, G. A.: Effect of the peptide bond on the singlet-
870 molecular-oxygen-mediated sensitized photo-oxidation of tyrosine and tryptophan
871 dipeptides. A kinetic study, *Journal of Photochemistry and Photobiology B: Biology*, 10,
872 57-70, 1991.
- 873 Bielski, B.: Evaluation of the reactivities of HO₂/O₂ with compounds of biological interest, *Oxy*
874 *Radicals and Their Scavenger Systems*. G. Cohen and RA Greenwald (Editors), 1, 1-7,
875 1983.
- 876 Bielski, B. H. J., Cabelli, D. E., Arudi, R. L., and Ross, A. B.: Reactivity of HO₂/O₂⁻ radicals in
877 aqueous solution, *Journal of Physical and Chemical Reference Data*, 14, 1041-1100,
878 1985.
- 879 Bilski, P., Holt, R. N., and Chignell, C. F.: Properties of singlet molecular oxygen O₂ (1Δg) in
880 binary solvent mixtures of different polarity and proticity, *Journal of Photochemistry and*
881 *Photobiology A: Chemistry*, 109, 243-249, 1997.

882 Buxton, G. V., Greenstock, C. L., Helman, W. P., and Ross, A. B.: Critical review of rate
883 constants for reactions of hydrated electrons, hydrogen atoms and hydroxyl radicals
884 ($\cdot\text{OH}/\text{O}^-$) in aqueous solution, *J. Phys. Chem. Ref. Data*, 17, 513-886, 1988a.
885 Buxton, G. V., Wood, N. D., and Dyster, S.: Ionisation Constants of $\cdot\text{OH}$ And HO_2 in Aqueous
886 Solution up to 200°C. A Pulse Radiolysis Study, *J. Chem. Soc., Faraday Trans.*, 84,
887 1113-1121, 1988b.
888 California Air Resources Board, iADAM database: Air Quality Data Statistics:
889 <https://www.arb.ca.gov/adam>, access: June 6, 2018.
890 Canonica, S., Hellrung, B., and Wirz, J.: Oxidation of phenols by triplet aromatic ketones in
891 aqueous solution, *J. Phys. Chem. A*, 104, 1226-1232, 2000.
892 Canonica, S., Kohn, T., Mac, M., Real, F. J., Wirz, J., and von Gunten, U.: Photosensitizer
893 method to determine rate constants for the reaction of carbonate radical with organic
894 compounds, *Environmental science & technology*, 39, 9182-9188, 2005.
895 Chen, S.-N., Hoffman, M. Z., and Parsons Jr, G. H.: Reactivity of the carbonate radical toward
896 aromatic compounds in aqueous solution, *J. Phys. Chem.*, 79, 1911-1912, 1975.
897 Chen, Z., Chu, L., Galbavy, E. S., Ram, K., and Anastasio, C.: Hydroxyl radical in/on
898 illuminated polar snow: Formation rates, lifetimes, and steady-state concentrations,
899 *Atmos. Chem. Phys.*, 16, 9579-9590, 2016.
900 Deguillaume, L., Leriche, M., Monod, A., and Chaumerliac, N.: The role of transition metal ions
901 on HO_x radicals in clouds: a numerical evaluation of its impact on multiphase chemistry,
902 *Atmos Chem Phys*, 4, 95-110, 2004.
903 Demerjian, K. L.: The mechanism of photochemical smog formation, *Adv. Environ. Sci.*
904 *Technol.*, 4, 1-262, 1974.
905 Hess, M., Koepke, P., and Schult, I.: Optical properties of aerosols and clouds: The software
906 package OPAC, *Bulletin of the American meteorological society*, 79, 831-844, 1998.
907 Hoigné, J., and Bader, H.: Rate constants of reactions of ozone with organic and inorganic
908 compounds in water—II: dissociating organic compounds, *Water Res.*, 17, 185-194,
909 1983.
910 Huang, J., and Mabury, S. A.: Steady-state concentrations of carbonate radicals in field waters,
911 *Environmental Toxicology and Chemistry*, 19, 2181-2188, 2000.
912 Hunter, T.: Radiationless transition $T_1 \rightarrow S_0$ in aromatic ketones, *Transactions of the Faraday*
913 *Society*, 66, 300-309, 1970.
914 Jen, C. N., Hatch, L. E., Selimovic, V., Yokelson, R. J., Weber, R., Fernandez, A. E., Kreisberg,
915 N. M., Barsanti, K. C., and Goldstein, A. H.: Speciated and total emission factors of
916 particulate organics from burning western US wildland fuels and their dependence on
917 combustion efficiency, *Atmos. Chem. Phys.*, 19, 1013-1026, 2019.
918 Kaur, R., and Anastasio, C.: Light absorption and the photoformation of hydroxyl radical and
919 singlet oxygen in fog waters, *Atmos. Environ.*, 164, 387-397, 2017.
920 Kaur, R., and Anastasio, C.: First measurements of organic triplet excited states in atmospheric
921 waters, *Environ. Sci. Technol.*, 52, 5218-5226, 2018.
922 Kozmér, Z., Arany, E., Alapi, T., Takács, E., Wojnárovits, L., and Dombi, A.: Determination of
923 the rate constant of hydroperoxyl radical reaction with phenol, *Radiat. Phys. Chem.*, 102,
924 135-138, 2014.
925 Lauraguais, A., Coeur-Tourneur, C., Cassez, A., and Seydi, A.: Rate constant and secondary
926 organic aerosol yields for the gas-phase reaction of hydroxyl radicals with syringol (2, 6-
927 dimethoxyphenol), *Atmos. Environ.*, 55, 43-48, 2012.

928 Lilie, J.: Pulsradiolytische untersuchung der oxydativen ringöffnung von furan, thiophen und
929 pyrrol/pulsradiolytic investigations of the oxydativ ring scission of furan, thiophen and
930 pyrrol, Zeitschrift für Naturforschung B, 26, 197-202, 1971.

931 McGregor, K. G., and Anastasio, C.: Chemistry of fog waters in California's Central Valley: 2.
932 Photochemical transformations of amino acids and alkyl amines, Atmos. Environ., 35,
933 1091-1104, 2001.

934 Meylan, W. M., and Howard, P. H.: Computer estimation of the atmospheric gas-phase reaction
935 rate of organic compounds with hydroxyl radicals and ozone, Chemosphere, 26, 2293-
936 2299, 1993.

937 Neta, P., and Schuler, R. H.: Rate constants for reaction of hydrogen atoms with aromatic and
938 heterocyclic compounds. Electrophilic nature of hydrogen atoms, Journal of the
939 American Chemical Society, 94, 1056-1059, 1972.

940 O'Neill, P., Steenken, S., and Schulte-Frohlinde, D.: Formation of radical cations of
941 methoxylated benzenes by reaction with OH radicals, Ti²⁺, Ag²⁺, and SO₄²⁻-in
942 aqueous solution. An optical and conductometric pulse radiolysis and in situ radiolysis
943 electron spin resonance study, Journal of Physical Chemistry, 79, 2773-2779, 1975.

944 O'Neill, P., and Steenken, S.: Pulse radiolysis and electron spin resonance studies on the
945 formation of phenoxyl radicals by reaction of OH radicals with methoxylated phenols and
946 hydroxybenzoic acids, Ber. Bunsenges. Phys. Chem., 81, 550-556, 1977.

947 Parworth, C. L., Young, D. E., Kim, H., Zhang, X., Cappa, C. D., Collier, S., and Zhang, Q.:
948 Wintertime water-soluble aerosol composition and particle water content in Fresno,
949 California, J. Geophys. Res. Atmos., 122, 3155-3170, 2017.

950 Piechowski, M. V., Nauser, T., Hoignè, J., and Bühler, R. E.: O₂⁻ decay catalyzed by Cu²⁺ and
951 Cu⁺ ions in aqueous solutions: a pulse radiolysis study for atmospheric chemistry,
952 Berichte der Bunsengesellschaft für physikalische Chemie, 97, 762-771, 1993.

953 Rehorek, D., and Seidel, A.: A. Leifer. The kinetics of environmental aquatic photochemistry.
954 ACS professional and reference book. American Chemical Society, Washington 1988,
955 304 S., 41 Abb., 35 Tab., Kart, Preis: US & Canada \$59.95, Export \$71.95, ISBN 0-
956 8412-1464-6, Cryst. Res. Technol., 24, 732-732, 1989.

957 Richards-Henderson, N. K., Hansel, A. K., Valsaraj, K. T., and Anastasio, C.: Aqueous oxidation
958 of green leaf volatiles by hydroxyl radical as a source of SOA: Kinetics and SOA yields,
959 Atmos. Environ., 95, 105-112, 2014a.

960 Richards-Henderson, N. K., Pham, A. T., Kirk, B. B., and Anastasio, C.: Secondary organic
961 aerosol from aqueous reactions of green leaf volatiles with organic triplet excited states
962 and singlet molecular oxygen, Environ. Sci. Technol., 49, 268-276, 2014b.

963 Rinke, M., and Zetzsch, C.: Rate Constants for the Reactions of OH Radicals with Aromatics:
964 Benzene, Phenol, Aniline, and 1, 2, 4-Trichlorobenzene, Ber. Bunsenges. Phys. Chem.,
965 88, 55-62, 1984.

966 Rosario-Ortiz, F. L., and Canonica, S.: Probe compounds to assess the photochemical activity of
967 dissolved organic matter, Environ. Sci. Technol., 50, 12532-12547, 2016.

968 Seinfeld, J. H., and Pandis, S. N.: Atmospheric chemistry and physics: From air pollution to
969 climate change, John Wiley & Sons, 2012.

970 Smith, J. D., Sio, V., Yu, L., Zhang, Q., and Anastasio, C.: Secondary organic aerosol production
971 from aqueous reactions of atmospheric phenols with an organic triplet excited state,
972 Environ. Sci. Technol., 48, 1049-1057, 2014.

973 Smith, J. D., Kinney, H., and Anastasio, C.: Aqueous benzene-diols react with an organic triplet
974 excited state and hydroxyl radical to form secondary organic aerosol, *Phys. Chem. Chem.*
975 *Phys.*, 17, 10227-10237, 2015.

976 Solar, S., Solar, W., and Getoff, N.: Reactivity of hydroxyl with tyrosine in aqueous solution
977 studied by pulse radiolysis, *J. Phys. Chem.*, 88, 2091-2095, 1984.

978 Tetreau, C., Lavalette, D., Land, E., and Peradejordi, F.: Sensitized triplet-triplet absorption of
979 biphenylene, *Chem. Phys. Lett.*, 17, 245-247, 1972.

980 Tratnyek, P. G., and Hoigne, J.: Oxidation of substituted phenols in the environment: A QSAR
981 analysis of rate constants for reaction with singlet oxygen, *Environ. Sci. Technol.*, 25,
982 1596-1604, 1991a.

983 Tratnyek, P. G., and Hoigne, J.: Oxidation of substituted phenols in the environment: a QSAR
984 analysis of rate constants for reaction with singlet oxygen, *Environmental science &*
985 *technology*, 25, 1596-1604, 1991b.

986 USEPA: Estimation Programs Interface Suite™ for Microsoft® Windows, v 4.11, United States
987 Environmental Protection Agency, Washington, DC, USA, 2012.

988 USGS: U.S. Geological Survey. Water Properties - Dissolved Oxygen. Available at
989 <https://water.usgs.gov/edu/dissolvedoxygen.html> [last accessed: January 23, 2018], 2018.

990 Vempati, H. S.: Physico-chemical properties of green leaf volatiles, 2014.

991 Vione, D., Minella, M., Maurino, V., and Minero, C.: Indirect photochemistry in sunlit surface
992 waters: photoinduced production of reactive transient species, *Chemistry-A European*
993 *Journal*, 20, 10590-10606, 2014.

994 Wilkinson, F., Helman, W. P., and Ross, A. B.: Quantum yields for the photosensitized
995 formation of the lowest electronically excited singlet state of molecular oxygen in
996 solution, *J. Phys. Chem. Ref. Data*, 22, 113-262, 1993.

997 Wilkinson, F., Helman, W. P., and Ross, A. B.: Rate constants for the decay and reactions of the
998 lowest electronically excited singlet state of molecular oxygen in solution. An expanded
999 and revised compilation, *J. Phys. Chem. Ref. Data*, 24, 663-677, 1995.

1000 Yasuhisa, T., Hideki, H., and Muneyoshi, Y.: Superoxide radical scavenging activity of phenolic
1001 compounds, *International journal of biochemistry*, 25, 491-494, 1993.

1002 Young, D. E., Kim, H., Parworth, C., Zhou, S., Zhang, X., Cappa, C. D., Seco, R., Kim, S., and
1003 Zhang, Q.: Influences of emission sources and meteorology on aerosol chemistry in a
1004 polluted urban environment: results from DISCOVER-AQ California, *Atmos. Chem.*
1005 *Phys.*, 16, 5427-5451, 2016.

1006 Zein, A. E., Coeur, C. c., Obeid, E., Lauraguais, A. l., and Fagniez, T.: Reaction kinetics of
1007 catechol (1, 2-benzenediol) and guaiacol (2-methoxyphenol) with ozone, *The Journal of*
1008 *Physical Chemistry A*, 119, 6759-6765, 2015.

1009 Zeng, T., and Arnold, W. A.: Pesticide photolysis in prairie potholes: probing photosensitized
1010 processes, *Environmental science & technology*, 47, 6735-6745, 2012.

1011 Zepp, R. G., Braun, A. M., Hoigne, J., and Leenheer, J. A.: Photoproduction of hydrated
1012 electrons from natural organic solutes in aquatic environments, *Environmental science &*
1013 *technology*, 21, 485-490, 1987.

1014 Zhou, X., and Mopper, K.: Determination of photochemically produced hydroxyl radicals in
1015 seawater and freshwater, *Mar. Chem.*, 30, 71-88, 1990.

1016